Urinary Proteomics Guides Artificial Intelligence to Discover New Digital Biomarkers for Type 2 Diabetic Nephropathy Classification

Nicholas Lucarelli[1,*], Donghwan Yun[2,*], Dohyun Han[3,*], Brandon Ginley[1], Kyung Chul Moon[4], Avi Z. Rosenberg[5], John E. Tomaszewski[1], Jarcy Zee[6], Kuang-Yu Jen[7], Seung Seok Han[7,†], and Pinaki Sarder[1,†]

[1]Department of Pathology & Anatomical Sciences, University at Buffalo, NY, USA

[2]Department of Biomedical Sciences, [4]Department of Pathology, and [7]Department of Internal Medicine, Seoul National University College of Medicine, Seoul, Republic of Korea

[3]Proteomics Core Facility, Biomedical Research Institute, Seoul National University Hospital, Seoul, Republic of Korea

[5]Department of Pathology, John Hopkins University, MD, USA

[6]Department of Biostatistics, Epidemiology, and Informatics, University of Pennsylvania and Children's Hospital of Philadelphia, PA, USA

[7]Department of Pathology and Laboratory Medicine, University of California, Davis Medical Center, CA, USA.

[†]Correspondence:

Seung Seok Han

Department of Internal Medicine, Seoul National University College of Medicine

103 Daehakro, Jongno-gu, Seoul, 03080, Republic of Korea

Tel: +82-2-2072-4785; Fax: +82-2-745-2264; E-mail: hansway7@snu.ac.kr

Pinaki Sarder

Department of Pathology and Anatomical Sciences, University at Buffalo

955 Main Street, Buffalo, New York, 14203

Tel: 716-829-2265; E-mail: pinakisa@buffalo.edu

Abstract

Background: ~~Type 2~~ Diabetic Nephropathy (~~T2~~DN), in the setting of type 2 diabetes, is the world's leading cause of chronic kidney disease and end-stage kidney disease (ESKD). The increasing prevalence and heterogeneous phenotype of ~~T2~~DN complicate the approach to treating patients. While kidney biopsy is the gold standard for (1) exclusion of non-DN diagnoses and (2) confirming diagnosis of DN, it is imperfect in predicting progression to ESKD. Artificial intelligence (AI) has the potential to improve classification of ~~T2~~DN, predict progression risk, and via integration with urinary proteomic profiles identify novel urinary biomarkers, taken together augmenting and going beyond current pathology practice.

Methods: We studied whole slide images (WSIs) of periodic acid-Schiff stained renal biopsies from 56 DN patients with associated urinary proteomics data ~~for 2038 proteins~~. We identified urinary proteins differentially expressed in patients that developed ESKD within two years of biopsy. Six renal subcompartments were computationally segmented from each WSI using our previously published H-AI-L pipeline. Hand-engineered image features for glomeruli and tubules, and urinary proteins were used as inputs to deep learning frameworks to predict patient's ESKD status two years after biopsy. Differentially measured proteins were spatially registered using available snRNA-seq data from early stage diabetics, and were correlated with digital image features from the same spatial compartment using Spearman rank sum coefficient.

Results: Differentially abundant urinary proteins were most predictive of ESKD, with AUC = 0.95, with weaker performance of tubular and glomerular features, AUC = 0.73 and AUC = 0.66, respectively. Additionally, some proteins were associated in renal parenchymal cell types/compartments correlated with differential digital image features (i.e., EGF with tubular basement membrane contrast, and C7 with glomerular PAS-stain contrast).

Conclusions: By integrating urinary biomarkers with image biomarkers we demonstrate that

urinary proteins can robustly predict progression to ESKD, outperforming tubular and glomerular computational features. Using computational methods like ours can be useful more broadly to investigate links between molecular profiles and image features to improve pathophysiological understanding of the nature of DN progression with translational potential.

Introduction

~~Type 2~~ Diabetic Nephropathy (~~T2~~DN), in the setting of type 2 diabetes, is the leading driver of chronic kidney disease (CKD) and end-stage kidney disease (ESKD) worldwide[1]. The incidence of DN is increasing due to high prevalence of diabetes, with subsequent kidney complications such as proteinuria and a decline in kidney function affect more than 40% of the patients[2-4]. The result is an increased burden of cardiovascular morbidity and mortality[5], but the current therapeutic tools including lifestyle modification, blockers of renin-angiotensin-aldosterone system and SGLT2 inhibitors are insufficient to manage the rising incidence of DN and comorbidities. The heterogeneous phenotype of DN further complicates a comprehensive approach, with a subset of patients have an abrupt decline in kidney function requiring dialysis within a few years of diabetes diagnosis[6].

Kidney biopsy is the gold standard for the diagnosis of kidney disease, and histology aids in predicting the outcome and/or response to therapy[7]. The utility of a renal biopsy in the setting of diabetes, beyond staging of DN, is critical to identify non-diabetic processes (up to 30% of cases) [8,9] with a different etiology and disease trajectory compared with DN [10,11]. For improved classification and staging of DN, the Renal Pathology Society generated a DN classification schema[12]. This system reflects the course of progressive DN well[13,14], but has been hindered by the lack of practical application and implementation[15]. Recent approaches have interrogated molecular profiles with classical grading systems of tissue histology[16-18], but this has not yet been reported for the RPS DN classification schema.

Artificial intelligence (AI) has potential to classify histology of kidney diseases in an automated fashion, which reduces the burden on pathologists and promises to improve reproducibility and robustness[19]. Our previous work demonstrated digital classification of diabetic glomerulopathy in renal biopsies [20,21] where our models achieved high levels of

agreement with routine pathologist classification. To demonstrate the value added by these computational techniques, AI-based supervision for morphological changes related with molecular profiles or patient outcomes but imperceptible to the human eye are a promising next step [22-24]. Herein, we integrated urinary proteomic profiles with AI-based histology images from biopsy-confirmed DN cases. The urinary proteomic model had a greater performance than the AI-based image feature models in predicting early deterioration of kidney function. Several significant proteins and/or relevant pathways were associated with histological changes at the pixel and morphological level. These results suggest that the urinary proteomic dataset could guide better annotation of meaningful image features by AI, which were both within and beyond range of human eye. Based on the results, AI will enable the extraction of histologic data related with encoded molecular implications, as the next revolution in the histology-guided care of DN and generate new hypothesis for discovering novel pathobiology with diagnostic and prognostic implications pertaining to diabetes.

Results

Renal Tissue Multicompartment Segmentation

From each subject, one PAS-stained renal tissue biopsy whole slide image (WSI) was segmented into 6 classes: image background, renal interstitium (excluding perivascular stroma), non-sclerotic glomeruli, globally sclerotic glomeruli, tubules, and arteries/arterioles. The segmentation was first performed by our trained Panoptic segmentation network, and each slide was then manually corrected for any errors or missed segmentations. Examples of corrected network predictions are shown in ***Fig. 1.*** For this study, only cortical regions of the biopsies were used for analyses. Therefore, medullary regions were manually annotated and excluded from further analyses. Panoptic Quality (PQ)[25,26], was measured for segmentation of glomeruli, globally sclerotic glomeruli, and tubules in cortical regions. On average, we measured PQ = 0.76, 0.79, and 0.89 for segmenting glomeruli, globally sclerotic glomeruli, and tubules, respectively.

Renal Tissue Sub-Compartmentalization

Glomerular sub-compartmentalization was done similarly to the method described by Ginley *et al.*[20] in our earlier work. Following the same motivation, tubular sub-compartmentalization was performed to simplify the description of the structure. Each instance of glomerulus and tubule was further segmented into three components: (1) nuclear component, (2) PAS-positive component, and (3) white space component. Examples of the tubular sub-compartmentalization are shown in ***Fig. 2.*** This method of compartmentalization has been shown previously to be useful in classifying patients into stages of DN, by using features extracted from the compartmentalized glomeruli[20]. However, this method is novel for tubules, and in predicting the progression of DN. We assessed the validity of these methods in this work, but did not analyze artery and arteriolar morphometrics.

Renal Tissue Image Feature Quantification

Hand-engineered digital image features were measured from each compartmentalized instance of glomeruli and tubules. The features measured per glomerulus have been previously described by Ginley *et al.*[20] in our earlier work. New features were also defined in addition to our existing set, including component-specific distance metrics, such as quantiles of pixel distance from the glomerular border. In total, there were 315 digital image features measured for each glomerulus. The full feature definitions are listed in ***Supp. Doc. 2.***

Similar digital image features were measured for each renal tubule. From the three components segmented from each tubule (see *Renal Tissue Sub-Compartmentalization*), features were measured on pixel colors, textures, morphology, containment, and inter- and intra-structural distances. Examples of these feature extractions are shown in ***Fig. 3.*** One unique aspect of this set was the features added to measure more specific morphology of the tubules. While glomeruli typically appear circular in histological sections, tubules can have a highly variable shape. To account for this variance, we measured tubular curl[27], major axis length, perimeter, and area. These features can describe the tortuosity and thickness of each tubule. Also, features were defined to quantify the morphology of the tubular basement membrane (TBM). During feature extraction, the TBM was segmented from the rest of the PAS+ area, and color, textural, and size features were measured using the resulting segmentation. Some examples of TBM thickness quantifications are shown in ***Fig. 3.*** The TBM has previously been shown to display renal damage in patients with diabetic kidney disease[28]. In total, 207 digital image features were measured for each segmented tubule. These features are listed in ***Supp. Doc. 2.***

Urinary Proteomics Data Feature Manifold Classification

The feature sets used in this study were initially analyzed using Seurat[29,30]. Each feature set (urinary proteins, glomerular image features, tubular image features) was visualized separately

using Uniform Manifold Approximation and Projection (UMAP) to project the high-dimensional feature-space to a 2-dimensional plot. For patient-wise visualization of image feature sets in UMAP space, each feature was averaged across all object instances (namely, for all the segmented glomeruli or tubules) in a single biopsy. An SVM was trained on each feature set to classify patients on whether they progressed to ESKD within 2 years of biopsy. To account for the imbalance in outcomes, the class weights were adjusted inversely proportional to class frequencies[31]. For aggregated glomerular image features, the SVM achieved Matthews Correlation Coefficient (*MCC*), $MCC = 0.31$. For tubular image features, we achieved $MCC = 0.39$, and for the full urine protein set, $MCC = 0.60$. The simplified feature spaces and SVM hyperplanes are shown in ***Fig. 4***.

Using Seurat, we were also able to identify 45 proteins that were differentially measured ($p < 0.05$) in patients that progressed to ESKD within 2 years. Cluster biomarkers were found using the *FindMarkers* function. Of these proteins, several were measured to be significantly higher in patients progressing to ESKD (***Table 1A***), and others were measured to be significantly lower (***Table 1B***). After reducing the number of features in the urine protein set, we retrained the SVM, and achieved an improved $MCC = 0.72$.

Mapping Urinary Proteomics Features to Pertinent Renal Cells using Single-Nuclei RNA Sequencing

The percentage of cells and average expression for each of the 45 differentially measured urinary proteins were quantified using single-nuclei RNA (snRNA) sequencing data for both non-diabetic and diabetic kidney tissues ($n = 6$). Cell type candidate biomarkers, and protein expression for the differentially measured urinary proteins are shown in ***Fig. 5***. A total of 11 clusters including proximal convoluted tubule, parietal epithelial cell, thick ascending loop, distal convoluted tubule, collecting duct (principal cell, intercalated cell type A and B),

podocyte, endothelial cell, mesangial cell & fibroblast, and immune cells were identified by cell marker genes, and sub-clustering of mesangial cell and fibroblast yielded three subclusters (fibroblast, myofibroblast, and mesangial cell, ***Fig. 5A-B)***. The gene expression of urine proteins increased and decreased in progressed patients is summarized in ***Fig. 5C.*** This result provides insights on which protein types are expressed in renal cell types, since it is hard to precisely localize urinary proteins. Additionally, we quantified the changes in protein expression between non-diabetic and diabetic cases. For example, there was a clear increase in the number of fibroblasts expressing the *C7* gene in diabetic kidneys, and it can be visualized in the UMAP plot with subclustered mesangial cells and fibroblasts (***Fig. 5E***). This relationship was further explored in the study below correlating image and molecular features.

Disease Progression Prediction using AI

AI was implemented to predict disease progression in patients with DN because of its unique ability to detect and model nonlinear relationships[32], which is important for studying nonlinear disease progression such as that of CKD[33].

We used two neural network architectures to predict progression in DN patients. Urinary proteins are patient-level measurements, and therefore these features can be used directly to produce a classification through a series of dense layers, in a Fully Connected Neural Network (FCNN). However, the digital image features measured in this study are measured from multiple instances (namely, multiple segmented glomeruli or tubules) per patient, and must be aggregated to form a single prediction for a patient. We therefore used a Recurrent Neural Network (RNN) to incorporate all glomeruli or tubules to form predictions following recipes discussed in our previous publication[20]. Since some of our data is unlabeled, we trained our networks using a self-training semi-supervised scheme[34]. The results are aggregated from each patient when used in the holdout set during 10-fold cross-validation. We compared the SoftMax

predictions of each network to the patient's ground truth label, and assessed the performance with the Area Under the Curve (AUC) of the Receiver Operating Characteristic (ROC) curve. These results are shown in ***Fig. 6***.

We achieved the best performance when training on differentially measured urinary proteins in an FCNN, with $AUC = 0.95$. This score indicates nearly perfect agreement between the classifier network and the ground truth label. Between the image feature types, those measured for tubules outperformed glomeruli. Tubular image features achieved $AUC = 0.73$, while glomerular image features achieved $AUC = 0.66$. The imbalance between the number of glomeruli and tubules present in a biopsy could explain the difference in network performance, but these biopsies are standard for pathologists' diagnoses. Therefore, tubular features could be considered better indicators of disease progression.

Correlation of Renal Tissue Morphometry and Urinary Proteomics Data

Using Spearman's rank correlation coefficient, we measured the degree of correlation between digital image features and urinary protein measurements, while controlling for confounding variables. We were interested in understanding how a urinary proteome may be reflected in tissue sections and analyzing the significance of these relationships. Each digital image feature across all structures in each patient subject was matched with the subject's urinary proteomic profile, and with their associated molecular pathway scores. The measured correlation coefficients were aggregated into the heatmaps shown in ***Fig. 7***.

The associated heatmap color represents the degree of correlation between an image feature and a urinary protein or pathway, indicated by the colorbar. On average, correlation coefficients with glomerular image features were greater than those with tubules, but *p*-values were lower for tubules, likely due to differences in sample size. We were most interested in the correlations with the largest magnitude, and these molecular-image pairs were ranked accordingly. A full

list of the corresponding image features, along with the corresponding urinary proteins, and pathways, is listed in ***Supp. Doc. 2.***

Discovery via Renal Tissue Image Pixel Parsing

Of the many Spearman rank correlation coefficients measured between image features and urinary proteomics molecular data, we were most interested in those with greatest magnitude. The goal is to identify the image features and proteins/pathways that may have some direct or indirect relationship.

As a select example, when looking at the correlation coefficients calculated between non-sclerotic glomerular image features and urinary proteins, the most highly correlated pair consisted of the protein Complement C7, and the standard deviation of green pixel values in PAS-positive region, with a coefficient value of -0.43 ($p < 0.05$). Along with this image feature, Complement C7 was also more highly correlated with the standard deviations of red and blue pixel values in PAS-positive regions, with coefficient values of -0.39 and -0.37 ($p < 0.05$), respectively. These pixel values are directly related to the perceived brightness in an image, and of the three channels, the green channel has the most significant effect[35]. Furthermore, the standard deviation of the pixel values in an image is related to the image contrast[36], specifically within the PAS-positive region of the segmented glomerulus. Therefore, since this feature and protein have an inverse correlation, as the amount of C7 present in the urine increases, one should expect to see a decrease in this image feature. C7 is a protein expressed in renal fibroblasts, as demonstrated in our snRNA sequencing and urinary proteomics mapping data. C7 is one of the proteins of the membrane attack complex (MAC)[37], which may target the glomerulus based on this correlation. Furthermore, one can link this relationship to outcome, since C7 is also a urinary protein that is differentially elevated in patients developing ESKD within 2 years post-biopsy/urinalysis. Some image feature examples are shown in ***Fig. 8.***

When looking at correlation coefficients between tubular image features and urinary proteins, a few interesting cases arose. One of the most highly correlated pairs consisted of the protein Epidermal Growth Factor (EGF), and the standard deviation of green pixel values in the TBM regions, with a coefficient value of 0.21 ($p < 0.05$). Similar to the glomerular example, EGF was also relatively highly correlated with the standard deviations of the red and blue pixels in the TBM regions. As the amount of EGF present in the urine decreases, one should also expect to see a decrease in these features in the image data. EGF has previously been implicated in the development of AKI and CKD[38], and is expressed in renal tubular cells, as supported by our snRNA-seq results. Additionally, five of the other six most highly correlated feature-protein pairs involve the protein Osteopontin (SPP1). SPP1 is another protein that is found in renal tubular cells, as shown in both our snRNAseq results, and previous studies[39], while the receptor is found in immune cells[40]. These urinary proteins were elucidated by this study for their relations to renal morphology in histological images, but their specific roles in kidney diseases are currently not fully understood[41].

Discussion

The ability to predict disease progression in patients with DN is valuable in identifying at-risk patients. Identifying risk early in disease progression allows the clinicians to make informed decisions about screening and treatments for patients[42]. Using AI, we were able to show that urinary proteins can predict which DN patients would progress to ESKD within two years of urine collection. However, digital image features were proven to be of lesser value than urinary proteins. Between the two sets of digital image features, those measured at the individual tubules level still had higher prognostic power in DN progression than the previously published glomerular based features.

Biopsy is the current gold standard for diagnosis and outcome prediction of kidney disease, and predicting response to therapy. In this work, we examined the digital morphology of glomeruli and tubules as seen in renal biopsies. It is much more manageable for a pathologist to analyze individual glomeruli, since these structures are significantly less present in the biopsy as compared to tubules. The large number of tubules present in a biopsy makes it difficult for pathologists to integrate data over the entire WSI and make an objective prognosis. In this work, we suggest that tubular image features from a standard needle biopsy are more predictive of disease progression than glomerular features. Therefore, we also suggest that computational methods like those we have demonstrated provide an advantage over current diagnosis standards, since our methods can provide a reproducible and comprehensive view of the tubular morphology.

We have also demonstrated the ability to link urinary proteomics data to quantitative image features. Qualitative image analysis has long been the standard for assessing pathology, but our results show that proteomics are robust in assessing progression in DN. Therefore, discovering and investigating links between image features and molecular profiles can aid in further

research to increase our understanding of the nonlinear nature of DN. This methodology is also not limited to DN, or specific to renal pathology. Investigating these links further could lead to discoveries in the area of diabetic kidney disease. Integration of other data types are also applicable in this case, depending on investigative goals and resources.

As mentioned by Ginley *et al.*[20], actual compartmental distinction in both glomeruli and tubules is complex. This sub-compartmentalization does not fully reflect actual components of the glomerulus and tubule. The simplification of each structure into three components based on their colorimetric appearance is a limitation to our performance in quantifying disease progression. Also, we largely analyzed each data source (image and molecular) individually, and there is a potential value in integrating image and molecular data to make prognoses, which can be an area of future investigations. Lastly, our snRNA sequencing data comes from non-diabetics and early diabetic, while the urinary proteomics and histology are sampled from various stages of DN. Therefore, the sequencing data may not be fully reflective of the conclusions we have made. To mitigate this shortcoming, in the future we will focus on generating image, urinary proteomics, and snRNA sequencing data from same subject to tighten the conclusions made in this work.

Methods

Human Samples

Study subjects were from Seoul National University Hospital. Human data collection followed protocols approved by the Institutional Review Board at the Seoul National University (SNU) College of Medicine (H-1812-159-998), Seoul, Korea. All experiments were performed according to federal guidelines and regulations. Individual subject data contain patient demographic and medical history information, including height, weight, age, history of diabetes, stroke, and presence of hypertension. Blood tests were administered to the subjects at the time of biopsy. Serum creatinine was used to measure the estimated glomerular filtration rate (eGFR) at the time of biopsy using the CKD-EPI equation[43]. Patients were re-evaluated and new blood samples were collected at one- and two-years following the initial biopsy and urine collection, and eGFR was recalculated. For each timepoint, it was determined whether serum creatinine had doubled compared with baseline, whether eGFR had reached 50% of the baseline value, and whether the patient had reached end stage kidney disease (ESKD). A full description of patient baseline characteristics can be found in ***Supp. Doc. 1.***

Whole Slide Image Data

Image data for this study consisted of brightfield microscopy whole-slide images (WSIs) of periodic acid-Schiff (PAS)-stained renal biopsies from n = 56 human DN subjects. An additional n = 30 WSIs from human DN patients were added as an additional set, but outcome data was not available for these patients. Whole slide imaging was done using a digital slide scanner (Aperio AT2, Leica Biosystems, Wetzlar, Germany). Pixel resolution of the images is 0.25 μm per pixel. Each biopsy was graded by a pathologist for glomerular lesions, following the Renal Pathology Society DN scoring system[12]. Other features scored included for interstitial fibrosis and tubular atrophy (IFTA), interstitial inflammation, arteriolar hyalinosis,

and arteriosclerosis.

Urine Sample Preparation

For protein digestion, 1-2 ml urine sample from each subject was concentrated to 250 ul using a spin filter with a molecular weight cut-off of 3 kDa (Millipore, Billerica, MA). The protein concentration was measured according to the Bradford assay protocol (Bio-Rad protein assay kit, Bio-Rad, Hercules, CA). For protein digestion, 50 µg of urine proteins was precipitated by adding a 5-fold volume of ice-cold acetone. The precipitated samples were reconstituted in 50 µl of SDT buffer (2% SDS, 0.1 M dithiothreitol in 0.1 M Tris HCl; pH, 8.0). After being heated at 95°C, the denatured proteins were digested by a filter-aided sample preparation (FASP) method as previously described[44] with some modifications. Briefly, protein samples were loaded onto a 30K amicon filter (Millipore, Billerica, MA), and buffer was exchanged with UA solution (8M UREA in 0.1M Tris-HCl; pH, 8.5) via centrifugation. After three buffer exchanges with UA solution, the reduced cysteines were alkylated with 0.05 M iodoacetamide (IAA) in UA solution for 30 min at room temperature in the dark. Thereafter, UA buffer was exchanged for 40 mM ammonium bicarbonate (ABC) twice. The protein samples were digested with trypsin/LysC (enzyme to substrate ratio of 1:100) at 37°C for 16 h. The resulting peptides were collected in new tubes via centrifugation, and an additional elution step was performed using 40 mM ABC and 0.5 M NaCl. All resulting peptides were acidified with 10% trifluoroacetic acid and desalted using a homemade styrene divinylbenzene reversed-phase sulfonate (SDB-RPS)-StageTips[45,46]. The peptides were initially washed with 0.2% TFA, and were then sequentially eluted with 40, 60, and 80% acetonitrile (ACN) containing 1% ammonia. Fractionated peptides were completely dried with a vacuum dryer and stored at -80°C.

Establishment of a Matching Spectral Library

To construct a matching spectral library for matching between runs, pooled urine samples were

digested using the two-step filter-aided sample preparation as described previously[46,47]. Digested peptides were desalted using Oasis HLB solid-phase extraction (SPE). For the in-depth data set, 100 µg of purified peptides were fractionated using an Agilent 1260 bioinert HPLC (Agilent, Santa Clara, CA) equipped with an analytical column (4.6 × 250 mm, 5-µm particle). High-pH reversed-phase peptide fractionation was performed at a flow rate of 0.8 ml/min over a 60-min gradient using solvent A (15 mm ammonium hydroxide in water) and solvent B (15 mM ammonium hydroxide in 90% acetonitrile). A total of 96 fractions was collected each minute and non-contiguously pooled into 24 fractions. The fractions were dried in a vacuum centrifuge and stored at -80°C until liquid chromatography-tandem mass spectrometry (LC-MS/MS).

LC-MS/MS Analysis

LC-MS/MS analysis was performed using Quadrupole Orbitrap mass spectrometers, Q-exactive plus (Thermo Fisher Scientific, Waltham, MA) coupled to an Ultimate 3000 RSLC systems (Dionex, Sunnyvale, CA) with a nano-electrospray source as previously described with some modifications[44,45]. Peptide samples were separated on a two-column setup with a trap column (300 µm I.D. × 0.5 cm, C18 3 µm, 100 Å) and analytical column (50 µm I.D. × 50 cm, C18 1.9 µm, 100 Å). Prior to sample injection, the dried peptide samples were redissolved in solvent A (2% acetonitrile and 0.1% formic acid). After the samples were loaded onto the nano LC, a 90-min gradient from 8% to 30% solvent B (100% acetonitrile and 0.1% formic acid) was applied to all samples. The spray voltage was 2.0 kV in positive ion mode and the temperature of the heated capillary was set to 320°C. Mass spectra were acquired in data-dependent mode using a top 15 method on a Q-Exactive. The Orbitrap analyser scanned precursor ions with a mass range of 300–1650 m/z and resolution of 70,000 at m/z 200. Higher-energy collisional dissociation (HCD) scans were acquired on the Q-Exactive at a resolution

of 17,500. HCD peptide fragments were acquired at a normalized collision energy of 28. The maximum ion injection times for the survey and MS/MS scans were 20 and 120 ms, respectively.

Data Processing for Label-Free Quantification

Mass spectra were processed with MaxQuant (version 1.6.1.0)[48]. MS/MS spectra were searched against the Human Uniprot protein sequence database (December 2014, 88,657 entries) using the Andromeda search engine[49]. Primary searches were performed using a six-ppm precursor ion tolerance for total protein level analysis. The MS/MS ion tolerance was set to 20 ppm. Cysteine carbamido-methylation was set as a fixed modification. *N*-Acetylation of proteins and oxidation of methionine were set as variable modifications. Enzyme specificity was set to full tryptic digestion. Peptides with a minimum length of six amino acids and up to two missed cleavages were considered. The required false discovery rate (FDR) was set to 1% at the peptide, protein, and modification levels. To maximize the number of quantification events across samples, matching between runs was performed using the pooled urine sample as a library.

Human AI Loop (HAIL) Pipeline

To conduct computational segmentation of renal micro-compartments, we used our previously published, publicly available HAIL pipeline[50]. This pipeline allows users to train segmentation CNNs directly from annotations produced in the WSI viewer Aperio ImageScope®. HAIL allows for an iterative process of network training, where the network's own predictions produced after each training iteration can be manually corrected and used to bootstrap further annotation data.

Panoptic Segmentation

Panoptic segmentation[26] was performed on PAS stained WSIs to classify pixels into six

categories, and to resolve separate instances (e.g., individual tubules) of the same class. These six categories include image background, renal interstitium (excluding perivascular stroma), non-sclerotic glomeruli, globally sclerotic glomeruli, renal tubules, and arteries/arterioles. To train the model, 126 WSIs of kidney biopsy from native diabetic, lupus nephritis, and transplant patients were selected due to the presence of minimal cortex (<10%) in the slide, and fully annotated for all six categories. The network architecture was modelled closely after Google's Panoptic-Deeplab model[51]. There are three primary differences between our network model, and DeepLab-Panoptic. First, to reduce the memory overhead, the feature encoding backbone used is a ResNet50[52]. Second, the output stride of our encoder is only 8 as opposed to 16 as used in the DeepLab-Panoptic model. Finally, for the output of our instance decoder branch, rather than predicting a Hough transform, this branch predicts the distance transform of each object. Then, instance segmentation is performed by computing a watershed transform[53] on the predicted output distance transform map. Classification IDs of the predicted objects are settled with the majority voting rule used in Panoptic-DeepLab. The network was trained on cropped image patches of 560 × 560 pixel size and batch size 2 for approximately 3.8M steps. The trained network was then used for prediction where medullary regions were manually annotated and excluded from the analysis. Finally, glomeruli and tubules with artefact were manually removed from the final segmentations to eliminate erroneous quantification. Segmentation accuracy was assessed using the Panoptic Quality (PQ) metric[25], created by the original developers of Panoptic segmentation. This metric joins segmentation quality and recognition quality to assess both semantic and instance segmentation performance. PQ was only measured for segmentation of glomeruli, globally sclerotic glomeruli, and tubules, since these were the classes used in later analyses. We selected 5 random WSIs from patients that progressed to ESKD within 2 years and 5 random WSIs from patients that did not, and these

images were used for performance analysis. Our manually corrected annotations for these slides were further corrected by a pathologist, and used as a ground truth.

Glomerular and Tubular Sub-Compartmentalization

To simplify compartmentalization of the annotated regions, glomerular pixels are assigned to one of three components based on their appearance in the PAS-stained biopsies, according to Ginley *et. al*[20]: (1) nuclear components, (2) PAS-positive components, containing the glomerular basement membrane, mesangium, and Bowman's capsule, and (3) luminal components consisting of capillary lumina and the Bowman's space. For tubular sub-compartmentalization, the three components were similar.

Nuclei were detected in the tissue by a custom coded Panoptic segmentation network. This network was trained on previously annotated data described by Ginley *et. al*[20]. In both glomerular and tubular images, nuclei were segmented by the same network. In glomeruli, PAS+ components were segmented by a several step process. First, the original RGB image was transformed to the hue-saturation-value color space[54], the saturation channel was isolated, and the dark regions were brightened using a gamma transform[55]. For each glomerulus, this gamma was set at a constant of 0.7. Otsu's thresholding method[56] was then applied to segment the PAS+ area, excluding the already segmented nuclei. Once the nuclear and PAS+ components were segmented, the remaining pixels not contained in these components were classified as luminal pixels. PAS+ components of the tubules were segmented in a slightly different fashion. First, the RGB image was transformed to the LAB color space[57]. Second, the lightness color channel (L) was isolated and a constant threshold of 80 was applied to the 8-bit pixels. All pixels, not already classified as nuclei, above this threshold were classified as luminal components. All other pixels not contained in the nuclear or luminal segmentation were classified as PAS+ components.

Feature Engineering

For glomerular images, several digital image feature types are defined according to the methods described by Ginley *et al*[20]. These feature types included color, texture, morphology, containment, interstructural distances, and intrastructural distances. A total of 315 image features were measured for each glomerulus. For tubular images, similar digital features are measured for the same respective structures. However, additional features are defined for the tubular basement membrane, and to measure the tortuosity of the tubules. A total of 207 image features are measured for each tubule. A full list of both digital image feature sets can be found in ***Supp. Doc. 2.***

Image/ Proteomic Feature Manifold Classification

Image/proteomic feature manifolds were studied in low dimensional space using a state-of-the-art software Seurat[29,30]. Seurat is typically used for studying single-cell RNA-sequencing (scRNAseq) data, but can be extended to other high-dimensional data, such as digital image features and urinary proteomics. For image feature analysis, each datapoint is modelled as a computationally segmented individual microcompartment (e.g., tubule, glomerulus), and corresponding feature values are quantified engineered feature data. For urinary proteomics analysis, each datapoint is modelled as a single subject, and corresponding feature values are measured urinary proteomics features. As a first step, the data is normalized by a global-scaling normalization method. This method normalizes each feature by min-max scaling values between 0-1, multiplying by a scale factor, and then log-transforming the result. The data is then scaled to zero mean and unit variance. Principal component analysis was then performed on the scaled data. Non-linear dimensionality reduction using UMAP (Uniform Manifold Approximation and Projection)[58] is performed using the first 20 principal components per datapoint. Class labels (e.g., subjects with two-year ESKD vs the rest) of interest are applied

to these points following dimensionality reduction.

We analyzed differentially measured image or proteomics between various data classes to characterize these classes. Features that are differentially expressed between classes are discovered using the *FindMarkers* function in Seurat, which uses the Wilcoxon rank sum test[59] to determine statistical significance. This function also automatically performs *p*-value adjustment using Bonferroni correction, based on the number of features in the dataset. Features with an adjusted $p < 0.05$ were identified as differentially expressed.

To classify subjects based on two-year ESKD binary outcome measure, we performed binary classification of the UMAP feature data using a support vector classifier[60]. One-dimensional hyperplanes were optimized using a radial basis function kernel, with balanced class weight, to classify the subjects. The performance of the classifier was quantified using Matthews correlation coefficient[61].

Mapping Urinary Proteins to Source Renal Parenchymal Cells using Single-Nuclei RNA Sequencing Data

While fusing urinary proteomics data and digital renal tissue image features is an important goal of our study, it is important to map the urinary proteomics data to pertinent renal cell types to investigate biological relevance of our findings. For this mapping, as a quality control, pooled single-nuclei RNA sequencing (snRNAseq) data of early diabetic (n = 3) and nondiabetic (n = 3) patients from a previous study[62] were used. Genes expressed in ≥3 cells, cells with ≥500 unique molecular identifier counts were used. The R[63] and Seurat[64] software packages as well as pheatmap (version 1.0.12) package embedded in R were used for data analyses and visualization. For the mapping the following functionalities from these software packages were used: *SCTransform* for merging data with adjusting batch-effects; *FindNeighbors* and *FindClusters* for finding clusters; *RunUMAP, FeaturePlot, DotPlot,* and

pheatmap for data visualization; and *Findmarkers* for identifying differentially expressed genes.

Disease Progression Prediction using Urinary Proteins by Semi-Supervised Fully Connected Neural Network

For each patient, 2038 unique urinary proteins were measured at the time of the biopsy, and for the additional (n = 30) set, 2313 urinary proteins. To predict patient progression to ESKD, we designed a fully connected neural network (FCNN). For all the AI networks, a binary outcome for ESKD progression within two years of biopsy was used as ground truth. Due to the small sample size, using the entire protein set caused overfitting of the network. Therefore, only differentially measured proteins are used as input. The network architecture consists of an input layer for protein data, then a series of two dense layers, each with 30 hidden nodes. These dense layers both contain leaky rectified linear unit (ReLU) activation functions, and 50% dropout during training. The last dense layer connects to a two-node prediction layer, with a SoftMax activation function. Cross-entropy was used to compute the loss for this network. The network was trained with an Adam optimizer, with the learning rate set at 0.001.The network was trained using self-supervised semi-supervision[34] with n = 56 labelled cases and n = 30 unlabelled cases. First, the labelled dataset was split into 90% training and 10% testing, and the network was trained using just this training set for 500 iterations with batch size 50. Then, predictions were produced for the additional dataset of n = 30 that did not have any outcome label. The SoftMax output was clipped at a threshold over 0.90, so any network predictions with more than 90% confidence were kept, and assigned the label produced by the network. Next, the newly labelled cases were added to the original set, and a single training step of batch 50 was run. Then, predictions are reproduced for the second dataset of n = 30, and the process is repeated for a total of 100 iterations. Lastly, predictions are run on the 10% holdout labelled set, and compiled

into the final predictions. The network is then reset, and a different 10% holdout is taken for testing. This was repeated for 10 folds and the results reported are compiled from 100 trials of 10-fold cross validation. Performance was calculated using the area under the receiver operator characteristic curve. The generalized network architecture is shown in ***Supp. Doc. 1.***

Disease Progression Prediction using Image features by Semi-Supervised Recurrent Neural Network

To predict DN progression in our cohort using quantified image features from glomerular or tubular compartments, we employed the recurrent neural network (RNN) architecture designed by Ginley *et al*[20]. The goal is to predict an outcome label for a given WSI by incorporating at the network input the ensemble of quantified image features per compartment basis serially with respect to all the glomeruli or tubules in a biopsy. The main modification of the network architecture with that described in Ginley *et al.*[20] is the final prediction layer, where we use two prediction nodes for our binary outcome (ESKD vs no-ESKD in two years after biopsy), with a SoftMax activation. All training parameters, including learning rate, batch size, and training steps were kept the same. Semi-supervised training was coded similarly to the FCNN above. First, 500 training steps of batch size 256 and 10-time steps were completed with 90% of the labelled dataset. Predictions were run on the unlabelled patients, and those with prediction confidence > 75% were kept, assigned the predicted label, and added back to the training set. Then, 100 additional training steps are run with the expanded training set, and predictions on all the unlabelled data are rerun. This process is repeated 5 times for 500 additional training steps. Final predictions are compiled from 10 trials of 10-fold cross-validation. The generalized network architecture is shown in ***Supp. Doc. 1.***

Correlation of Renal Tissue Morphometry and Molecular Data

Our previous experiments investigate how urine proteins and digital image features of renal

structures relate to DN outcome. We next sought to understand how these two orthogonal data modes are related. These relationships were quantified using partial Spearman's rank correlation coefficient, which controlled for several covariates, including sex, age, height, weight, hypertension, number of years with diagnosed diabetes, and history of stroke and ischemic heart disease. For this analysis, we used *partialcorr* command embedded in MATLAB (Mathworks, Natick, MA)[65]. Coefficients were measured for one-to-one relationships between quantified structural image features and protein expression or scores of molecular pathways formed by an ensemble of proteins. We adjusted the *p*-values of the correlation measures using the Benjamini-Hochberg method[66].

For the above correlative study, to quantify the functionality of the measured urinary proteins at pathway level, we developed a scoring method for upregulation and downregulation of molecular pathways, using Ingenuity Pathway Analysis (IPA; Qiagen, Hilden, Germany)[67]. First, the proteins included in each pathway were identified. Then, the raw protein measurements were added by one, and the resulting values were log-transformed. The resulting data were then min-max scaled between 0-1 per protein basis. Following scaling, values were adjusted by their biological expectation of upregulation/downregulation in pertinent pathways, according to the analytical algorithms embedded in IPA. Namely, the scores of the proteins that were expected to be upregulated during the upregulation of a particular pathway were kept the same. Scores of the proteins that were expected to be downregulated during the upregulation of a particular pathway were revised by subtracting their pertinent values from 1. This was done so that all protein values would increase/decrease the same during upregulation/downregulation of a pathway, respectively. Lastly, the scaled values of the proteins for each pathway were summed for each patient, to obtain one score per pathway.

Discovery via Renal Tissue Image Pixel Parsing

Of the most highly correlated pairs (structural image features vs protein expression or pathway scores), we focused our studies on proteins or molecular pathways with biological relevance to renal pathology. This focus limited the proteins of interest to those expressed in renal cell types, and molecular pathways of interest to those involving aspects of renal function. Distributions across patients were investigated for structural image features highly correlated with these biologically relevant molecular candidates. Discovered image features were visualized in MATLAB, via mapping the quantified image features in the image space. Projected maps were qualitatively studied by renal pathology experts, and relationships with compelling trends were used for future hypothesis generation.

Data Availability

Codes are available at [insert github link here].

Author Contributions

NL corrected computational segmentations, conceptualized and performed the quantitative analyses, designed, and conducted the computational methods, completed all statistical analyses, interpreted the results, and wrote the manuscript. DY …. DH …. BG guided NL in conducting the work, reviewed the codes, as well as critically analyzed results. KCM …. AR and JET critically analyzed the results of the correlation study to decipher the biological meaning of the image level features corresponding to molecular markers pertinent from the urinary proteomic data. JZ contributed with the statistical analysis conducted in the study. KYJ generated ground-truth segmentation boundaries for analyzing the performance of the multi-compartment renal tissue segmentation. SSH co-conceived the overall study with PS integrating urinary proteomics data with renal tissue image data, optimized urinary proteomics data generation, as well as spearheaded the database generation with matching renal tissue whole slide image data as well as with corresponding outcome data. PS co-conceived the study with SSH, assisted in manuscript preparation, coordinated with the study team, assisted in study design, supervised the computational implementation, and critically analyzed the results.

Acknowledgement

The project was supported by NIDDK grant R01 DK114485 (PS), a glue grant (PS) from the NIDDK Kidney Precision Medicine Project, a multi-disciplinary small team grant RSG201047.2 (PS) from the State University of New York, a pilot grant (PS) from the University of Buffalo's Clinical and Translational Science Institute (CTSI) grant 3UL1TR00141206 S1, a DiaComp Pilot & Feasibility Project 21AU4180 (PS) with support from NIDDK Diabetic Complications Consortium grants U24 DK076169 and U24 DK115255,

NIH-OD grant U54 HL145608 (PS), and NIDDK grant R01 DK131189 (PS).

References

1 Koye, D. N., Magliano, D. J., Nelson, R. G. & Pavkov, M. E. The Global Epidemiology of Diabetes and Kidney Disease. *Advances in chronic kidney disease* **25**, 121-132, doi:10.1053/j.ackd.2017.10.011 (2018).

2 Doshi, S. M. & Friedman, A. N. Diagnosis and Management of Type 2 Diabetic Kidney Disease. *Clinical journal of the American Society of Nephrology : CJASN* **12**, 1366-1373, doi:10.2215/cjn.11111016 (2017).

3 Adler, A. I. *et al.* Development and progression of nephropathy in type 2 diabetes: the United Kingdom Prospective Diabetes Study (UKPDS 64). *Kidney international* **63**, 225-232, doi:10.1046/j.1523-1755.2003.00712.x (2003).

4 Fiorentino, M. *et al.* Renal biopsy in patients with diabetes: a pooled meta-analysis of 48 studies. *Nephrology, dialysis, transplantation : official publication of the European Dialysis and Transplant Association - European Renal Association* **32**, 97-110, doi:10.1093/ndt/gfw070 (2017).

5 Tuttle, K. R. *et al.* Diabetic kidney disease: a report from an ADA Consensus Conference. *Diabetes care* **37**, 2864-2883, doi:10.2337/dc14-1296 (2014).

6 Jiang, G. *et al.* Progression of diabetic kidney disease and trajectory of kidney function decline in Chinese patients with Type 2 diabetes. *Kidney international* **95**, 178-187, doi:10.1016/j.kint.2018.08.026 (2019).

7 Luciano, R. L. & Moeckel, G. W. Update on the Native Kidney Biopsy: Core Curriculum 2019. *American journal of kidney diseases : the official journal of the National Kidney Foundation* **73**, 404-415, doi:10.1053/j.ajkd.2018.10.011 (2019).

8 Sharma, S. G. *et al.* The modern spectrum of renal biopsy findings in patients with diabetes. *Clinical journal of the American Society of Nephrology : CJASN* **8**, 1718-1724, doi:10.2215/CJN.02510213 (2013).

9 Mazzucco, G. *et al.* Different patterns of renal damage in type 2 diabetes mellitus: a multicentric study on 393 biopsies. *American journal of kidney diseases : the official journal of the National Kidney Foundation* **39**, 713-720, doi:10.1053/ajkd.2002.31988 (2002).

10 Wong, T. Y. *et al.* Renal outcome in type 2 diabetic patients with or without coexisting nondiabetic nephropathies. *Diabetes care* **25**, 900-905, doi:10.2337/diacare.25.5.900 (2002).

11 Li, L. *et al.* Renal pathological implications in type 2 diabetes mellitus patients with renal involvement. *Journal of diabetes and its complications* **31**, 114-121, doi:10.1016/j.jdiacomp.2016.10.024 (2017).

12 Tervaert, T. W. *et al.* Pathologic classification of diabetic nephropathy. *J Am Soc Nephrol* **21**, 556-563, doi:10.1681/ASN.2010010010 (2010).

13 An, Y. *et al.* Renal histologic changes and the outcome in patients with diabetic nephropathy. *Nephrology, dialysis, transplantation : official publication of the European Dialysis and Transplant Association - European Renal Association* **30**, 257-266, doi:10.1093/ndt/gfu250 (2015).

14 Mise, K. *et al.* Renal prognosis a long time after renal biopsy on patients with diabetic nephropathy. *Nephrology, dialysis, transplantation : official publication of the European Dialysis and Transplant Association - European Renal Association* **29**, 109-118, doi:10.1093/ndt/gft349 (2014).

15 Qi, C., Mao, X., Zhang, Z. & Wu, H. Classification and Differential Diagnosis of

Diabetic Nephropathy. *Journal of diabetes research* **2017**, 8637138, doi:10.1155/2017/8637138 (2017).

16 Loupy, A. *et al.* The Banff 2019 Kidney Meeting Report (I): Updates on and clarification of criteria for T cell- and antibody-mediated rejection. *American journal of transplantation : official journal of the American Society of Transplantation and the American Society of Transplant Surgeons* **20**, 2318-2331, doi:10.1111/ajt.15898 (2020).

17 Sethi, S. & Fervenza, F. C. Standardized classification and reporting of glomerulonephritis. *Nephrology, dialysis, transplantation : official publication of the European Dialysis and Transplant Association - European Renal Association* **34**, 193-199, doi:10.1093/ndt/gfy220 (2019).

18 Gadegbeku, C. A. *et al.* Design of the Nephrotic Syndrome Study Network (NEPTUNE) to evaluate primary glomerular nephropathy by a multidisciplinary approach. *Kidney international* **83**, 749-756, doi:10.1038/ki.2012.428 (2013).

19 Huo, Y., Deng, R., Liu, Q., Fogo, A. B. & Yang, H. AI applications in renal pathology. *Kidney international*, doi:10.1016/j.kint.2021.01.015 (2021).

20 Ginley, B. *et al.* Computational Segmentation and Classification of Diabetic Glomerulosclerosis. *Journal of the American Society of Nephrology : JASN* **30**, 1953-1967, doi:10.1681/asn.2018121259 (2019).

21 Ginley, B. *et al.* Automated Computational Detection of Interstitial Fibrosis, Tubular Atrophy, and Glomerulosclerosis. *Journal of the American Society of Nephrology : JASN* **32**, 837-850, doi:10.1681/asn.2020050652 (2021).

22 Coudray, N. *et al.* Classification and mutation prediction from non-small cell lung cancer histopathology images using deep learning. *Nature medicine* **24**, 1559-1567, doi:10.1038/s41591-018-0177-5 (2018).

23 Kather, J. N. *et al.* Deep learning can predict microsatellite instability directly from histology in gastrointestinal cancer. *Nature medicine* **25**, 1054-1056, doi:10.1038/s41591-019-0462-y (2019).

24 Mobadersany, P. *et al.* Predicting cancer outcomes from histology and genomics using convolutional networks. *Proceedings of the National Academy of Sciences of the United States of America* **115**, E2970-E2979, doi:10.1073/pnas.1717139115 (2018).

25 Kirillov, A., He, K., Girshick, R., Rother, C. & Dollár, P. in *Proceedings of the IEEE/CVF Conference on Computer Vision and Pattern Recognition.* 9404-9413.

26 Kirillov, A., He, K., Girshick, R. B., Rother, C. & Dollár, P. Panoptic Segmentation. *2019 IEEE/CVF Conference on Computer Vision and Pattern Recognition (CVPR)*, 9396-9405 (2019).

27 Wirth, M. A. (Purdue University Cytometry Laboratories, 2004).

28 Tyagi, I., Agrawal, U., Amitabh, V., Jain, A. K. & Saxena, S. Thickness of glomerular and tubular basement membranes in preclinical and clinical stages of diabetic nephropathy. *Indian J Nephrol* **18**, 64-69, doi:10.4103/0971-4065.42336 (2008).

29 Stuart, T. *et al.* Comprehensive Integration of Single-Cell Data. *Cell* **177**, 1888-1902.e1821, doi:10.1016/j.cell.2019.05.031 (2019).

30 Butler, A., Hoffman, P., Smibert, P., Papalexi, E. & Satija, R. Integrating single-cell transcriptomic data across different conditions, technologies, and species. *Nature Biotechnology* **36**, 411-420, doi:10.1038/nbt.4096 (2018).

31 Yi-Min, H. & Shu-Xin, D. in *2005 International Conference on Machine Learning and Cybernetics.* 4365-4369 Vol. 4367.

32 Tu, J. V. Advantages and disadvantages of using artificial neural networks versus

logistic regression for predicting medical outcomes. *Journal of Clinical Epidemiology* **49**, 1225-1231, doi:https://doi.org/10.1016/S0895-4356(96)00002-9 (1996).

33 Li, L. *et al.* Longitudinal Progression Trajectory of GFR Among Patients With CKD. *American Journal of Kidney Diseases* **59**, 504-512, doi:https://doi.org/10.1053/j.ajkd.2011.12.009 (2012).

34 Fazakis, N., Karlos, S., Kotsiantis, S. & Sgarbas, K. Self-Trained LMT for Semisupervised Learning. *Comput Intell Neurosci* **2016**, 3057481-3057481, doi:10.1155/2016/3057481 (2016).

35 Bezryadin, S., Bourov, P. & Ilinih, D. Brightness Calculation in Digital Image Processing. *International Symposium on Technologies for Digital Photo Fulfillment* **2007**, 10-15, doi:10.2352/ISSN.2169-4672.2007.1.0.10 (2007).

36 Moulden, B., Kingdom, F. & Gatley, L. The Standard Deviation of Luminance as a Metric for Contrast in Random-Dot Images. *Perception* **19**, 79-101, doi:10.1068/p190079 (1990).

37 Würzner, R. Modulation of complement membrane attack by local C7 synthesis. *Clin Exp Immunol* **121**, 8-10, doi:10.1046/j.1365-2249.2000.01263.x (2000).

38 Zepeda-Orozco, D., Wen, H. M., Hamilton, B. A., Raikwar, N. S. & Thomas, C. P. EGF regulation of proximal tubule cell proliferation and VEGF-A secretion. *Physiol Rep* **5**, e13453, doi:10.14814/phy2.13453 (2017).

39 Kaleta, B. The role of osteopontin in kidney diseases.

40 MacDonald, L. *et al.* COVID-19 and RA share an SPP1 myeloid pathway that drives PD-L1+ neutrophils and CD14+ monocytes. *JCI Insight* **6**, e147413, doi:10.1172/jci.insight.147413 (2021).

41 Isaka, Y. Epidermal growth factor as a prognostic biomarker in chronic kidney diseases. *Ann Transl Med* **4**, S62-S62, doi:10.21037/atm.2016.10.64 (2016).

42 Ahuja, K. & Schaar, M. V. D. Risk-Stratify: Confident Stratification Of Patients Based On Risk. *ArXiv* **abs/1811.00753** (2018).

43 Levey, A. S. *et al.* A new equation to estimate glomerular filtration rate. *Ann Intern Med* **150**, 604-612, doi:10.7326/0003-4819-150-9-200905050-00006 (2009).

44 Grzegorski, S. J. *et al.* Disruption of the kringle 1 domain of prothrombin leads to late onset mortality in zebrafish. *Scientific reports* **10**, 4049-4049, doi:10.1038/s41598-020-60840-7 (2020).

45 Rhee, S. J. *et al.* Comparison of serum protein profiles between major depressive disorder and bipolar disorder. *BMC Psychiatry* **20**, 145-145, doi:10.1186/s12888-020-02540-0 (2020).

46 Han, D., Jin, J., Woo, J., Min, H. & Kim, Y. Proteomic analysis of mouse astrocytes and their secretome by a combination of FASP and StageTip-based, high pH, reversed-phase fractionation. *PROTEOMICS* **14**, 1604-1609, doi:https://doi.org/10.1002/pmic.201300495 (2014).

47 Han, D., Jin, J., Yu, J., Kim, K. & Kim, Y. Integrated approach using multistep enzyme digestion, TiO2 enrichment, and database search for in-depth phosphoproteomic profiling. *PROTEOMICS* **15**, 618-623, doi:https://doi.org/10.1002/pmic.201400102 (2015).

48 Tyanova, S., Temu, T. & Cox, J. The MaxQuant computational platform for mass spectrometry-based shotgun proteomics. *Nature Protocols* **11**, 2301-2319, doi:10.1038/nprot.2016.136 (2016).

49 Cox, J. *et al.* Andromeda: A Peptide Search Engine Integrated into the MaxQuant

Environment. *Journal of Proteome Research* **10**, 1794-1805, doi:10.1021/pr101065j (2011).

50 Lutnick, B. *et al.* An integrated iterative annotation technique for easing neural network training in medical image analysis. *Nature Machine Intelligence* **1**, 112-119, doi:10.1038/s42256-019-0018-3 (2019).

51 Cheng, B. *et al.* Panoptic-DeepLab: A Simple, Strong, and Fast Baseline for Bottom-Up Panoptic Segmentation. *arXiv e-prints*, arXiv:1911.10194 (2019).

52 He, K., Zhang, X., Ren, S. & Sun, J. Deep Residual Learning for Image Recognition. *arXiv e-prints*, arXiv:1512.03385 (2015).

53 Gonzalez, R. C. & Woods, R. E. *Digital Image Processing*. 3 edn, 1-976 (Prentice Hall, 2007).

54 Ganesan, P., Rajini, V., Sathish, B. S. & Shaik, K. B. in *2014 International Conference on Control, Instrumentation, Communication and Computational Technologies (ICCICCT).* 101-105.

55 Guan, X., Jian, S., Hongda, P., Zhiguo, Z. & Haibin, G. in *2009 Second International Symposium on Computational Intelligence and Design.* 60-63.

56 Bangare, S., Dubal, A., Bangare, P. & Patil, S. Reviewing Otsu's Method For Image Thresholding. *International Journal of Applied Engineering Research* **10**, 21777-21783, doi:10.37622/IJAER/10.9.2015.21777-21783 (2015).

57 Connolly, C. & Fleiss, T. A study of efficiency and accuracy in the transformation from RGB to CIELAB color space. *IEEE Transactions on Image Processing* **6**, 1046-1048, doi:10.1109/83.597279 (1997).

58 McInnes, L., Healy, J. & Melville, J. UMAP: Uniform Manifold Approximation and Projection for Dimension Reduction. *arXiv e-prints*, arXiv:1802.03426 (2018).

59 Gallant, A. R. *Nonlinear Statistical Models*. (Wiley, 1987).

60 Hastie, T., Tibshirani, R., Friedman, J.H. *The Elements of Statistical Learning: Data Mining, Inference, and Prediction*. 2 edn, 768 (Springer, 2009).

61 McHugh, M. L. Interrater reliability: the kappa statistic. *Biochem Med (Zagreb)* **22**, 276-282 (2012).

62 Wilson, P. C. *et al.* The single-cell transcriptomic landscape of early human diabetic nephropathy. *Proceedings of the National Academy of Sciences* **116**, 19619, doi:10.1073/pnas.1908706116 (2019).

63 *The Comprehensive R Archive Network (V 4.0.3)*, <http://cran.r-project.org> (

64 *Seurat (V 3.2.3)*, <https://satijalab.org/seurat/> (

65 *MATLAB*, <https://www.mathworks.com/products/matlab.html> (

66 Benjamini, Y. & Hochberg, Y. Controlling the False Discovery Rate: A Practical and Powerful Approach to Multiple Testing. *Journal of the Royal Statistical Society. Series B (Methodological)* **57**, 289-300 (1995).

67 *Ingenuity Pathways Analysis (IPA)*, <https://www.nihlibrary.nih.gov/resources/tools/ingenuity-pathways-analysis-ipa> (

Results Figures.

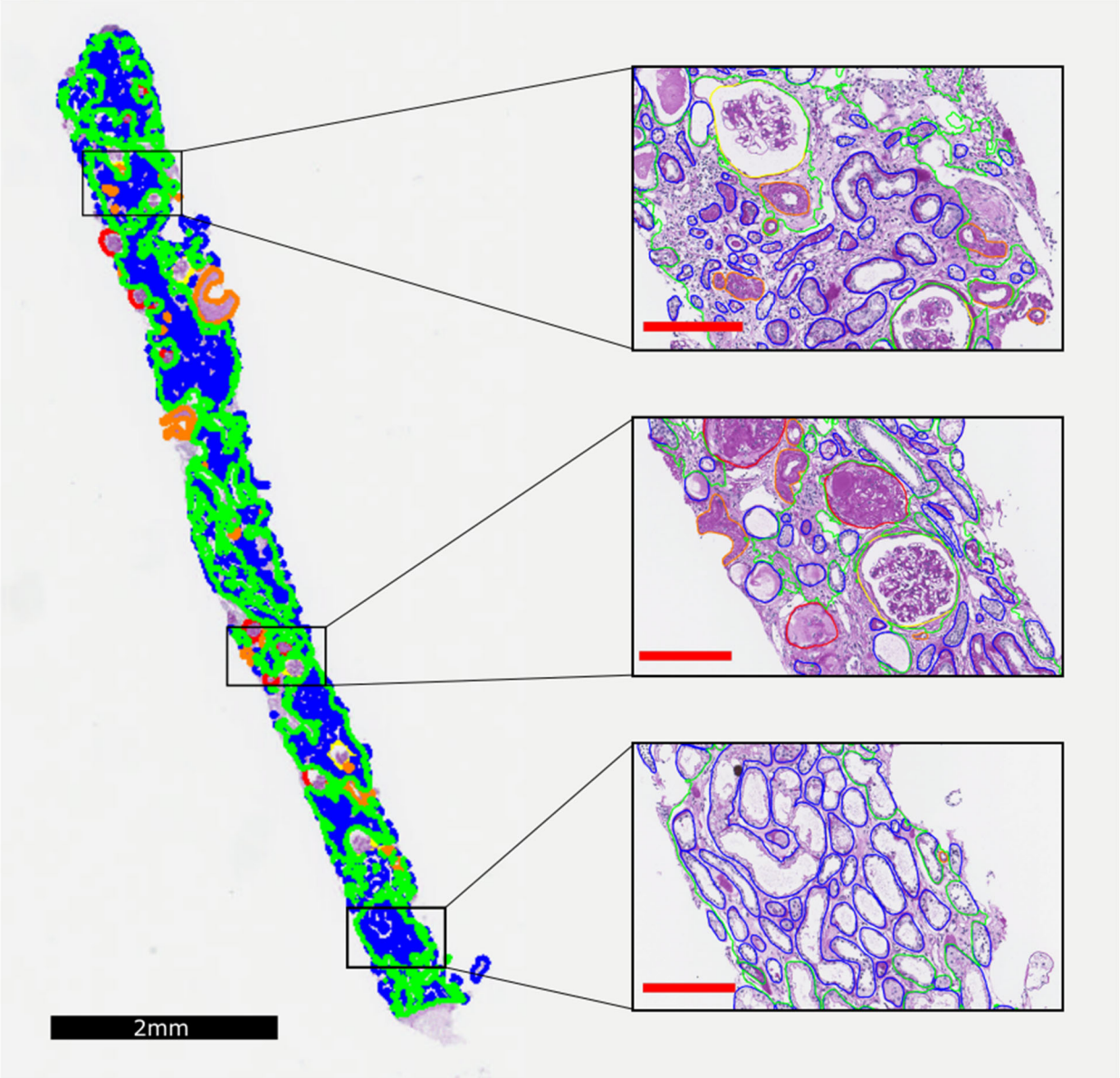

Figure 1. Whole Slide Image Segmentation of Renal Biopsy. Biopsy level predictions mapped back in WSI viewer Aperio ImageScope. Background (none), interstitium (green), glomeruli (yellow), globally sclerotic glomeruli (red), tubules (blue), arteries and arterioles (orange). Black scale bar: 2mm. Red scale bars: 200µm

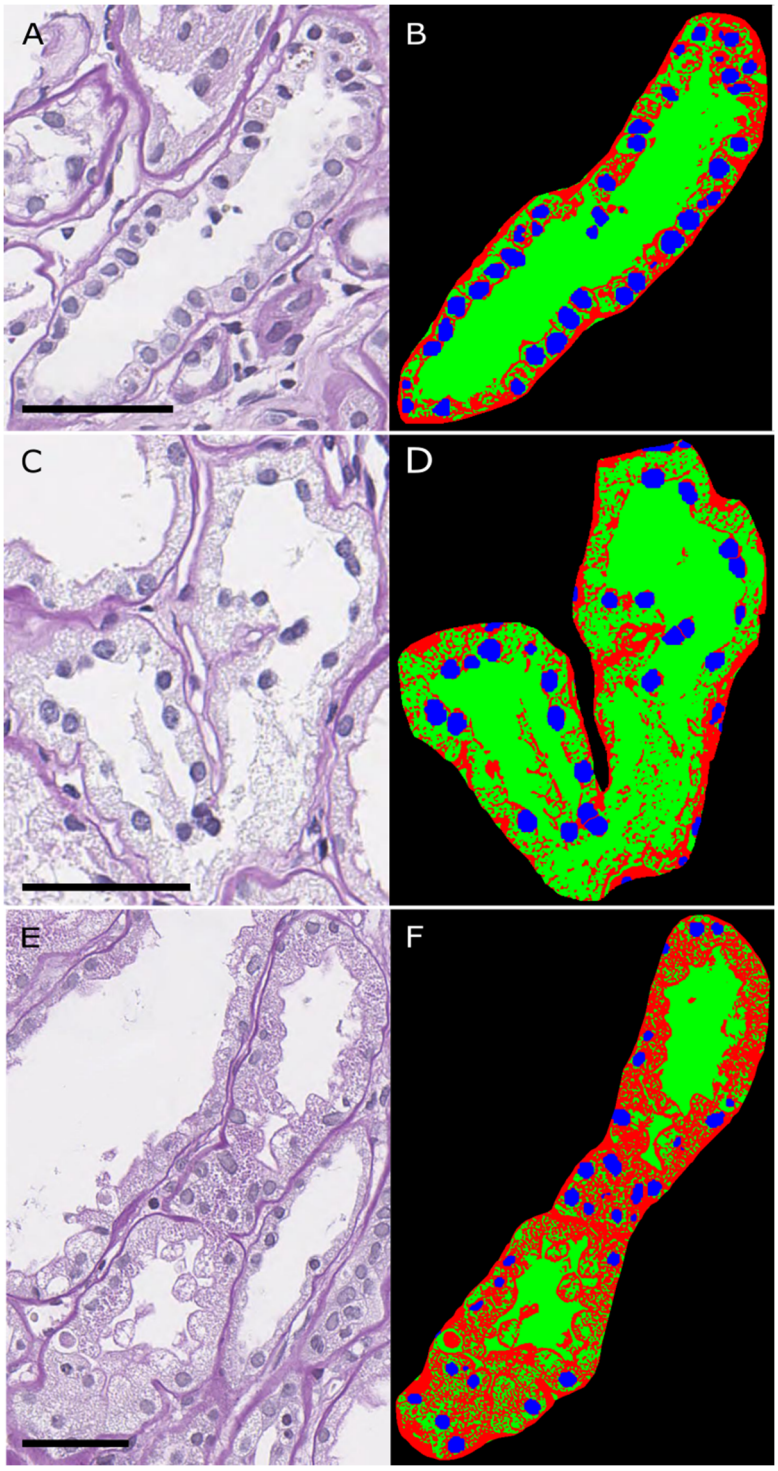

Figure 2. Component segmentation of Renal Tubules. Tubules segmented into nuclear component (blue), PAS+ component (red), and luminal/white space component (green). Scale Bars: 25µm

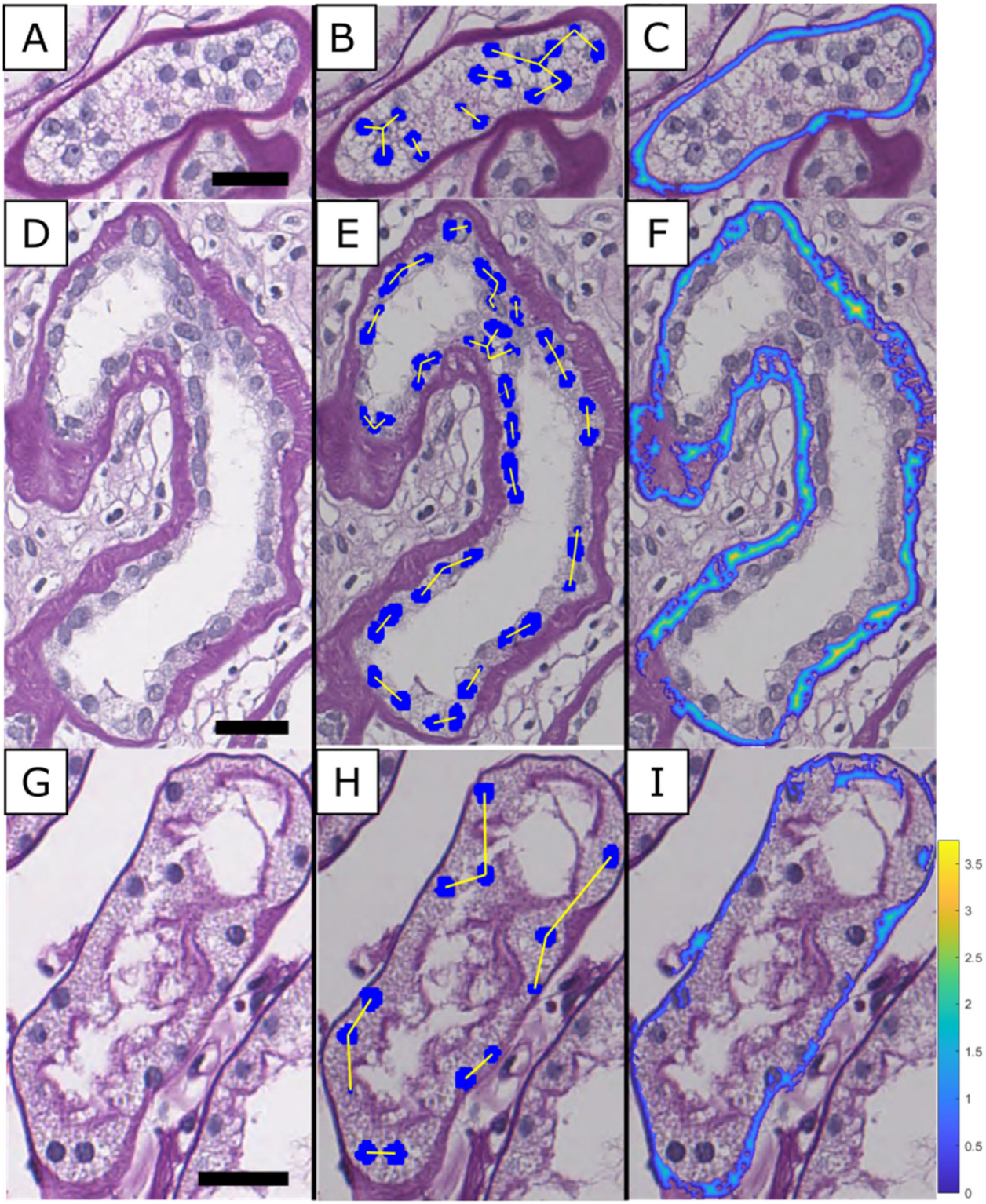

Figure 3. Feature Extraction from Renal Tubules. (A,D,G) Original images from WSI. (B,E,H) Representation of closest internuclear distance. (C,F,I) Representation of tubular basement membrane thickness. Scale Bars = 25µm

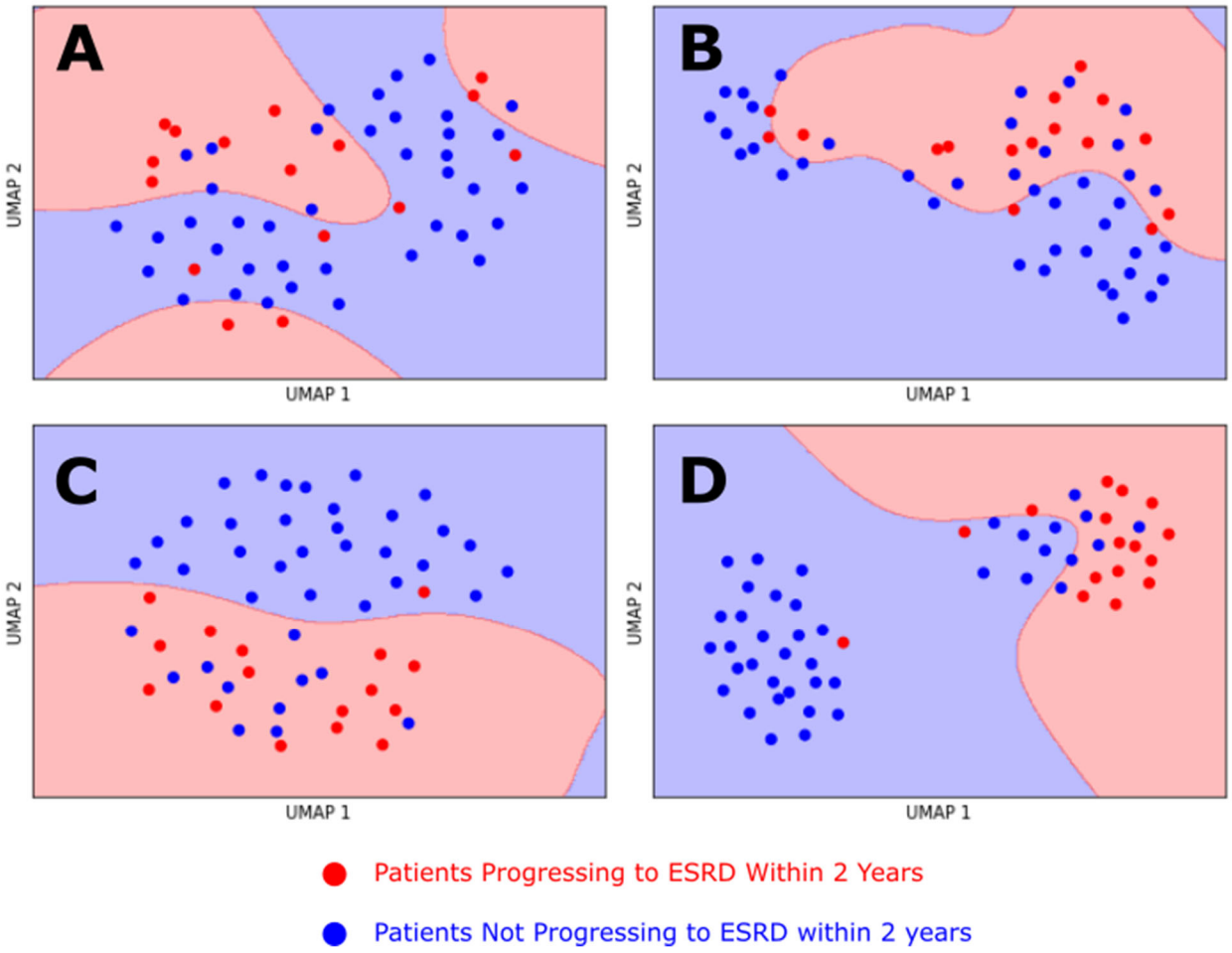

Figure 4. UMAP Dimensionality reduction for various feature types. (A) Aggregated glomerular features, (B) Aggregated tubular features, (C) Full urine proteomics set, (D) Significant 2yESRD protein biomarkers. Red dots represent patients progressing to ESRD within 2 years of biopsy/urine collection. Blue dots represent patients that did not. Red background represents SVM prediction of progressing to ESRD within 2 years. Blue background represents SVM prediction of not progressing to ESRD within 2 years.

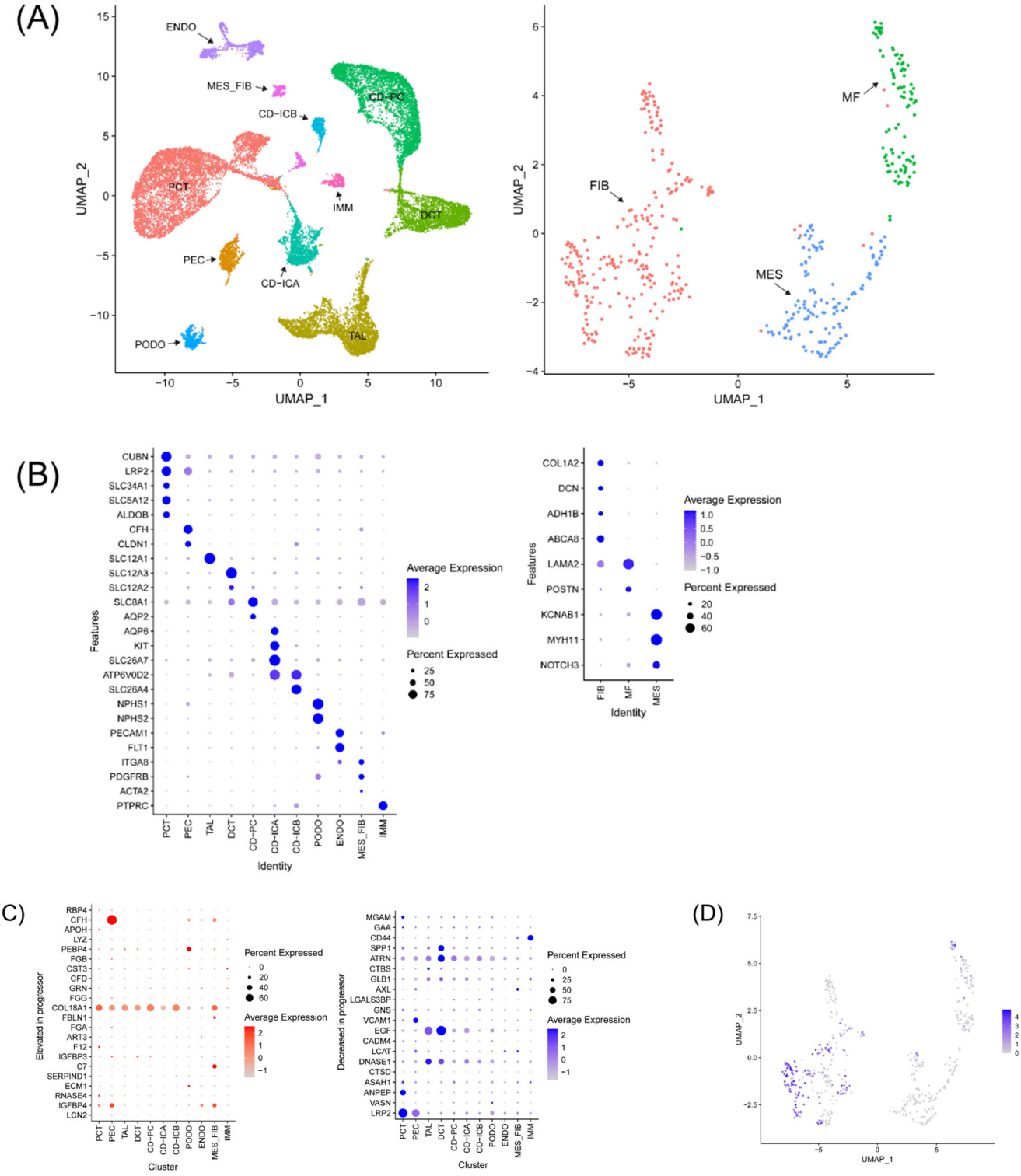
(A)
ENDO
MES_FIB
CD−ICB
CD−PC
PCT
IMM
DCT
PEC
CD−ICA
TAL
PODO
UMAP_2
UMAP_1
MF
FIB
MES
(B)
CUBN
LRP2
SLC34A1
SLC5A12
ALDOB
CFH
CLDN1
SLC12A1
SLC12A3
SLC12A2
SLC8A1
AQP2
AQP6
KIT
SLC26A7
ATP6V0D2
SLC26A4
NPHS1
NPHS2
PECAM1
FLT1
ITGA8
PDGFRB
ACTA2
PTPRC
Features
Identity
PCT
PEC
TAL
DCT
CD−PC
CD−ICA
CD−ICB
PODO
ENDO
MES_FIB
IMM
Average Expression
Percent Expressed
COL1A2
DCN
ADH1B
ABCA8
LAMA2
POSTN
KCNAB1
MYH11
NOTCH3
FIB
MF
MES
(C)
RBP4
CFH
APOH
LYZ
PEBP4
FGB
CST3
CFD
GRN
FGG
COL18A1
FBLN1
FGA
ART3
F12
IGFBP3
C7
SERPIND1
ECM1
RNASE4
IGFBP4
LCN2
Elevated in progressor
Cluster
MGAM
GAA
CD44
SPP1
ATRN
CTBS
GLB1
AXL
LGALS3BP
GNS
VCAM1
EGF
CADM4
LCAT
DNASE1
CTSD
ASAH1
ANPEP
VASN
LRP2
Decreased in progressor
(D)
UMAP_2
UMAP_1

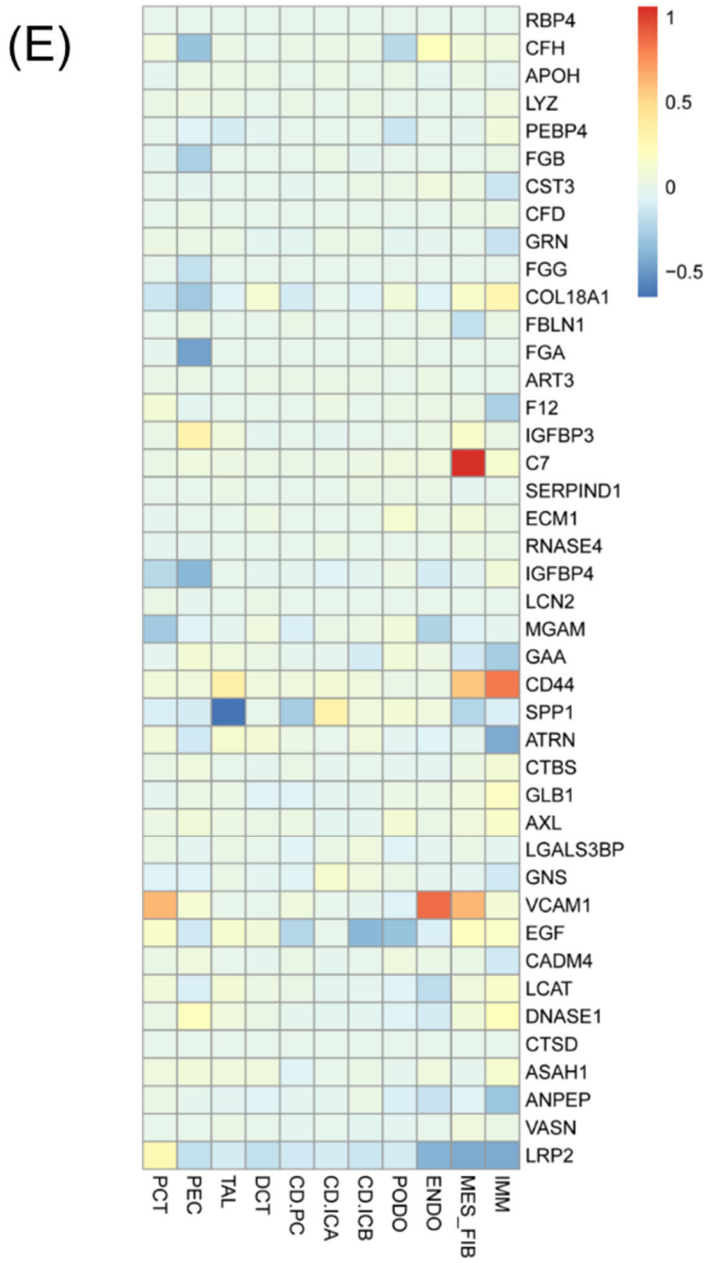

Figure 5. (A) UMAP plot of 23,987 cells pooled from a source with human kidneys (left) and a plot subclustered from a MES_FIB cluster (right). (B) Dot plots to identify clusters (left) and a MES_FIB cluster (right). (C) Dot plots for the gene expression of urine proteins related with progression of T2DN. Left, increased urine proteins in progressed patients. Right, decreased urine proteins in progressed patients. (D) Expression of the C7 gene in the UMAP plot. (E) Heatmap of logarithmic fold changes of genes in diabetic kidneys compared with non-diabetic kidneys.

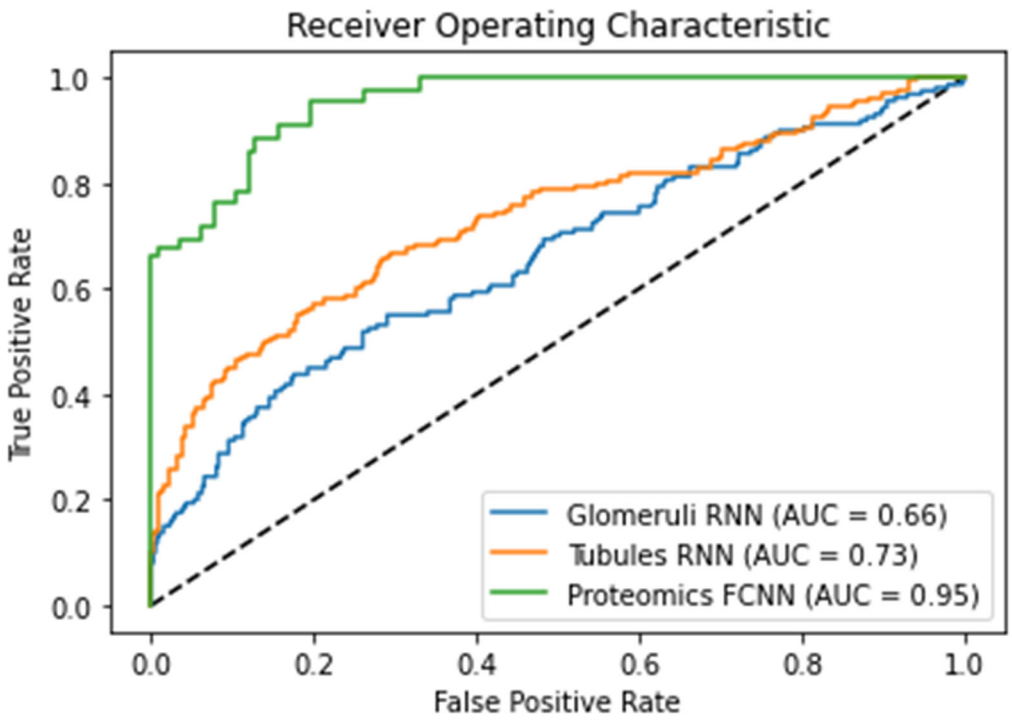

Figure 6. AI Network 2yESRD Prediction Performance. Results shown from FCNN using 2yESRD marker proteins (green), RNN using tubular digital image features (orange), and RNN using glomerular digital image features (blue). AI predictions compared to ground truth labels for *n* = 56. FCNN results shown for 100 trials of 10-fold cross validation. RNN results shown for 10 trials of 10-fold cross-validation.

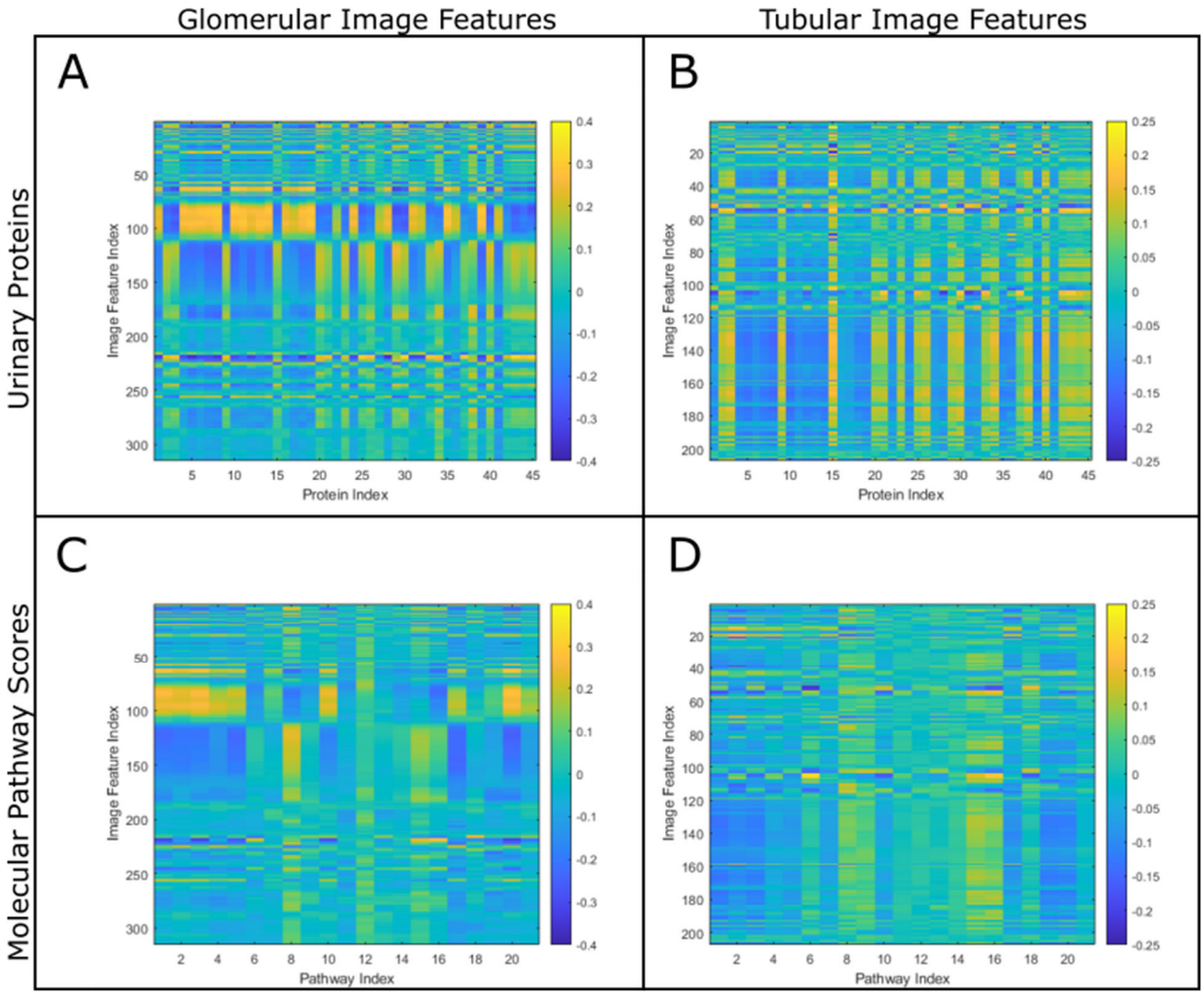

Figure 7. Spearman Rank Correlation Coefficients between Digital Image Features and Urinary Protein Measurements or Molecular Pathway Scores. Color at intersection represents single spearman coefficient between pairs.

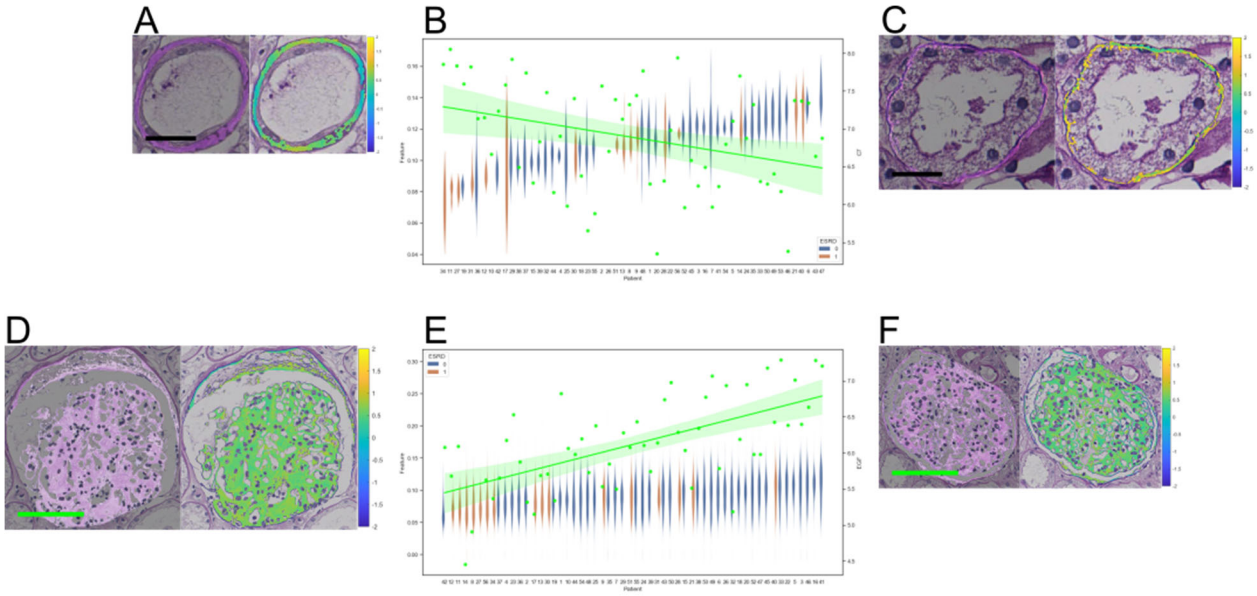

Figure 8. Pixel parsing discovery result for significant correlations between urinary proteomics and digital image features. (E) Violin plot of the standard deviation of Green pixel values in the Tubular basement membrane region, plotted for each patient in order of increasing mean feature value. Scatter plot of urinary proteomic measurements for Epidermal Growth Factor. (D) Image of candidate tubule with low feature value, and (F) image of candidate tubule with high feature value. First image highlights Tubular Basement Membrane (TBM) segmented area, while second image shows z-scores of green pixel values in the TBM. Black scale bars = 25µm

(B) Violin plot of the standard deviation of Green pixel values in the PAS+ regions of the glomerulus, plotted for each patient in order of increasing mean feature value. Scatter plot of urinary proteomic measurements for Complement C7. (A) Image of candidate glomerulus with low feature value, and (C) image of candidate glomerulus with high feature value. First image highlights PAS+ segmented area, while second image shows z scores of green pixel values in PAS+ areas. Green scale bars = 100µm

Gene	Protein Name
RBP4	Retinol-binding protein 4
CFH	Complement factor H
CFHR1	Complement factor H-related protein 1
CFHR2	Complement factor H-related protein 2
APOH	Beta-2-glycoprotein 1
LYZ	Lysozyme C
PEBP4	Phosphatidylethanolamine-binding protein 4
FGB	Fibrinogen beta chain
FGG	Fibrinogen gamma chain
FGA	Fibrinogen alpha chain
CST3	Cystatin-C
CFD	Complement factor D
GRN	Granulins
COL18A1	Collagen alpha-1(XVIII) chain
FBLN1	Fibulin-1
ART3	Ecto-ADP-ribosyltransferase 3
F12	Coagulation factor XII
IGFBP3	Insulin-like growth factor-binding protein 3
IGFBP4	Insulin-like growth factor-binding protein 4
C7	Complement component C7
SERPIND1	Heparin cofactor 2
GKN1	Gastrokine-1
ECM1	Extracellular matrix protein 1
RNASE4	Ribonuclease 4
LCN2	Neutrophil gelatinase-associated lipocalin

Table 1A. 2yESRD Upregulated Proteins

Gene	Protein Name
MGAM	Maltase-glucoamylase, intestinal
GAA	Lysosomal alpha-glucosidase
CD44	CD44 antigen
SPP1	Osteopontin
ATRN	Attractin
CTBS	Di-N-acetylchitobiase
GLB1	Beta-galactosidase
AXL	Tyrosine-protein kinase receptor UFO
LGALS3BP	Galectin-3-binding protein
GNS	N-acetylglucosamine-6-sulfatase
VCAM1	Vascular cell adhesion protein 1
EGF	Pro-epidermal growth factor
CADM4	Cell adhesion molecule 4
LCAT	Phosphatidylcholine-sterol acyltransferase
DNASE1	Deoxyribonuclease-1
CTSD	Cathepsin D
ASAH1	Acid ceramidase
ANPEP	Aminopeptidase N
VASN	Vasorin
LRP2	Low-density lipoprotein receptor-related protein 2

Table 1B. 2yESRD Downregulated Proteins

Supplementary Table 1A. Baseline Characteristics

	Total (n = 56)	Non-ESRD (n = 40)	ESRD (n = 16)	*P*
Age (years)	51.6 ± 10.9	51.1 ± 10.9	52.9 ± 11.2	0.575
Male (%)	75.0	75.0	75.0	1.000
Body mass index (kg/m²)	25.3 ± 3.5	25.4 ± 3.7	25.1 ± 3.3	0.712
Duration of diabetes mellitus (years)	10.0 (4.8–15.0)	9.5 (3.8–14.2)	11.5 (9.2–18.5)	0.063
Comorbidities (%)				
Hypertension	94.6	95	93.8	1.000
History of ischemic heart disease	7.1	7.5	6.2	1.000
History of cerebrovascular disease	3.6	2.5	6.2	0.494
Laboratory findings				
HbA1c (%)	7.2 (6.6–8.0)	7.2 (6.6–8.5)	6.6 (6.5–7.3)	0.059
Blood urea nitrogen (mg/dl)	24.5 (18.8–44.5)	20.5 (16.0–31.0)	52.5 (44.2–62.8)	<0.001
Creatinine (mg/dl)	1.54 (1.16–2.4)	1.38 (1.09–1.58)	4.47 (2.48–5.98)	<0.001
eGFR (ml/min/1.73 m²)	48.3 (23.7–69.9)	56.8 (46.5–76.7)	12.0 (9.3–24.5)	<0.001
uPCR (g/g)	5.5 (2.4–9.1)	3.8 (1.9–7.2)	9.0 (7.3–10.7)	0.003
Pathologic findings				
Glomerular classification (%)				0.385
I	5.4	7.5	0	
IIa	10.7	12.5	6.2	
IIb	28.6	32.5	18.8	
III	14.3	15	12.5	
IV	41.1	32.5	62.5	
IFTA score	2 (1–3)	2 (1–2)	3 (3–3)	<0.001
Interstitial inflammation score	1 (1–1)	1 (1–1)	1 (1–1)	0.805
Arteriolar hyalinosis score	2 (1–2)	2 (1–2)	2 (2–2)	0.016
Presence of large vessels (%)	91.1	87.5	100	0.307
Arteriosclerosis score	1 (1–2)	1 (1–2)	2 (1–2)	0.170

Abbreviation: ESRD, end-stage renal disease; HbA1c, hemoglobin A1c; eGFR, estimated glomerular filtration rate; uPCR, random urine protein-to-creatinine ratio; IFTA, interstitial fibrosis and tubular atrophy.

Supplementary Table 1B. Baseline characteristics of the patients in the validation cohort

	Total (n = 30)
Age (years)	60.0 ± 10.9
Male (%)	66.7
Body mass index (kg/m²)	24.4 ± 3.2
Duration of diabetes mellitus (years)	10.0 (3.0–19.0)
Comorbidities (%)	
Hypertension	96.7
History of ischemic heart disease	6.7
History of cerebrovascular disease	13.3
Laboratory findings	
HbA1c (%)	6.8 (6.2–8.4)
Blood urea nitrogen (mg/dl)	26.0 (22.0–35.0)
Creatinine (mg/dl)	1.56 (1.17–2.14)
eGFR (ml/min/1.73 m²)	37.3 (21.4–59.3)
uPCR (g/g)	3.1 (1.5–7.0)
Pathologic findings	
Glomerular classification (%)	
I	13.3
IIa	13.3
IIb	26.7
III	16.7
IV	30.0
IFTA score	2 (1–3)
Interstitial inflammation score	1 (1–1)
Arteriolar hyalinosis score	1 (0–2)
Presence of large vessels (%)	83.3
Arteriosclerosis score	1 (0–2)

Abbreviation: ESRD, end-stage renal disease; HbA1c, hemoglobin A1c; eGFR, estimated glomerular filtration rate; uPCR, random urine protein-to-creatinine ratio; IFTA, interstitial fibrosis and tubular atrophy.

Supplementary Document 1

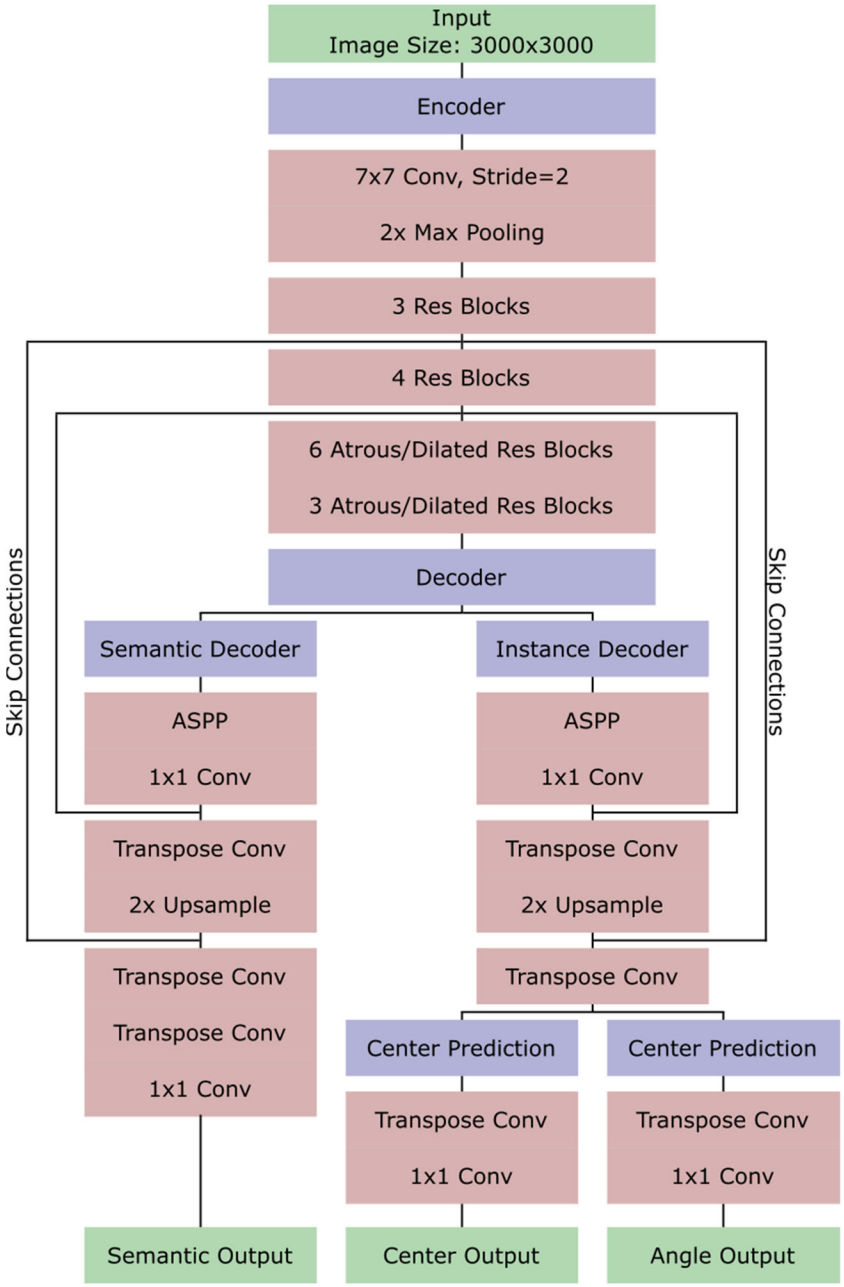

Supplementary Figure 1. Panoptic Segmentation Architecture.

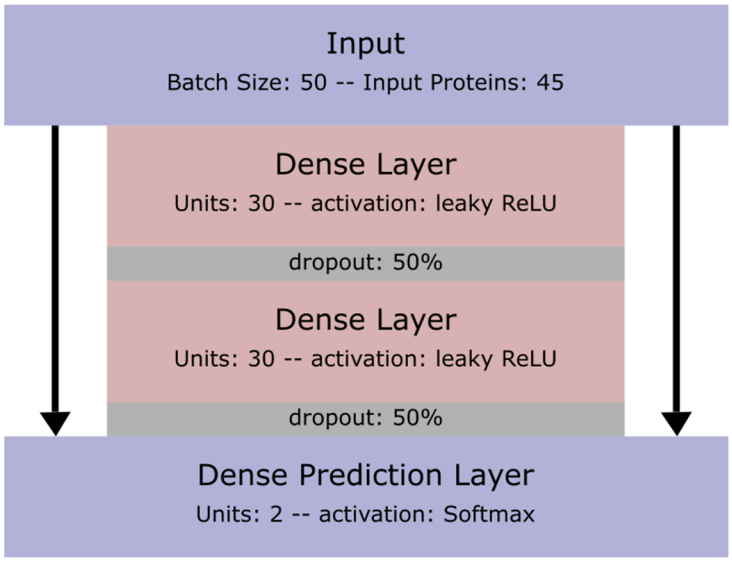

Supplementary Figure 2. Fully Connected Neural Network (FCNN) Architecture

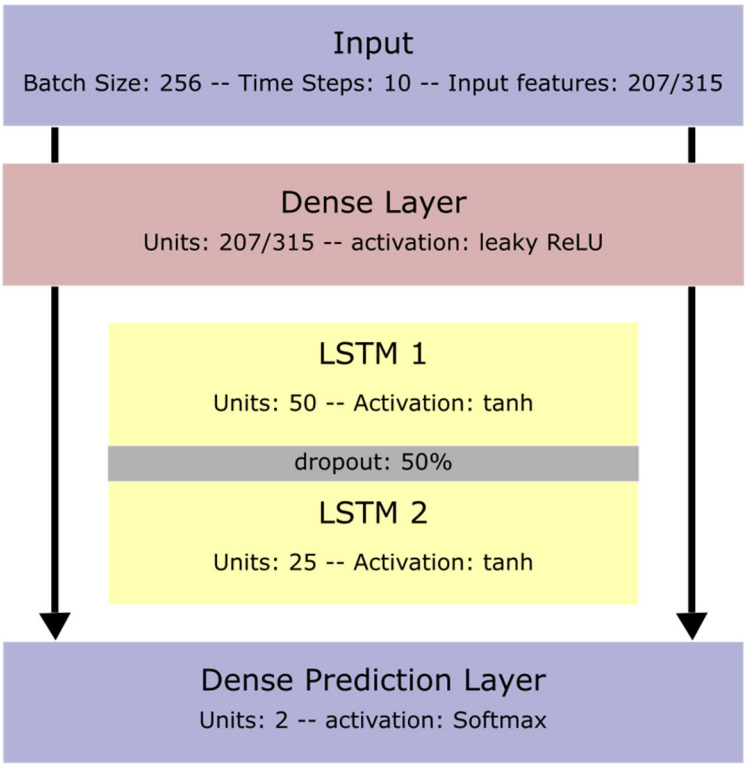

Supplementary Figure 3. Recurrent Neural Network (RNN) Architecture

Supplementary Document 2.

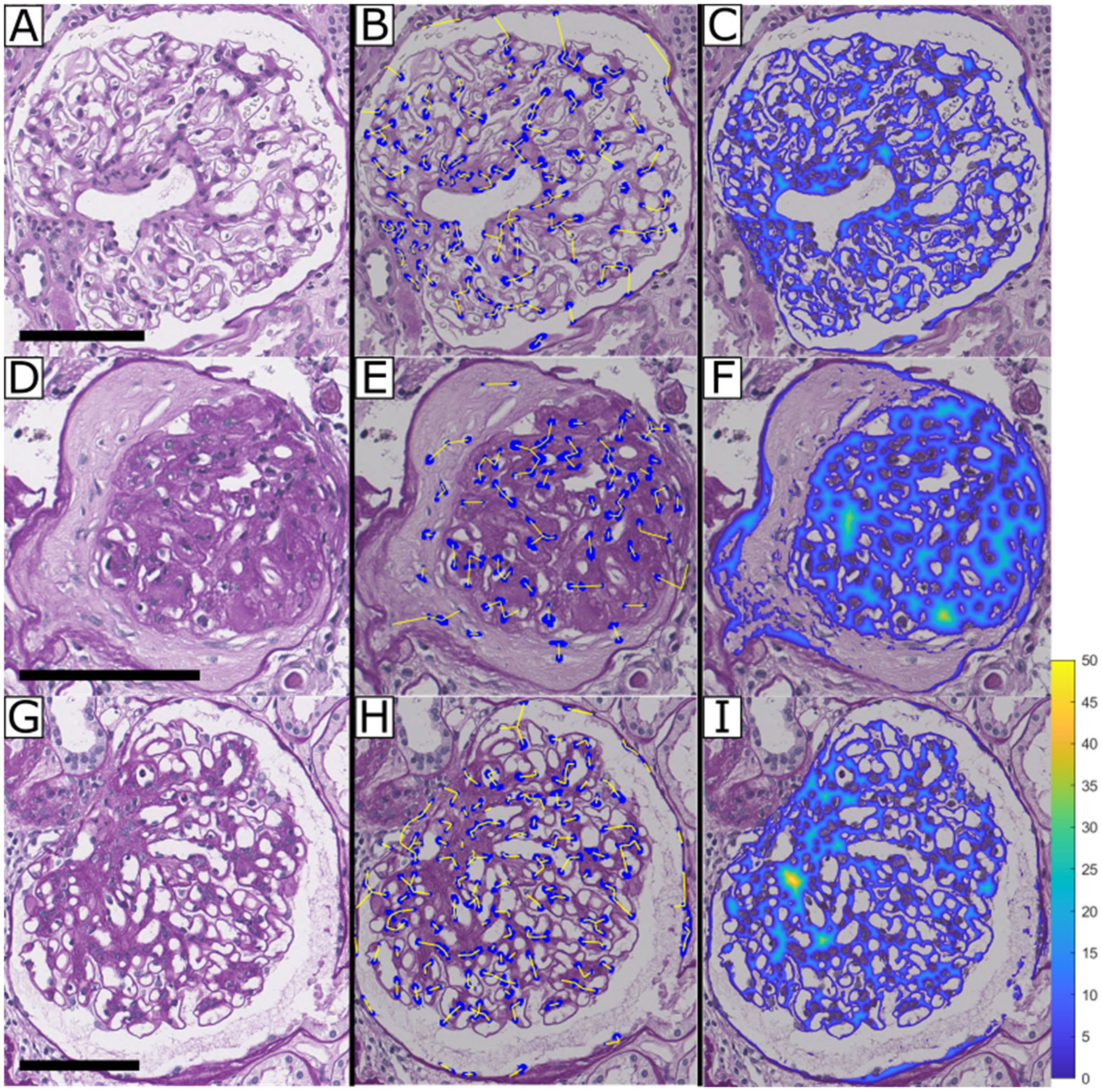

Supplementary Figure 4. Glomerular Feature Extraction.

Supplementary Table 2. Glomerular Image Features

Feature No.	Feature Description
1	Average luminal object solidity
2	Average PAS+ region contained in luminal object boundaries
3	Average nuclear region contained in luminal object boundaries
4	Sum total luminal objects' areas
5	Mean of luminal objects' areas
6	Median of luminal objects' areas
7	Luminal textural contrast
8	Luminal textural correlation
9	Luminal textural energy
10	Luminal textural homogeneity
11	Average PAS+ object solidity
12	Average lumina region contained in PAS+ object boundaries
13	Average nuclear region contained in PAS+ object boundaries
14	Sum total PAS+ objects' areas
15	Mean of PAS+ objects' areas
16	Median of PAS+ objects' areas
17	PAS+ textural contrast
18	PAS+ textural correlation
19	PAS+ textural energy
20	PAS+ textural homogeneity
21	Mean ratio of PAS+ pixels lying just outside nuclear perimeter to length of perimeter
22	Mean ratio of luminal pixels lying just outside nuclear perimeter to length of perimeter
23	Mean nuclear perimeter pixel count
24	Sum total nuclear area
25	Mean nuclear areas
26	Mode nuclear areas
27	Nuclear textural contrast
28	Nuclear textural correlation
29	Nuclear textural energy
30	Nuclear textural homogeneity
31	Mean distance of luminal object centroids from glomerular centroid
32	Mean of mean distances of luminal object centroids from glomerular boundary
33	Mean of maximum distances of luminal object centroids from glomerular boudnary
34	Mean of minimum distances of luminal object centroids from glomerular boudnary
35	Mean of mean distances of luminal object centroids from themselves
36	Mean of maximum distances of luminal object centroids from themselves
37	Mean of minimum distances of luminal object centroids from themselves
38	Mean distance of PAS+ object centroids from glomerular centroid
39	Mean of mean distances of PAS+ object centroids from glomerular boundary
40	Mean of maximum distances of PAS+ object centroids from glomerular boudnary

41	Mean of minimum distances of PAS+ object centroids from glomerular boudnary
42	Mean of mean distances of PAS+ object centroids from themselves
43	Mean of maximum distances of PAS+ object centroids from themselves
44	Mean of minimum distances of PAS+ object centroids from themselves
45	Mean distance of nuclear object centroids from glomerular centroid
46	Mean of mean distances of nuclear object centroids from glomerular boundary
47	Mean of maximum distances of nuclear object centroids from glomerular boudnary
48	Mean of minimum distances of nuclear object centroids from glomerular boudnary
49	Mean of mean distances of nuclear object centroids from themselves
50	Mean of maximum distances of nuclear object centroids from themselves
51	Mean of minimum distances of nuclear object centroids from themselves
52	Total glomerular area
53	Total PAS+ object number
54	Total luminal object number
55	Total nucleus number
56	Sum of PAS+ distance transform values 0<d<=10
57	Sum of PAS+ distance transform values 10<d<=20
58	Sum of PAS+ distance transform values 20<d<=1000
59	Maximum PAS+ distance transform value 10<d<=20
60	Number of connected objects with PAS+ distance transform value 0<d<=10
61	Number of connected objects with PAS+ distance transform value 10<d<=20
62	Mean of PAS+ distance transform values 0<d<=10
63	Mean of PAS+ distance transform values 10<d<=20
64	Median of PAS+ distance transform values 0<d<=10
65	Median of PAS+ distance transform values 10<d<=20
66	Mean area of objects with PAS+ distance transform value 0<d<=10
67	Median area of objects with PAS+ distance transform value 0<d<=10
68	Maximum area of objects with PAS+ distance transform value 0<d<=10
69	Mean area of objects with PAS+ distance transform value 10<d<=20
70	Median area of objects with PAS+ distance transform value 10<d<=20
71	Count of pixels with PAS+ distance transform value 1<d<=3
72	Count of pixels with PAS+ distance transform value 3<d<=5
73	Count of pixels with PAS+ distance transform value 5<d<=7
74	Count of pixels with PAS+ distance transform value 7<d<=9
75	Count of pixels with PAS+ distance transform value 9<d<=11
76	Count of pixels with PAS+ distance transform value 11<d<=13
77	Count of pixels with PAS+ distance transform value 13<d<=15
78	Count of pixels with PAS+ distance transform value 15<d<=17
79	Count of pixels with PAS+ distance transform value 17<d<=19
80	Count of pixels with PAS+ distance transform value 19<d<=21
81	Count of pixels with PAS+ distance transform value 21<d<=23
82	Count of pixels with PAS+ distance transform value 23<d<=25
83	Count of pixels with PAS+ distance transform value 25<d<=27

84	Count of pixels with PAS+ distance transform value 27<d<=29
85	Count of pixels with PAS+ distance transform value 29<d<=31
86	Count of pixels with PAS+ distance transform value 31<d<=33
87	Count of pixels with PAS+ distance transform value 33<d<=35
88	Count of pixels with PAS+ distance transform value 35<d<=37
89	Count of pixels with PAS+ distance transform value 37<d<=39
90	Count of pixels with PAS+ distance transform value 39<d<=41
91	Count of pixels with PAS+ distance transform value 41<d<=43
92	Count of pixels with PAS+ distance transform value 43<d<=45
93	Count of pixels with PAS+ distance transform value 45<d<=47
94	Count of pixels with PAS+ distance transform value 47<d<=49
95	Count of pixels with PAS+ distance transform value 49<d<=51
96	Count of pixels with PAS+ distance transform value 51<d<=53
97	Count of pixels with PAS+ distance transform value 53<d<=55
98	Count of pixels with PAS+ distance transform value 55<d<=57
99	Count of pixels with PAS+ distance transform value 57<d<=59
100	Count of pixels with PAS+ distance transform value 59<d<=61
101	Count of pixels with PAS+ distance transform value 61<d<=63
102	Count of pixels with PAS+ distance transform value 63<d<=65
103	Count of pixels with PAS+ distance transform value 65<d<=67
104	Count of pixels with PAS+ distance transform value 67<d<=69
105	Count of pixels with PAS+ distance transform value 69<d<=71
106	Count of pixels with PAS+ distance transform value 71<d<=73
107	Count of pixels with PAS+ distance transform value 73<d<=75
108	Count of pixels with PAS+ distance transform value 75<d<=77
109	Count of pixels with PAS+ distance transform value 77<d<=79
110	Count of pixels with PAS+ distance transform value 79<d<=2000
111	Count of pixels with luminal distance transform value 1<d<=2
112	Count of pixels with luminal distance transform value 2<d<=3
113	Count of pixels with luminal distance transform value 3<d<=4
114	Count of pixels with luminal distance transform value 4<d<=5
115	Count of pixels with luminal distance transform value 5<d<=6
116	Count of pixels with luminal distance transform value 6<d<=7
117	Count of pixels with luminal distance transform value 7<d<=8
118	Count of pixels with luminal distance transform value 8<d<=9
119	Count of pixels with luminal distance transform value 9<d<=10
120	Count of pixels with luminal distance transform value 10<d<=11
121	Count of pixels with luminal distance transform value 11<d<=12
122	Count of pixels with luminal distance transform value 12<d<=13
123	Count of pixels with luminal distance transform value 13<d<=14
124	Count of pixels with luminal distance transform value 14<d<=15
125	Count of pixels with luminal distance transform value 15<d<=16
126	Count of pixels with luminal distance transform value 16<d<=17

127	Count of pixels with luminal distance transform value 17<d<=18
128	Count of pixels with luminal distance transform value 18<d<=19
129	Count of pixels with luminal distance transform value 19<d<=20
130	Count of pixels with luminal distance transform value 20<d<=21
131	Count of pixels with luminal distance transform value 21<d<=22
132	Count of pixels with luminal distance transform value 22<d<=23
133	Count of pixels with luminal distance transform value 23<d<=24
134	Count of pixels with luminal distance transform value 24<d<=25
135	Count of pixels with luminal distance transform value 25<d<=26
136	Count of pixels with luminal distance transform value 26<d<=27
137	Count of pixels with luminal distance transform value 27<d<=28
138	Count of pixels with luminal distance transform value 28<d<=29
139	Count of pixels with luminal distance transform value 29<d<=30
140	Count of pixels with luminal distance transform value 30<d<=31
141	Count of pixels with luminal distance transform value 31<d<=32
142	Count of pixels with luminal distance transform value 32<d<=33
143	Count of pixels with luminal distance transform value 33<d<=34
144	Count of pixels with luminal distance transform value 34<d<=35
145	Count of pixels with luminal distance transform value 35<d<=36
146	Count of pixels with luminal distance transform value 36<d<=37
147	Count of pixels with luminal distance transform value 37<d<=38
148	Count of pixels with luminal distance transform value 38<d<=39
149	Count of pixels with luminal distance transform value 39<d<=40
150	Count of pixels with luminal distance transform value 40<d<=41
151	Count of pixels with luminal distance transform value 41<d<=42
152	Count of pixels with luminal distance transform value 42<d<=43
153	Count of pixels with luminal distance transform value 43<d<=44
154	Count of pixels with luminal distance transform value 44<d<=45
155	Count of pixels with luminal distance transform value 45<d<=46
156	Count of pixels with luminal distance transform value 46<d<=47
157	Count of pixels with luminal distance transform value 47<d<=48
158	Count of pixels with luminal distance transform value 48<d<=49
159	Count of pixels with luminal distance transform value 49<d<=50
160	Count of pixels with luminal distance transform value 50<d<=51
161	Count of pixels with luminal distance transform value 51<d<=52
162	Count of pixels with luminal distance transform value 52<d<=53
163	Count of pixels with luminal distance transform value 53<d<=54
164	Count of pixels with luminal distance transform value 54<d<=55
165	Count of pixels with luminal distance transform value 55<d<=56
166	Count of pixels with luminal distance transform value 56<d<=57
167	Count of pixels with luminal distance transform value 57<d<=58
168	Count of pixels with luminal distance transform value 58<d<=59
169	Count of pixels with luminal distance transform value 59<d<=60

170	Count of pixels with luminal distance transform value 60<d<=2000
171	Count of pixels with nuclear distance transform value 1<d<=2
172	Count of pixels with nuclear distance transform value 2<d<=3
173	Count of pixels with nuclear distance transform value 3<d<=4
174	Count of pixels with nuclear distance transform value 4<d<=5
175	Count of pixels with nuclear distance transform value 5<d<=6
176	Count of pixels with nuclear distance transform value 6<d<=7
177	Count of pixels with nuclear distance transform value 7<d<=8
178	Count of pixels with nuclear distance transform value 8<d<=9
179	Count of pixels with nuclear distance transform value 9<d<=10
180	Count of pixels with nuclear distance transform value 10<d<=11
181	Count of pixels with nuclear distance transform value 11<d<=12
182	Count of pixels with nuclear distance transform value 12<d<=13
183	Count of pixels with nuclear distance transform value 13<d<=14
184	Count of pixels with nuclear distance transform value 14<d<=15
185	Count of pixels with nuclear distance transform value 15<d<=16
186	Count of pixels with nuclear distance transform value 16<d<=17
187	Count of pixels with nuclear distance transform value 17<d<=18
188	Count of pixels with nuclear distance transform value 18<d<=19
189	Count of pixels with nuclear distance transform value 19<d<=20
190	Count of pixels with nuclear distance transform value 20<d<=2000
191	Count of pixels with glomerular distance transform value 2<d<=27
192	Count of pixels with glomerular distance transform value 27<d<=52
193	Count of pixels with glomerular distance transform value 52<d<=77
194	Count of pixels with glomerular distance transform value 77<d<=102
195	Count of pixels with glomerular distance transform value 102<d<=127
196	Count of pixels with glomerular distance transform value 127<d<=152
197	Count of pixels with glomerular distance transform value 152<d<=177
198	Count of pixels with glomerular distance transform value 177<d<=202
199	Count of pixels with glomerular distance transform value 202<d<=227
200	Count of pixels with glomerular distance transform value 227<d<=252
201	Count of pixels with glomerular distance transform value 252<d<=277
202	Count of pixels with glomerular distance transform value 277<d<=302
203	Count of pixels with glomerular distance transform value 302<d<=327
204	Count of pixels with glomerular distance transform value 327<d<=352
205	Count of pixels with glomerular distance transform value 352<d<=377
206	Count of pixels with glomerular distance transform value 377<d<=402
207	Count of pixels with glomerular distance transform value 402<d<=427
208	Count of pixels with glomerular distance transform value 427<d<=452
209	Count of pixels with glomerular distance transform value 452<d<=477
210	Count of pixels with glomerular distance transform value 477<d<=502
211	Count of pixels with glomerular distance transform value 502<d<=527
212	Count of pixels with glomerular distance transform value 527<d<=552

213 Count of pixels with glomerular distance transform value 552<d<=577
214 Count of pixels with glomerular distance transform value 577<d<=20000
215 Mean of red values in PAS+ regions
216 Mean of green values in PAS+ regions
217 Mean of blue values in PAS+ regions
218 Std of red values in PAS+ regions
219 Std of green values in PAS+ regions
220 Std of blue values in PAS+ regions
221 Mean of red values in luminal regions
222 Mean of green values in luminal regions
223 Mean of blue values in luminal regions
224 Std of red values in luminal regions
225 Std of green values in luminal regions
226 Std of blue values in luminal regions
227 Mean of red values in nuclear regions
228 Mean of green values in nuclear regions
229 Mean of blue values in nuclear regions
230 Std of red values in nuclear regions
231 Std of green values in nuclear regions
232 Std of blue values in nuclear regions
233 Number nuclear pixels contained radius 0<r<100
234 Number nuclear pixels contained radius 100<r<200
235 Number nuclear pixels contained radius 200<r<300
236 Number nuclear pixels contained radius 300<r<400
237 Number nuclear pixels contained radius 400<r<500
238 Number nuclear pixels contained radius 500<r<600
239 Number nuclear pixels contained radius 600<r<700
240 Number nuclear pixels contained radius 700<r<800
241 Number nuclear pixels contained radius 800<r<900
242 Number nuclear pixels contained radius 900<r<1000
243 Number nuclear pixels contained radius 1000<r<1300
244 Number luminal pixels contained radius 0<r<100
245 Number luminal pixels contained radius 100<r<200
246 Number luminal pixels contained radius 200<r<300
247 Number luminal pixels contained radius 300<r<400
248 Number luminal pixels contained radius 400<r<500
249 Number luminal pixels contained radius 500<r<600
250 Number luminal pixels contained radius 600<r<700
251 Number luminal pixels contained radius 700<r<800
252 Number luminal pixels contained radius 800<r<900
253 Number luminal pixels contained radius 900<r<1000
254 Number luminal pixels contained radius 1000<r<1300
255 Number PAS+ pixels contained radius 0<r<100

256 Number PAS+ pixels contained radius 100<r<200
257 Number PAS+ pixels contained radius 200<r<300
258 Number PAS+ pixels contained radius 300<r<400
259 Number PAS+ pixels contained radius 400<r<500
260 Number PAS+ pixels contained radius 500<r<600
261 Number PAS+ pixels contained radius 600<r<700
262 Number PAS+ pixels contained radius 700<r<800
263 Number PAS+ pixels contained radius 800<r<900
264 Number PAS+ pixels contained radius 900<r<1000
265 Number PAS+ pixels contained radius 1000<r<1300
266 Number nuclear pixels contained between theta -180<Θ<-162
267 Number nuclear pixels contained between theta -162<Θ<-144
268 Number nuclear pixels contained between theta -144<Θ<-126
269 Number nuclear pixels contained between theta -126<Θ<-108
270 Number nuclear pixels contained between theta -108<Θ<-90
271 Number nuclear pixels contained between theta -90<Θ<-72
272 Number nuclear pixels contained between theta -72<Θ<-54
273 Number nuclear pixels contained between theta -54<Θ<-36
274 Number nuclear pixels contained between theta -36<Θ<-18
275 Number nuclear pixels contained between theta -18<Θ<0
276 Number nuclear pixels contained between theta 0<Θ<18
277 Number nuclear pixels contained between theta 18<Θ<36
278 Number nuclear pixels contained between theta 36<Θ<54
279 Number nuclear pixels contained between theta 54<Θ<72
280 Number nuclear pixels contained between theta 72<Θ<90
281 Number nuclear pixels contained between theta 90<Θ<108
282 Number nuclear pixels contained between theta 108<Θ<126
283 Number nuclear pixels contained between theta 126<Θ<144
284 Number nuclear pixels contained between theta 144<Θ<162
285 Number nuclear pixels contained between theta 162<Θ<180
286 0.1 quantile of nuclear pixels from the boundary line
287 0.2 quantile of nuclear pixels from the boundary line
288 0.3 quantile of nuclear pixels from the boundary line
289 0.4 quantile of nuclear pixels from the boundary line
290 0.5 quantile of nuclear pixels from the boundary line
291 0.6 quantile of nuclear pixels from the boundary line
292 0.7 quantile of nuclear pixels from the boundary line
293 0.8 quantile of nuclear pixels from the boundary line
294 0.9 quantile of nuclear pixels from the boundary line
295 1 quantile of nuclear pixels from the boundary line
296 0.1 quantile of luminal pixels from the boundary line
297 0.2 quantile of luminal pixels from the boundary line
298 0.3 quantile of luminal pixels from the boundary line

299	0.4 quantile of luminal pixels from the boundary line
300	0.5 quantile of luminal pixels from the boundary line
301	0.6 quantile of luminal pixels from the boundary line
302	0.7 quantile of luminal pixels from the boundary line
303	0.8 quantile of luminal pixels from the boundary line
304	0.9 quantile of luminal pixels from the boundary line
305	1 quantile of luminal pixels from the boundary line
306	0.1 quantile of mesangial pixels from the boundary line
307	0.2 quantile of mesangial pixels from the boundary line
308	0.3 quantile of mesangial pixels from the boundary line
309	0.4 quantile of mesangial pixels from the boundary line
310	0.5 quantile of mesangial pixels from the boundary line
311	0.6 quantile of mesangial pixels from the boundary line
312	0.7 quantile of mesangial pixels from the boundary line
313	0.8 quantile of mesangial pixels from the boundary line
314	0.9 quantile of mesangial pixels from the boundary line
315	1 quantile of mesangial pixels from the boundary line

Supplementary Table 3. Tubular Image Features

Feature No.	Feature Description
1	Average luminal object solidity
2	Average PAS+ region contained in luminal object boundaries
3	Average nuclear region contained in luminal object boundaries
4	Sum total luminal objects' areas
5	Mean of luminal objects' areas
6	Median of luminal objects' areas
7	Luminal textural contrast
8	Luminal textural correlation
9	Luminal textural energy
10	Luminal textural homogeneity
11	Average PAS+ object solidity
12	Average lumina region contained in PAS+ object boundaries
13	Average nuclear region contained in PAS+ object boundaries
14	Sum total PAS+ objects' areas
15	Mean of PAS+ objects' areas
16	Median of PAS+ objects' areas
17	PAS+ textural contrast
18	PAS+ textural correlation
19	PAS+ textural energy
20	PAS+ textural homogeneity
21	Mean ratio of PAS+ pixels lying just outside nuclear perimeter to length of perimeter
22	Mean ratio of luminal pixels lying just outside nuclear perimeter to length of perimeter
23	Mean nuclear perimeter pixel count
24	Sum total nuclear area
25	Mean nuclear areas
26	Mode nuclear areas
27	Nuclear textural contrast
28	Nuclear textural correlation
29	Nuclear textural energy
30	Nuclear textural homogeneity
31	Mean distance of nuclear object centroids from tubular centroid
32	Mean of mean distances of nuclear object centroids from tubular boundary
33	Mean of maximum distances of nuclear object centroids from tubular boundary
34	Mean of minimum distances of nuclear object centroids from tubular boundary
35	Mean of mean distances of nuclear object centroids from themselves
36	Mean of maximum distances of nuclear object centroids from themselves
37	Mean of minimum distances of nuclear object centroids from themselves
38	Total tubular area
39	Total PAS+ object number
40	Total luminal object number

41	Total nucleus number
42	Average TBM thickness per perimeter length
43	Maximum TBM thickness per perimeter length
44	Minimum TBM thickness per perimeter length
45	Average value of TBM distance transform
46	Maximum value of TBM distance transform
47	TBM textural energy
48	TBM textural correlation
49	TBM textural contrast
50	TBM textural homogeneity
51	Mean of red values in TBM regions
52	Mean of green values in TBM regions
53	Mean of blue values in TBM regions
54	Standard deviation of red values in TBM regions
55	Standard deviation of green values in TBM regions
56	Standard deviation of blue values in TBM regions
57	Sum total TBM area
58	Average solidity of TBM
59	Mean distance of TBM object centroids from tubular centroid
60	Mean of mean distances of TBM object centroids from tubular boundary
61	Mean of maximum distances of TBM object centroids from tubular boundary
62	Mean of minimum distances of TBM object centroids from tubular boundary
63	Mean of mean distances of TBM object centroids from themselves
64	Mean of maximum distances of TBM object centroids from themselves
65	Mean of minimum distances of TBM object centroids from themselves
66	Average ITO thickness per perimeter length
67	Maximum ITO thickness per perimeter length
68	Minimum ITO thickness per perimeter length
69	Average value of ITO distance transform
70	Maximum value of ITO distance transform
71	ITO textural energy
72	ITO textural correlation
73	ITO textural contrast
74	ITO textural homogeneity
75	Mean of red values in ITO regions
76	Mean of green values in ITO regions
77	Mean of blue values in ITO regions
78	Standard deviation of red values in ITO regions
79	Standard deviation of green values in ITO regions
80	Standard deviation of blue values in ITO regions
81	Standard deviation of blue values in ITO regions
82	Sum total ITO area
83	Average solidity of ITO

84	Mean distance of ITO object centroids from tubular centroid
85	Mean of mean distances of ITO object centroids from tubular boundary
86	Mean of maximum distances of ITO object centroids from tubular boundary
87	Mean of minimum distances of ITO object centroids from tubular boundary
88	Mean of mean distances of ITO object centroids from themselves
89	Mean of maximum distances of ITO object centroids from themselves
90	Mean of minimum distances of ITO object centroids from themselves
91	Tubular compactness
92	Tubular eccentricity
93	Equivalent diameter of a circle with measured tubular area
94	Tubule major axis length
95	Tubule minor axis length
96	Tubular perimeter
97	Tubular fiber length
98	Tubular fiber width
99	Tubular curl
100	Tubular solidity
101	Mean of red values in PAS+ regions
102	Mean of green values in PAS+ regions
103	Mean of blue values in PAS+ regions
104	Std of red values in PAS+ regions
105	Std of green values in PAS+ regions
106	Std of blue values in PAS+ regions
107	Mean of red values in luminal regions
108	Mean of green values in luminal regions
109	Mean of blue values in luminal regions
110	Std of red values in luminal regions
111	Std of green values in luminal regions
112	Std of blue values in luminal regions
113	Mean of red values in nuclear regions
114	Mean of green values in nuclear regions
115	Mean of blue values in nuclear regions
116	Std of red values in nuclear regions
117	Std of green values in nuclear regions
118	Std of blue values in nuclear regions
119	Minimum of luminal pixels weighted inversely by distance from tubular boundary
120	Maximum of luminal pixels weighted inversely by distance from tubular boundary
121	Mean of luminal pixels weighted inversely by distance from tubular boundary
122	Median of luminal pixels weighted inversely by distance from tubular boundary
123	Standard deviation of luminal pixels weighted inversely by distance from tubular boundary
124	Minimum of PAS+ pixels weighted inversely by distance from tubular boundary
125	Maximum of PAS+ pixels weighted inversely by distance from tubular boundary
126	Mean of PAS+ pixels weighted inversely by distance from tubular boundary

127	Median of PAS+ pixels weighted inversely by distance from tubular boundary
128	Standard deviation of PAS+ pixels weighted inversely by distance from tubular boundary
129	0.1 quantile of nuclear pixels from the boundary line
130	0.2 quantile of nuclear pixels from the boundary line
131	0.3 quantile of nuclear pixels from the boundary line
132	0.4 quantile of nuclear pixels from the boundary line
133	0.5 quantile of nuclear pixels from the boundary line
134	0.6 quantile of nuclear pixels from the boundary line
135	0.7 quantile of nuclear pixels from the boundary line
136	0.8 quantile of nuclear pixels from the boundary line
137	0.9 quantile of nuclear pixels from the boundary line
138	1 quantile of nuclear pixels from the boundary line
139	0.1 quantile of luminal pixels from the boundary line
140	0.2 quantile of luminal pixels from the boundary line
141	0.3 quantile of luminal pixels from the boundary line
142	0.4 quantile of luminal pixels from the boundary line
143	0.5 quantile of luminal pixels from the boundary line
144	0.6 quantile of luminal pixels from the boundary line
145	0.7 quantile of luminal pixels from the boundary line
146	0.8 quantile of luminal pixels from the boundary line
147	0.9 quantile of luminal pixels from the boundary line
148	1 quantile of luminal pixels from the boundary line
149	0.1 quantile of mesangial pixels from the boundary line
150	0.2 quantile of mesangial pixels from the boundary line
151	0.3 quantile of mesangial pixels from the boundary line
152	0.4 quantile of mesangial pixels from the boundary line
153	0.5 quantile of mesangial pixels from the boundary line
154	0.6 quantile of mesangial pixels from the boundary line
155	0.7 quantile of mesangial pixels from the boundary line
156	0.8 quantile of mesangial pixels from the boundary line
157	0.9 quantile of mesangial pixels from the boundary line
158	1 quantile of mesangial pixels from the boundary line
159	Maximum value of PAS+ distance transform
160	Maximum value of luminal distance transform
161	Maximum value of nuclear distance transform
162	Maximum value of tubular distance transform
163	Maximum of mean pixel distance from boundary per nucleus
164	Maximum of minimum pixel distance from boundary per nucleus
165	Maximum of maximum pixel distance from boundary per nucleus
166	Mean of mean pixel distance from boundary per nucleus
167	Mean of minimum pixel distance from boundary per nucleus
168	Mean of maximum pixel distance from boundary per nucleus
169	Minimum of mean pixel distance from boundary per nucleus

170	Minimum of minimum pixel distance from boundary per nucleus
171	Minimum of maximum pixel distance from boundary per nucleus
172	Variance of mean pixel distance from boundary per nucleus
173	Variance of minimum pixel distance from boundary per nucleus
174	Variance of maximum pixel distance from boundary per nucleus
175	Median of mean pixel distance from boundary per nucleus
176	Median of minimum pixel distance from boundary per nucleus
177	Median of maximum pixel distance from boundary per nucleus
178	Maximum of mean pixel distance from boundary per TBM object
179	Maximum of minimum pixel distance from boundary per TBM object
180	Maximum of maximum pixel distance from boundary per TBM object
181	Mean of mean pixel distance from boundary per TBM object
182	Mean of minimum pixel distance from boundary per TBM object
183	Mean of maximum pixel distance from boundary per TBM object
184	Minimum of mean pixel distance from boundary per TBM object
185	Minimum of minimum pixel distance from boundary per TBM object
186	Minimum of maximum pixel distance from boundary per TBM object
187	Variance of mean pixel distance from boundary per TBM object
188	Variance of minimum pixel distance from boundary per TBM object
189	Variance of maximum pixel distance from boundary per TBM object
190	Median of mean pixel distance from boundary per TBM object
191	Median of minimum pixel distance from boundary per TBM object
192	Median of maximum pixel distance from boundary per TBM object
193	Maximum of mean pixel distance from boundary per ITO
194	Maximum of minimum pixel distance from boundary per ITO
195	Maximum of maximum pixel distance from boundary per ITO
196	Mean of mean pixel distance from boundary per ITO
197	Mean of minimum pixel distance from boundary per ITO
198	Mean of maximum pixel distance from boundary per ITO
199	Minimum of mean pixel distance from boundary per ITO
200	Minimum of minimum pixel distance from boundary per ITO
201	Minimum of maximum pixel distance from boundary per ITO
202	Variance of mean pixel distance from boundary per ITO
203	Variance of minimum pixel distance from boundary per ITO
204	Variance of maximum pixel distance from boundary per ITO
205	Median of mean pixel distance from boundary per ITO
206	Median of minimum pixel distance from boundary per ITO
207	Median of maximum pixel distance from boundary per ITO

Supplementary Table 4. All Urinary Proteins Measured

Protein No.	Protein names	Gene names
1		
2		
3	Nuclear speckle splicing regulatory protein 1	CCDC55
4	Serpin B6	SERPINB6
5	EH domain-containing protein 1	EHD1
6	Sushi, von Willebrand factor type A, EGF and pentraxin domain-containing protein 1	SVEP1
7	Ig kappa chain V-III region VH	IGKV3-7
8		IGLV4-69
9		IGLV8-61
10		IGLV4-60
11		IGLV6-57
12	Ig lambda chain V-I region NIG-64	IGLV1-51
13		IGLV1-47
14		IGLV7-46
15		IGLV1-40
16		IGLV5-37
17		IGLV3-27
18		IGLV3-25
19		IGLV3-21
20		IGLV3-19
21		IGLV2-18
22		IGLV2-14
23		IGLV2-11
24		IGLV3-10
25		IGLV3-9
26	Ig lambda-2 chain C regions	IGLC2
27	Ig lambda-7 chain C region	IGLC7
28		IGHA2
29		IGHV3-64
30		IGHV4-4
31		IGKV2D-24
32	Ig kappa chain V-II region RPMI 6410	IGKV2-30
33		IGKV2D-30
34		IGKV1D-37
35		PECAM1
36		IGHV3OR16-12
37		IGHV1OR15-1
38		IGHV3OR15-7
39	TATA-binding protein-associated factor 2N	TAF15
40		IGLV5-45

41	Ig heavy chain V-III region 23	IGHV3-23
42		IGHV3-53
43		
44		IGKV1D-8
45	Ester hydrolase C11orf54	C11orf54
46	Collagen alpha-2(I) chain	COL1A2
47	Ig kappa chain V-I region WAT	
48	Roundabout homolog 1	ROBO1
49	Ig kappa chain C region	IGKC
50	UBX domain-containing protein 1	UBXN1
51	Soluble scavenger receptor cysteine-rich domain-containing protein SSC5D	SSC5D
52		IGHV3-49
53	Heterogeneous nuclear ribonucleoproteins A2/B1	HNRNPA2B1
54	Bifunctional ATP-dependent dihydroxyacetone kinase/FAD-AMP lyase (cyclizing)	TKFC
55	Ig delta chain C region	IGHD
56	Chondroitin sulfate proteoglycan 5	CSPG5
57	Laminin subunit alpha-3	LAMA3
58		OSCAR
59	Aromatic-L-amino-acid decarboxylase	DDC
60		IGHG1
61	Testis-expressed sequence 2 protein	TEX2
62	Scavenger receptor class F member 2	SCARF2
63	CD177 antigen	CD177
64		IGKV1-27
65	Clathrin heavy chain	CLTC
66	Ig gamma-3 chain C region	IGHG3
67		IGHV3-72
68	Mucosal addressin cell adhesion molecule 1	MADCAM1
69	Immunoglobulin lambda-like polypeptide 5	IGLL5
70	Transmembrane protease serine 13	TMPRSS13
71		IGHV3-64
72	Mucin-like protein 1	MUCL1
73	Mucin-1	MUC1
74	Syntaxin-binding protein 2	STXBP2
75		ALB
76	Tropomyosin alpha-3 chain	TPM3
77	Gamma-adducin	ADD3
78	Integrin beta	ITGB2
79	Proteasomal ubiquitin receptor ADRM1	ADRM1
80	Cadherin-4	CDH4
81	IgGFc-binding protein	FCGBP
82	Folate receptor gamma	FOLR3
83		IGHG3

84	Basal cell adhesion molecule	BCAM
85	Collagen alpha-1(V) chain	COL5A1
86	Vacuolar protein sorting-associated protein VTA1 homolog	VTA1
87	Ig gamma-1 chain C region	IGHG1
88		IGHG1
89	Laminin subunit alpha-2	LAMA2
90	Ig mu chain C region	IGHM
91	Seizure 6-like protein 2	SEZ6L2
92		IGKC
93		IGLL5
94	UTP--glucose-1-phosphate uridylyltransferase	UGP2
95	Salivary acidic proline-rich phosphoprotein 1/2	PRH1
96	Plakophilin-1	PKP1
97	Tumor protein D54	TPD52L2
98	Integral membrane protein DGCR2/IDD	DGCR2
99	Myristoylated alanine-rich C-kinase substrate	MARCKS
100		IGKV1D-33
101	Receptor protein-tyrosine kinase	MERTK
102	Low affinity immunoglobulin gamma Fc region receptor III-B	FCGR3B
103	Colipase	CLPS
104		IGKV3-11
105		IGHG1
106	Hypoxia up-regulated protein 1	HYOU1
107		IGHG1
108	Natriuretic peptides A	NPPA
109	Pro-cathepsin H	CTSH
110	Collagen alpha-1(XV) chain	COL15A1
111		
112	Kinesin-like protein	CENPE
113		IGKV2D-29
114	Ig kappa chain V-II region Cum	IGKV2-40
115	Collagen alpha-1(VI) chain	COL6A1
116	Heterogeneous nuclear ribonucleoprotein M	HNRNPM
117		IGKC
118	Growth hormone receptor	GHR
119	Ras-related protein Rab-18	RAB18
120		IGHG1
121	15 kDa selenoprotein	SEP15
122	Glutathione peroxidase	GPX3
123	C-C motif chemokine 15	CCL15
124	Nebulin	NEB
125	Aggrecan core protein	ACAN
126	Ig kappa chain V-II region TEW	IGKC

127	Complement C1s subcomponent	C1S
128	AP-2 complex subunit beta	AP2B1
129	Basigin	BSG
130	Carcinoembryonic antigen-related cell adhesion molecule 8	CEACAM8
131	Inter-alpha-trypsin inhibitor heavy chain H5	ITIH5
132	Serum amyloid A-4 protein	SAA2-SAA4
133	Mucin-5AC	MUC5AC
134	Stathmin	STMN1
135	Major prion protein	PRNP
136	Flotillin-1	FLOT1
137	Neuroblastoma suppressor of tumorigenicity 1	NBL1
138	ADP-ribosyl cyclase/cyclic ADP-ribose hydrolase 2	BST1
139	Putative keratin-87 protein	KRT87P
140	IgLON family member 5	IGLON5
141	Leukocyte immunoglobulin-like receptor subfamily A member 5	LILRA5
142	Aminopeptidase B	RNPEP
143	N-acylglucosamine 2-epimerase	RENBP
144	Protein shisa-7	SHISA7
145	V-set and transmembrane domain-containing protein 2B	VSTM2B
146	Alpha-endosulfine	ENSA
147	Collagen alpha-6(VI) chain	COL6A6
148	Matrilin-4	MATN4
149	Tetraspanin	CD9
150	Inositol oxygenase	MIOX
151	BPI fold-containing family A member 1	BPIFA1
152	Trypsin-2	PRSS2
153	Insulin-like growth factor-binding protein 3	IGFBP3
154	Alpha-2-macroglobulin-like protein 1	A2ML1
155	Protein FAM3B	FAM3B
156	Small ubiquitin-related modifier 3	SUMO3
157	Leukocyte immunoglobulin-like receptor subfamily B member 1	LILRB1
158	Putative neutrophil cytosol factor 1C	NCF1C
159	G-protein coupled receptor family C group 5 member C	GPRC5C
160	Platelet-derived growth factor subunit B	PDGFB
161	Interleukin-2 receptor subunit beta	IL2RB
162	Seizure 6-like protein	SEZ6L
163	Apolipoprotein C-III	APOC3
164	Sulfurtransferase	MPST
165	Signal peptide, CUB and EGF-like domain-containing protein 1	SCUBE1
166	Receptor protein-tyrosine kinase	EPHB2
167	Astrocytic phosphoprotein PEA-15	PEA15
168	Latrophilin-2	ADGRL2
169	Lymphocyte function-associated antigen 3	CD58

170	Dyslexia-associated protein KIAA0319-like protein	KIAA0319L
171	Complement decay-accelerating factor	CD55
172	WASH complex subunit FAM21C	FAM21A
173	Protein FAM151A	FAM151A
174	Prosaposin	PSAP
175	Microfibrillar-associated protein 5	MFAP5
176	Myelin regulatory factor	MYRF
177	Sodium channel subunit beta-1	SCN1B
178	Citrate synthase	CS
179	Gamma-glutamyltransferase 6	GGT6
180	Complement C1r subcomponent	C1R
181	Complement factor B	CFB
182	Tumor necrosis factor receptor superfamily member 1B	TNFR1B
183	Transcobalamin-2	TCN2
184	Echinoderm microtubule-associated protein-like 4	EML4
185	Epithelial cell adhesion molecule	EPCAM
186	GTP-binding nuclear protein Ran	RAN
187	Abl interactor 1	ABI1
188	Serum albumin	ALB
189	Sodium/nucleoside cotransporter 1	SLC28A1
190	Inter-alpha-trypsin inhibitor heavy chain H4	ITIH4
191	CapZ-interacting protein	RCSD1
192	Metalloendopeptidase	MEP1A
193	Parvalbumin alpha	PVALB
194	10 kDa heat shock protein, mitochondrial	HSPE1
195	Interleukin-1 receptor type 1	IL1R1
196	Prothymosin alpha	PTMA
197	Butyrophilin subfamily 2 member A2	BTN2A2
198	Exostosin-like 2	EXTL2
199	Protein shisa-5	SHISA5
200	Mucin-13	MUC13
201	Type 2 lactosamine alpha-2,3-sialyltransferase	ST3GAL6
202	Charged multivesicular body protein 2b	CHMP2B
203	Profilin	PFN2
204	Sorcin	SRI
205	Protein FAM107B	FAM107B
206	Troponin C, skeletal muscle	TNNC2
207	Immunoglobulin superfamily member 8	IGSF8
208	40S ribosomal protein SA	RPSA
209		TF
210	Immunoglobulin superfamily member 11	IGSF11
211	Tissue factor pathway inhibitor	TFPI
212	Nuclear receptor-binding protein	NRBP1

213	Lipoma-preferred partner	LPP
214	Voltage-dependent calcium channel subunit alpha-2/delta-2	CACNA2D2
215	Protein lifeguard 3	TMBIM1
216	C-X-C chemokine receptor type 2	CXCR2
217	Paired immunoglobulin-like type 2 receptor alpha	PILRA
218	Acylamino-acid-releasing enzyme	APEH
219		TFPI
220	Transmembrane protease serine 2	TMPRSS2
221	V-type proton ATPase subunit B, kidney isoform	ATP6V1B1
222	Myotrophin	MTPN
223	HEPACAM family member 2	HEPACAM2
224	Zinc transporter ZIP5	SLC39A5
225	Echinoderm microtubule-associated protein-like 2	EML2
226	Leukocyte immunoglobulin-like receptor subfamily B member 4	LILRB4
227	Putative transmembrane protein INAFM1	INAFM1
228	Insulin-like growth factor-binding protein 1	IGFBP1
229	Transmembrane protein 198	TMEM198
230	Insulin-like growth factor-binding protein 5	IGFBP5
231	Synaptophysin-like protein 1	SYPL1
232	Vacuolar protein sorting-associated protein 37D	VPS37D
233	Procollagen C-endopeptidase enhancer 2	PCOLCE2
234	Neuronal cell adhesion molecule	NRCAM
235		TIGIT
236	SPARC	SPARC
237	Neuron-specific protein family member 1	D4S234E
238	Target of Nesh-SH3	ABI3BP
239	Glucosamine-6-phosphate isomerase	GNPDA1
240	Complement C1q subcomponent subunit B	C1QB
241	Protein NOXP20	FAM114A1
242	Matrix extracellular phosphoglycoprotein	MEPE
243	PDZ and LIM domain protein 7	PDLIM7
244	Vesicular integral-membrane protein VIP36	LMAN2
245	Rap guanine nucleotide exchange factor 6	RAPGEF6
246	Alpha-L-iduronidase	IDUA
247		GC
248	Cadherin-6	CDH6
249	Collagen alpha-1(XII) chain	COL12A1
250	Corticotropin-releasing factor-binding protein	CRHBP
251	Ribonuclease T2	RNASET2
252	Netrin receptor UNC5C	UNC5C
253	Proton-coupled amino acid transporter 2	SLC36A2
254		PDGFRB
255	Copper transport protein ATOX1	ATOX1

256	Zinc transporter ZIP14	SLC39A14
257	Tubulin-specific chaperone A	TBCA
258	Syndecan	SDC2
259	S-phase kinase-associated protein 1	SKP1
260	Latrophilin-3	ADGRL3
261	Vitamin K-dependent protein C	PROC
262	Protein-tyrosine-phosphatase	PTPRM
263	Tenascin-X	TNXB
264	Ezrin	EZR
265	Protein YIPF3	YIPF3
266	Maltase-glucoamylase, intestinal	MGAM
267	Neurexin-1	NRXN1
268	Calpastatin	CAST
269	Thrombospondin-4	THBS4
270	Calcitonin gene-related peptide 2	CALCB
271	Urokinase-type plasminogen activator	PLAU
272		
273	Lysosome-associated membrane glycoprotein 3	LAMP3
274	Folate receptor beta	FOLR2
275	Casein kinase II subunit alpha 3	CSNK2A1
276	Sodium/calcium exchanger 1	SLC8A1
277	Latent-transforming growth factor beta-binding protein 1	LTBP1
278	Microtubule-associated protein	MAP4
279	Hematopoietic lineage cell-specific protein	HCLS1
280	Mucin-4	MUC4
281	Neuropilin-1	NRP1
282	Properdin	CFP
283	Alpha-mannosidase	MAN2B2
284	Transporter	SLC6A19
285	Catenin beta-1	CTNNB1
286	Epsilon-sarcoglycan	SGCE
287	Macrophage colony-stimulating factor 1 receptor	CSF1R
288	Receptor protein-tyrosine kinase	EPHA4
289	ATP-binding cassette sub-family A member 2	ABCA2
290	Mucin-20	MUC20
291	Tetranectin	CLEC3B
292	Pro-opiomelanocortin	POMC
293	Band 4.1-like protein 2	EPB41L2
294	Thy-1 membrane glycoprotein	THY1
295	Mth938 domain-containing protein	AAMDC
296	Transmembrane protein 25	TMEM25
297	Mitogen-activated protein kinase	MAPK3
298	Sodium channel subunit beta-3	SCN3B

299	Ras-related protein R-Ras2	RRAS2
300	Junctional adhesion molecule-like	AMICA1
301	Ras-related protein Rab-2A	RAB2A
302	ADM	ADM
303	Ras-related protein Rab-1B	RAB1B
304	Puromycin-sensitive aminopeptidase	NPEPPS
305	Tetraspanin	CD151
306	Potassium voltage-gated channel subfamily E member 3	KCNE3
307	Brain-specific angiogenesis inhibitor 2	ADGRB2
308	Thioredoxin reductase 1, cytoplasmic	TXNRD1
309	Nucleosome assembly protein 1-like 4	NAP1L4
310	CD59 glycoprotein	CD59
311	Multivesicular body subunit 12A	MVB12A
312	Layilin	LAYN
313	Alpha-crystallin B chain	CRYAB
314	Serine protease 23	PRSS23
315	Cysteine and glycine-rich protein 1	CSRP1
316	Signal-regulatory protein beta-2	SIRPB2
317	Serine/threonine-protein kinase WNK1	WNK1
318	DNA damage-binding protein 1	DDB1
319	Maestro heat-like repeat-containing protein family member 2B	MROH2B
320	Amyloid-like protein 1	APLP1
321	4F2 cell-surface antigen heavy chain	SLC3A2
322	Scavenger receptor cysteine-rich type 1 protein M130	CD163
323	Malectin	MLEC
324	Ubiquitin-60S ribosomal protein L40	UBC
325	Testican-2	SPOCK2
326	Tumor susceptibility gene 101 protein	TSG101
327	Protein FAM198A	FAM198A
328	Limbic system-associated membrane protein	LSAMP
329	Activin receptor type-1B	ACVR1B
330	Sodium/calcium exchanger 2	SLC8A2
331	Neutral alpha-glucosidase AB	GANAB
332	Oxidized low-density lipoprotein receptor 1	OLR1
333	Coagulation factor VII	F7
334	Destrin	DSTN
335	Dickkopf-related protein 3	DKK3
336	Glyoxalase domain-containing protein 4	GLOD4
337	Tumor necrosis factor receptor superfamily member 14	TNFRSF14
338	Natural killer cells antigen CD94	KLRD1
339	Tetraspanin	CD63
340	LIM domain and actin-binding protein 1	LIMA1
341	Cadherin-19	CDH19

342	Dynactin subunit 2	DCTN2
343	Vacuolar protein sorting-associated protein 29	VPS29
344	Keratin, type I cytoskeletal 18	KRT18
345	Protein canopy homolog 2	CNPY2
346	Matrix metalloproteinase-19	MMP19
347	3(2),5-bisphosphate nucleotidase 1	BPNT1
348	Myosin light polypeptide 6	MYL6
349	Heterogeneous nuclear ribonucleoprotein A1	HNRNPA1
350	Protein sidekick-1	SDK1
351	Golgi integral membrane protein 4	GOLIM4
352	V-set and transmembrane domain-containing protein 2A	VSTM2A
353	Roundabout homolog 2	ROBO2
354	Disintegrin and metalloproteinase domain-containing protein 9	ADAM9
355		EPHB6
356	Endothelial cell-selective adhesion molecule	ESAM
357	Carboxylic ester hydrolase	BCHE
358	Elongation factor 1-beta	EEF1B2
359	Transferrin receptor protein 1	TFRC
360	Dipeptidyl peptidase 3	DPP3
361	Adenylate kinase 2, mitochondrial	AK2
362	Ubiquitin-conjugating enzyme E2 variant 1	UBE2V1
363	V-type proton ATPase subunit D	ATP6V1D
364	Protein unc-79 homolog	UNC79
365	Acylphosphatase	ACYP1
366	Protein Z-dependent protease inhibitor	SERPINA10
367		RNASE1
368		SERPINA3
369	Proteasome subunit alpha type	PSMA6
370	Latent-transforming growth factor beta-binding protein 2	LTBP2
371		FBLN5
372	Ectonucleoside triphosphate diphosphohydrolase 5	ENTPD5
373	Glia maturation factor beta	GMFB
374	Fibulin-5	FBLN5
375	Heterogeneous nuclear ribonucleoproteins C1/C2	HNRNPC
376	Melanoma inhibitory activity protein 2	MIA2
377	Protein NDRG2	NDRG2
378	Cochlin	COCH
379	Laminin subunit beta-1	LAMB1
380	Hepatocyte growth factor-like protein	MST1
381	Solute carrier family 12 member 2	SLC12A2
382	Complement factor I	CFI
383	Cartilage oligomeric matrix protein	COMP
384	Neurexin-2	NRXN2

385	Corneodesmosin	CDSN
386	Cadherin-23	CDH23
387	V-set and transmembrane domain-containing protein 1	VSTM1
388	Aldehyde dehydrogenase family 1 member A3	ALDH1A3
389	Zyxin	ZYX
390	Syntaxin-binding protein 5	STXBP5
391	Interleukin-10 receptor subunit beta	IL10RB
392	Serine/threonine-protein kinase SIK3	SIK3
393	CD99 antigen-like protein 2	CD99L2
394	Drebrin-like protein	DBNL
395	Glycodelin	PAEP
396	Low affinity immunoglobulin gamma Fc region receptor III-A	FCGR3A
397	Calmodulin	CALM2
398	Cyclic AMP-dependent transcription factor ATF-6 beta	ATF6B
399	Amphiphysin	AMPH
400	2-deoxynucleoside 5-phosphate N-hydrolase 1	DNPH1
401	ADP-ribosyl cyclase/cyclic ADP-ribose hydrolase 1	CD38
402	Adaptin ear-binding coat-associated protein 2	NECAP2
403	Thioredoxin domain-containing protein 15	TXNDC15
404	Interleukin-6 receptor subunit alpha	IL6R
405	Plasma kallikrein	KLKB1
406	Retinol-binding protein 1	RBP1
407	Nephronectin	NPNT
408	Latent-transforming growth factor beta-binding protein 3	LTBP3
409	Acetyltransferase component of pyruvate dehydrogenase complex	DLAT
410	ADP-sugar pyrophosphatase	NUDT5
411	Cysteine-rich protein 2	CRIP2
412	Transmembrane 7 superfamily member 3	TM7SF3
413	alpha-1,2-Mannosidase	MAN1B1
414	Receptor protein serine/threonine kinase	TGFBR1
415	Serine/arginine-rich splicing factor 9	SRSF9
416	Beta-2-microglobulin	B2M
417	Proteasome subunit alpha type	PSMA4
418	Acidic leucine-rich nuclear phosphoprotein 32 family member A	ANP32A
419	Signal peptide peptidase-like 2A	SPPL2A
420	Ras-related protein Rab-8B	RAB8B
421	TM2 domain-containing protein 3	TM2D3
422	Aflatoxin B1 aldehyde reductase member 2	AKR7A2
423	Probable ATP-dependent RNA helicase DDX17	DDX17
424	Cytochrome c oxidase subunit 5A, mitochondrial	COX5A
425	Protein CCSMST1	C16orf91
426	Hydroxyacylglutathione hydrolase, mitochondrial	HAGH
427	Dynein light chain roadblock-type 1	DYNLRB2

428	Interleukin-4 receptor subunit alpha	IL4R
429	Beta-hexosaminidase	HEXA
430	Cysteine-rich secretory protein LCCL domain-containing 2	CRISPLD2
431	Lysyl oxidase homolog 1	LOXL1
432	Ly6/PLAUR domain-containing protein 6B	LYPD6B
433	ATP-binding cassette sub-family B member 6, mitochondrial	ABCB6
434	Neurofascin	NFASC
435	Protein-L-isoaspartate O-methyltransferase	PCMT1
436	Proline-rich acidic protein 1	PRAP1
437	Platelet-derived growth factor subunit A	PDGFA
438	Zinc finger protein 185	ZNF185
439	Collagen alpha-1(XXVIII) chain	COL28A1
440	Reticulon-4 receptor	RTN4R
441	Translin	TSN
442	CD99 antigen	CD99
443	Grancalcin	GCA
444	Putative protein FAM10A4	ST13
445	Phospholipid scramblase 1	PLSCR1
446	Neural cell adhesion molecule 2	NCAM2
447	Sex hormone-binding globulin	SHBG
448	Eukaryotic translation initiation factor 5A	EIF5A
449	Brain-specific angiogenesis inhibitor 1-associated protein 2	BAIAP2
450	Sarcalumenin	SRL
451	C-type lectin domain family 10 member A	CLEC10A
452	Fibroblast growth factor receptor	FGFR3
453	Low-density lipoprotein receptor	LDLR
454	Cathelicidin antimicrobial peptide	CAMP
455	Semaphorin-4B	SEMA4B
456	Integrin alpha-7	ITGA7
457	Cysteine-rich secretory protein 3	CRISP3
458	Receptor protein-tyrosine kinase	FGFR4
459	Fructose-bisphosphate aldolase	ALDOA
460	Trans-Golgi network integral membrane protein 2	TGOLN2
461	Rho GDP-dissociation inhibitor 1	ARHGDIA
462	Cadherin-8	CDH8
463	L-xylulose reductase	DCXR
464		SECTM1
465	CMRF35-like molecule 1	CD300LF
466	Galectin	LGALS9
467	Uncharacterized protein C1orf159	C1orf159
468	Eukaryotic initiation factor 4A-I	EIF4A2
469	Secernin-2	SCRN2
470	Flotillin-2	FLOT2

471	T-cell antigen CD7	CD7
472	Receptor protein-tyrosine kinase	ERBB2
473		SECTM1
474	Intercellular adhesion molecule 2	ICAM2
475	Sodium channel protein	SCN4A
476	Fractalkine	CX3CL1
477	Unconventional myosin-Id	MYO1D
478	Myosin regulatory light chain 12A	MYL12A
479	Lutropin subunit beta	LHB
480	Collagen alpha-1(XIV) chain	COL14A1
481	Tryptase alpha/beta-1	TPSAB1
482	Low affinity immunoglobulin epsilon Fc receptor	FCER2
483	ICOS ligand	ICOSLG
484	WW domain-binding protein 2	WBP2
485	TAR DNA-binding protein 43	TARDBP
486	Kin of IRRE-like protein 2	KIRREL2
487	Tubulin-folding cofactor B	TBCB
488		PVRL2
489	Angiopoietin-related protein 6	ANGPTL6
490	Envoplakin	EVPL
491	Periplakin	PPL
492	Glucosidase 2 subunit beta	PRKCSH
493	Histone H3	H3F3B
494	Transmembrane protein 256	TMEM256
495	Cartilage intermediate layer protein 2	CILP2
496	Asialoglycoprotein receptor 1	ASGR1
497		MXRA7
498	Apolipoprotein C-II	APOC4-APOC2
499	Complement factor D	CFD
500	Apolipoprotein C-I	APOC1
501	Glutathione peroxidase	GPX4
502	ATP synthase subunit alpha, mitochondrial	ATP5A1
503	Follistatin-related protein 3	FSTL3
504	Calponin	CNN2
505	Microfibril-associated glycoprotein 4	MFAP4
506	IGF-like family receptor 1	IGFLR1
507	Aquaporin-1	AQP1
508	Iron/zinc purple acid phosphatase-like protein	PAPL
509		A1BG
510	CD209 antigen	CD209
511		C3
512	ER membrane protein complex subunit 10	EMC10
513	Deoxyribonuclease-2-alpha	DNASE2

514	PDZ and LIM domain protein 1	PDLIM1
515	Synaptosomal-associated protein 23	SNAP23
516	Mannan-binding lectin serine protease 2	MASP2
517	Signal-regulatory protein beta-1	SIRPB1
518	Membrane-associated progesterone receptor component 1	PGRMC1
519	Chloride intracellular channel protein 1	CLIC1
520	Uroplakin-1a	UPK1A
521	Prostaglandin E2 receptor EP3 subtype	PTGER3
522	Sulfhydryl oxidase 1	QSOX1
523	Beta-mannosidase	MANBA
524	Agrin	AGRN
525	Myc box-dependent-interacting protein 1	BIN1
526	Uroplakin-2	UPK2
527	Neural cell adhesion molecule L1-like protein	CHL1
528	Delta-like protein 1	DLL1
529	Syntenin-1	SDCBP
530	Syntenin-1	SDCBP
531	Podocalyxin	PODXL
532	Lysosomal alpha-mannosidase	MAN2B1
533	Fructose-1,6-bisphosphatase isozyme 2	FBP2
534	Pyridoxal kinase	PDXK
535	Immunoglobulin superfamily containing leucine-rich repeat protein	ISLR
536	Neurocan core protein	NCAN
537	Disintegrin and metalloproteinase domain-containing protein 10	ADAM10
538	Inositol monophosphatase 2	IMPA2
539	Na(+)/H(+) exchange regulatory cofactor NHE-RF1	SLC9A3R1
540	Tripeptidyl-peptidase 1	TPP1
541	Apolipoprotein L1	APOL1
542	Tumor necrosis factor receptor superfamily member 10C	TNFRSF10C
543	Proteasome subunit alpha type-7	PSMA7
544	Protocadherin-17	PCDH17
545	Plexin-B2	PLXNB2
546	A disintegrin and metalloproteinase with thrombospondin motifs 3	ADAMTS3
547	Actin-related protein 2/3 complex subunit 1B	ARPC1B
548	Actin-related protein 2/3 complex subunit 2	ARPC2
549	Actin-related protein 2/3 complex subunit 3	ARPC3
550	Ephrin type-B receptor 6	EPHB6
551	ADAM DEC1	ADAMDEC1
552	Laminin subunit alpha-5	LAMA5
553	Neurosecretory protein VGF	VGF
554	Synaptobrevin homolog YKT6	YKT6
555	Fatty acid-binding protein, brain	FABP7
556	Leucine-rich repeat transmembrane protein FLRT2	FLRT2

557	Kunitz-type protease inhibitor 1	SPINT1
558	Trehalase	TREH
559	Kunitz-type protease inhibitor 2	SPINT2
560	Zinc finger protein 749	ZNF749
561	Thioredoxin-like protein 1	TXNL1
562	Prominin-1	PROM1
563	Beta-1,4-glucuronyltransferase 1	B4GAT1
564	E3 ubiquitin-protein ligase RNF13	RNF13
565	Carbonic anhydrase 12	CA12
566	Charged multivesicular body protein 2a	CHMP2A
567	Prostate stem cell antigen	PSCA
568	Alpha-actinin-4	ACTN4
569	Calumenin	CALU
570	CD5 antigen-like	CD5L
571	Xaa-Pro aminopeptidase 2	XPNPEP2
572	Glia maturation factor gamma	GMFG
573	Transmembrane protease serine 11D	TMPRSS11D
574	Perilipin-1	PLIN1
575	Protocadherin-7	PCDH7
576	Guanine nucleotide-binding protein G(I)/G(S)/G(O) subunit gamma-7	GNG7
577	Sushi domain-containing protein 5	SUSD5
578	Lymphocyte antigen 75	LY75
579	Neuropilin-2	NRP2
580	Long-chain-fatty-acid--CoA ligase 4	ACSL4
581	Cubilin	CUBN
582	Beta-1,4-galactosyltransferase 3	B4GALT3
583	Toll-like receptor 2	TLR2
584	GDNF family receptor alpha-3	GFRA3
585	Tetraspanin-1	TSPAN1
586	Perilipin-3	PLIN3
587	Protein-tyrosine sulfotransferase 2	TPST2
588	Prosaposin receptor GPR37L1	GPR37L1
589	Protein CutA	CUTA
590	Sodium channel subunit beta-2	SCN2B
591	EF-hand calcium-binding domain-containing protein 14	EFCAB14
592	WD repeat-containing protein 1	WDR1
593	Slit homolog 3 protein	SLIT3
594	Copine-3	CPNE3
595	Gamma-glutamylcyclotransferase	GGCT
596	Cadherin-16	CDH16
597	Cartilage intermediate layer protein 1	CILP
598	Programmed cell death protein 6	PDCD6
599	Vacuolar protein sorting-associated protein 4B	VPS4B

600	Core histone macro-H2A.1	H2AFY
601	SH3 domain-binding glutamic acid-rich-like protein	SH3BGRL
602	Filamin-B	FLNB
603	Serine/threonine-protein kinase/endoribonuclease IRE1	ERN1
604	Glypican-4	GPC4
605	Ceroid-lipofuscinosis neuronal protein 5	CLN5
606	Tumor necrosis factor receptor superfamily member 21	TNFRSF21
607	Splicing factor 3B subunit 1	SF3B1
608	Peptidoglycan recognition protein 1	PGLYRP1
609	Protein CREG1	CREG1
610	Ficolin-3	FCN3
611	UDP-GalNAc:beta-1,3-N-acetylgalactosaminyltransferase 1	B3GALNT1
612	Renin receptor	ATP6AP2
613	Isocitrate dehydrogenase [NADP] cytoplasmic	IDH1
614	Attractin	ATRN
615	Cytosolic 10-formyltetrahydrofolate dehydrogenase	ALDH1L1
616	Dysferlin	DYSF
617	Gamma-butyrobetaine dioxygenase	BBOX1
618	Carboxypeptidase D	CPD
619	WNT1-inducible-signaling pathway protein 2	WISP2
620	N(G),N(G)-dimethylarginine dimethylaminohydrolase 1	DDAH1
621	Galactosylgalactosylxylosylprotein 3-beta-glucuronosyltransferase 3	B3GAT3
622	Lymphocyte antigen 6H	LY6H
623	Latrophilin-1	LPHN1
624	Endonuclease domain-containing 1 protein	ENDOD1
625	SLIT and NTRK-like protein 5	SLITRK5
626	Sciellin	SCEL
627	Reticulon-3	RTN3
628	Protocadherin-8	PCDH8
629	Ly6/PLAUR domain-containing protein 3	LYPD3
630	6-phosphogluconolactonase	PGLS
631	WNT1-inducible-signaling pathway protein 1	WISP1
632	Papilin	PAPLN
633	Apolipoprotein M	APOM
634	A disintegrin and metalloproteinase with thrombospondin motifs 2	ADAMTS2
635	Pantetheinase	VNN1
636	Neuronal pentraxin receptor	NPTXR
637	Serine/threonine-protein kinase OSR1	OXSR1
638	N(G),N(G)-dimethylarginine dimethylaminohydrolase 2	DDAH2
639	Formimidoyltransferase-cyclodeaminase	FTCD
640	EGF-containing fibulin-like extracellular matrix protein 2	EFEMP2
641	CD160 antigen	CD160
642	Reversion-inducing cysteine-rich protein with Kazal motifs	RECK

643	Interleukin-18-binding protein	IL18BP
644	Napsin-A	NAPSA
645	Molybdopterin synthase sulfur carrier subunit	MOCS2
646	Cytochrome b5	CYB5A
647	L-lactate dehydrogenase A chain	LDHA
648	Retinal dehydrogenase 1	ALDH1A1
649	Glutathione reductase, mitochondrial	GSR
650	Superoxide dismutase [Cu-Zn]	SOD1
651	Ceruloplasmin	CP
652	Coagulation factor VIII	F8
653	Purine nucleoside phosphorylase	PNP
654	Hypoxanthine-guanine phosphoribosyltransferase	HPRT1
655	Epidermal growth factor receptor	EGFR
656	Phosphoglycerate kinase 1	PGK1
657	Prothrombin	F2
658	Haptoglobin	HP
659	Haptoglobin-related protein	HPR
660	Coagulation factor IX	F9
661	Coagulation factor X	F10
662	Plasminogen	PLG
663	Coagulation factor XII	F12
664	Carbonic anhydrase 1	CA1
665	Carbonic anhydrase 2	CA2
666	Argininosuccinate synthase	ASS1
667	Pancreatic secretory trypsin inhibitor	SPINK1
668	Antithrombin-III	SERPINC1
669	Alpha-1-antitrypsin	SERPINA1
670	Alpha-1-antichymotrypsin	SERPINA3
671	Angiotensinogen	AGT
672	Alpha-2-macroglobulin	A2M
673	Complement C3	C3
674	Complement C5	C5
675	Cystatin-C	CST3
676	Cystatin-S	CST4
677	Cystatin-SN	CST1
678	Cystatin-A	CSTA
679	Kininogen-1	KNG1
680	Kininogen-1	KNG1
681	GTPase NRas	NRAS
682	Pro-epidermal growth factor	EGF
683	Proenkephalin-A	PENK
684	Follitropin subunit beta	FSHB
685	Calcitonin	CALCA

686	Insulin-like growth factor II	IGF2
687	Immunoglobulin J chain	IGJ
688	Ig kappa chain V-I region AU	
689	Ig kappa chain V-I region CAR	
690	Ig kappa chain V-I region DEE	
691	Ig kappa chain V-I region EU	
692	Ig kappa chain V-I region HK101	
693	Ig kappa chain V-I region HK102	IGKV1-5
694	Ig kappa chain V-I region Ka	
695	Ig kappa chain V-I region Kue	
696	Ig kappa chain V-I region Lay	
697	Ig kappa chain V-I region Rei	
698	Ig kappa chain V-I region Roy	
699	Ig kappa chain V-I region Scw	
700	Ig kappa chain V-I region WEA	
701	Ig kappa chain V-I region Wes	
702	Ig kappa chain V-I region Mev	
703	Ig kappa chain V-I region Ni	
704	Ig kappa chain V-II region FR	
705	Ig kappa chain V-II region MIL	
706	Ig kappa chain V-III region B6	
707	Ig kappa chain V-III region SIE	
708	Ig kappa chain V-III region NG9	
709	Ig kappa chain V-III region Ti	
710	Ig kappa chain V-III region POM	
711	Ig kappa chain V-IV region Len	
712	Ig lambda chain V-I region NEW	
713	Ig lambda chain V-II region TRO	
714	Ig lambda chain V-II region BUR	
715	Ig lambda chain V-III region SH	
716	Ig lambda chain V-IV region X	
717	Ig lambda chain V-IV region Hil	
718	Ig lambda chain V-V region DEL	
719	Ig lambda chain V-VI region AR	
720	Ig heavy chain V-I region HG3	
721	Ig heavy chain V-III region WEA	
722	Ig heavy chain V-III region TIL	
723	Ig heavy chain V-III region BUT	
724	Ig heavy chain V-III region NIE	
725	Ig heavy chain V-III region KOL	
726	Ig heavy chain V-III region BUR	
727	Ig heavy chain V-III region LAY	
728	Ig heavy chain V-III region WAS	

729	Ig heavy chain V-III region ZAP	
730	Ig heavy chain V-III region JON	
731	Ig heavy chain V-III region GAL	
732	Ig heavy chain V-II region WAH	
733	Ig heavy chain V-II region NEWM	
734	Polymeric immunoglobulin receptor	PIGR
735	Ig epsilon chain C region	IGHE
736	Ig gamma-2 chain C region	IGHG2
737	Ig gamma-4 chain C region	IGHG4
738	Ig alpha-1 chain C region	IGHA1
739	Ig alpha-2 chain C region	IGHA2
740	Hemoglobin subunit delta	HBD
741	Myoglobin	MB
742	Collagen alpha-1(I) chain	COL1A1
743	Collagen alpha-1(II) chain	COL2A1
744	Collagen alpha-1(III) chain	COL3A1
745	Collagen alpha-1(IV) chain	COL4A1
746	Prelamin-A/C	LMNA
747	Apolipoprotein A-I	APOA1
748	Apolipoprotein E	APOE
749	Fibrinogen alpha chain	FGA
750	Fibrinogen beta chain	FGB
751	Fibrinogen gamma chain	FGG
752	C-reactive protein	CRP
753	Serum amyloid P-component	APCS
754	Complement C1q subcomponent subunit C	C1QC
755	Complement component C9	C9
756	Beta-2-glycoprotein 1	APOH
757	Leucine-rich alpha-2-glycoprotein	LRG1
758	Fibronectin	FN1
759	Protein AMBP	AMBP
760	Alpha-1-acid glycoprotein 1	ORM1
761	Alpha-2-HS-glycoprotein	AHSG
762	Transthyretin	TTR
763	Vitamin D-binding protein	GC
764	Platelet basic protein	PPBP
765	Serotransferrin	TF
766	Lactotransferrin	LTF
767	Hemopexin	HPX
768	Ferritin light chain	FTL
769	Ferritin heavy chain	FTH1
770	Metallothionein-2	MT2A
771	Submaxillary gland androgen-regulated protein 3B	SMR3B

772	Angiogenin	ANG
773	Coagulation factor XI	F11
774	Antileukoproteinase	SLPI
775	C4b-binding protein alpha chain	C4BPA
776	Vitronectin	VTN
777	Catalase	CAT
778	Glucosylceramidase	GBA
779	Tissue alpha-L-fucosidase	FUCA1
780	Cystatin-B	CSTB
781	Annexin A1	ANXA1
782	Apolipoprotein B-100	APOB
783	Trefoil factor 1	TFF1
784	Superoxide dismutase [Mn], mitochondrial	SOD2
785	Phosphatidylcholine-sterol acyltransferase	LCAT
786	Histidine-rich glycoprotein	HRG
787	Ig kappa chain V-III region GOL	
788	Ig kappa chain V-III region CLL	
789	Ig lambda chain V-I region WAH	
790	Ig lambda chain V-II region NIG-84	
791	Ig lambda chain V region 4A	
792	Alpha-1B-glycoprotein	A1BG
793	Alpha-1B-glycoprotein	A1BG
794	HLA class II histocompatibility antigen gamma chain	CD74
795	von Willebrand factor	VWF
796	Semenogelin-1	SEMG1
797	Glyceraldehyde-3-phosphate dehydrogenase	GAPDH
798	Argininosuccinate lyase	ASL
799	Ig kappa chain V-I region BAN	
800	Ig kappa chain V-I region Walker	
801	Alpha-amylase 1	AMY1A
802	Pancreatic alpha-amylase	AMY2A
803	Heat shock protein beta-1	HSPB1
804	Guanine nucleotide-binding protein G(i) subunit alpha-2	GNAI2
805	Sodium/potassium-transporting ATPase subunit beta-1	ATP1B1
806	Secretogranin-1	CHGB
807	Fructose-bisphosphate aldolase B	ALDOB
808	Amyloid beta A4 protein	APP
809	Arginase-1	ARG1
810	Apolipoprotein D	APOD
811	Aldehyde dehydrogenase, mitochondrial	ALDH2
812	Protein S100-A8	S100A8
813	Plasminogen activator inhibitor 2	SERPINB2
814	Plasma serine protease inhibitor	SERPINA5

815	Plasma protease C1 inhibitor	SERPING1
816	Coagulation factor XIII B chain	F13B
817	Myeloperoxidase	MPO
818	Alkaline phosphatase, tissue-nonspecific isozyme	ALPL
819	Intercellular adhesion molecule 1	ICAM1
820	60S acidic ribosomal protein P2	RPLP2
821	Neuroendocrine protein 7B2	SCG5
822	Lithostathine-1-alpha	REG1A
823	HLA class I histocompatibility antigen, A-24 alpha chain	HLA-A
824	Thyroxine-binding globulin	SERPINA7
825	Heparin cofactor 2	SERPIND1
826	Integrin beta-1	ITGB1
827	Calbindin	CALB1
828	Myosin light chain 1/3, skeletal muscle isoform	MYL1
829	Serine protease hepsin	HPN
830	Collagen alpha-2(V) chain	COL5A2
831	Alpha-galactosidase A	GLA
832	Ig kappa chain V-III region IARC/BL41	
833	Ig kappa chain V-IV region	IGKV4-1
834	Ig kappa chain V-IV region B17	
835	Ig lambda chain V-VI region WLT	
836	Ig heavy chain V-I region Mot	
837	Ig heavy chain V-II region ARH-77	
838	Gelsolin	GSN
839	Gelsolin	GSN
840	ATP synthase subunit beta, mitochondrial	ATP5B
841	Complement C2	C2
842	Protein S100-A9	S100A9
843	Apolipoprotein A-IV	APOA4
844	Carcinoembryonic antigen-related cell adhesion molecule 5	CEACAM5
845	Alpha-enolase	ENO1
846	Glycogen phosphorylase, liver form	PYGL
847	Glucose-6-phosphate isomerase	GPI
848	Lipoprotein lipase	LPL
849	Kallikrein-1	KLK1
850	Ig lambda chain V-I region EPS	
851	Ig lambda chain V-IV region MOL	
852	Acyl-CoA-binding protein	DBI
853	Fatty acid-binding protein, liver	FABP1
854	L-lactate dehydrogenase B chain	LDHB
855	Thrombomodulin	THBD
856	Vitamin K-dependent protein S	PROS1
857	Protein disulfide-isomerase	P4HB

858	Prostate-specific antigen	KLK3
859	Asialoglycoprotein receptor 2	ASGR2
860	Cathepsin D	CTSD
861	Annexin A2	ANXA2
862	Complement component C8 alpha chain	C8A
863	Complement component C8 beta chain	C8B
864	Platelet glycoprotein Ib alpha chain	GP1BA
865	Complement component C8 gamma chain	C8G
866	Calpain-1 catalytic subunit	CAPN1
867	Carbonic anhydrase 3	CA3
868	Involucrin	IVL
869	Decorin	DCN
870	Beta-hexosaminidase subunit beta	HEXB
871	Cathepsin L1	CTSL
872	Profilin-1	PFN1
873	Adenine phosphoribosyltransferase	APRT
874	Cathepsin B	CTSB
875	Heat shock protein HSP 90-alpha	HSP90AA1
876	Ribonuclease pancreatic	RNASE1
877	Heat shock 70 kDa protein 1A	HSPA1A
878	Beta-microseminoprotein	MSMB
879	Annexin A6	ANXA6
880	Tumor necrosis factor receptor superfamily member 16	NGFR
881	Tumor necrosis factor receptor superfamily member 16	NGFR
882	Multidrug resistance protein 1	ABCB1
883	Corticosteroid-binding globulin	SERPINA6
884	Beta-glucuronidase	GUSB
885	Heat shock protein HSP 90-beta	HSP90AB1
886	Neutrophil elastase	ELANE
887	72 kDa type IV collagenase	MMP2
888	Stromelysin-1	MMP3
889	Extracellular superoxide dismutase [Cu-Zn]	SOD3
890	Cathepsin G	CTSG
891	Neprilysin	MME
892	Matrix Gla protein	MGP
893	Apolipoprotein(a)	LPA
894	Monocyte differentiation antigen CD14	CD14
895	Collagen alpha-2(IV) chain	COL4A2
896	Hepatocyte growth factor receptor	MET
897	Melanotransferrin	MFI2
898	Complement factor H	CFH
899	Vimentin	VIM
900	Alpha-2-antiplasmin	SERPINF2

901	Annexin A5	ANXA5
902	Chymotrypsin-like elastase family member 3A	CELA3A
903	Dopamine beta-hydroxylase	DBH
904	Glutathione S-transferase A2	GSTA2
905	Glutathione S-transferase P	GSTP1
906	Cystatin-SA	CST2
907	Matrilysin	MMP7
908	Villin-1	VIL1
909	Galectin-1	LGALS1
910	Dihydropteridine reductase	QDPR
911	Fructose-1,6-bisphosphatase 1	FBP1
912	2,3-cyclic-nucleotide 3-phosphodiesterase	CNP
913	Macrophage colony-stimulating factor 1	CSF1
914	Platelet-derived growth factor receptor beta	PDGFRB
915	Gastric inhibitory polypeptide	GIP
916	Tumor-associated calcium signal transducer 2	TACSTD2
917	Intestinal-type alkaline phosphatase	ALPI
918	Ubiquitin carboxyl-terminal hydrolase isozyme L1	UCHL1
919	Furin	FURIN
920	Leukotriene A-4 hydrolase	LTA4H
921	Fructose-bisphosphate aldolase C	ALDOC
922	Complement C4-A	C4A
923	Complement C4-B	C4B
924	Protein ELFN1	ELFN1
925	Pepsin A-3	PGA3
926	Serum amyloid A-1 protein	SAA1
927	Serum amyloid A-2 protein	SAA2
928	Putative transmembrane protein INAFM2	INAFM2
929	Adrenodoxin, mitochondrial	FDX1
930	Serglycin	SRGN
931	Non-secretory ribonuclease	RNASE2
932	Lysosomal alpha-glucosidase	GAA
933	Histone H1.4	HIST1H1E
934	Osteopontin	SPP1
935	Osteopontin	SPP1
936	Osteopontin	SPP1
937	Osteopontin	SPP1
938	Receptor-type tyrosine-protein phosphatase F	PTPRF
939	Thioredoxin	TXN
940	Complement component C7	C7
941	Chromogranin-A	CHGA
942	Mast/stem cell growth factor receptor Kit	KIT
943	S-formylglutathione hydrolase	ESD

944	60 kDa heat shock protein, mitochondrial	HSPD1
945	Clusterin	CLU
946	78 kDa glucose-regulated protein	HSPA5
947	Laminin subunit gamma-1	LAMC1
948	Lysosomal acid phosphatase	ACP2
949	Heat shock cognate 71 kDa protein	HSPA8
950	Integrin alpha-M	ITGAM
951	Mannose-binding protein C	MBL2
952	Ras-related protein Ral-A	RALA
953	Ras-related protein Ral-B	RALB
954	Lysosome-associated membrane glycoprotein 1	LAMP1
955	Fibroblast growth factor receptor 1	FGFR1
956	Cholesteryl ester transfer protein	CETP
957	Uteroglobin	SCGB1A1
958	Cation-independent mannose-6-phosphate receptor	IGF2R
959	Alcohol dehydrogenase class-3	ADH5
960	Fatty acid-binding protein, intestinal	FABP2
961	Collagen alpha-2(VI) chain	COL6A2
962	Collagen alpha-2(VI) chain	COL6A2
963	Collagen alpha-3(VI) chain	COL6A3
964	Coagulation factor V	F5
965	Nucleoprotein TPR	TPR
966	Prolactin-inducible protein	PIP
967	Creatine kinase B-type	CKB
968	Low affinity immunoglobulin gamma Fc region receptor II-a	FCGR2A
969	High affinity immunoglobulin epsilon receptor subunit alpha	FCER1A
970	Annexin A3	ANXA3
971	Eosinophil cationic protein	RNASE3
972	Alpha-actinin-1	ACTN1
973	Angiotensin-converting enzyme	ACE
974	Cadherin-1	CDH1
975	Promotilin	MLN
976	Myosin-7	MYH7
977	Proto-oncogene tyrosine-protein kinase Src	SRC
978	Xaa-Pro dipeptidase	PEPD
979	Gamma-interferon-inducible lysosomal thiol reductase	IFI30
980	Lysosome-associated membrane glycoprotein 2	LAMP2
981	Ribonuclease inhibitor	RNH1
982	Secretogranin-2	SCG2
983	Neural cell adhesion molecule 1	NCAM1
984	Versican core protein	VCAN
985	Elongation factor 2	EEF2
986	Protein disulfide-isomerase A4	PDIA4

987	Complement component C6	C6
988	Carcinoembryonic antigen-related cell adhesion molecule 1	CEACAM1
989	Carcinoembryonic antigen-related cell adhesion molecule 1	CEACAM1
990	Bone marrow proteoglycan	PRG2
991	HLA class II histocompatibility antigen, DRB1-4 beta chain	HLA-DRB1
992	Plastin-2	LCP1
993	Plastin-3	PLS3
994	Collagen alpha-2(XI) chain	COL11A2
995	L-selectin	SELL
996	Macrophage migration inhibitory factor	MIF
997	Farnesyl pyrophosphate synthase	FDPS
998	Carboxypeptidase M	CPM
999	Nidogen-1	NID1
1000	Alcohol dehydrogenase [NADP(+)]	AKR1A1
1001	Pyruvate kinase PKM	PKM
1002	Endoplasmin	HSP90B1
1003	Matrix metalloproteinase-9	MMP9
1004	Carboxypeptidase A1	CPA1
1005	Carboxypeptidase B	CPB1
1006	Fatty acid-binding protein, adipocyte	FABP4
1007	Glutamine synthetase	GLUL
1008	Aldose reductase	AKR1B1
1009	Aminopeptidase N	ANPEP
1010	Poliovirus receptor	PVR
1011	Ras-related C3 botulinum toxin substrate 2	RAC2
1012	Carboxypeptidase N catalytic chain	CPN1
1013	Arylsulfatase A	ARSA
1014	Beta-1,4-galactosyltransferase 1	B4GALT1
1015	Prostatic acid phosphatase	ACPP
1016	Folate receptor alpha	FOLR1
1017	15-hydroxyprostaglandin dehydrogenase [NAD(+)]	HPGD
1018	Membrane cofactor protein	CD46
1019	N-acetylglucosamine-6-sulfatase	GNS
1020	Immunoglobulin lambda-like polypeptide 1	IGLL1
1021	Arylsulfatase B	ARSB
1022	Beta-galactoside alpha-2,6-sialyltransferase 1	ST6GAL1
1023	Desmoplakin	DSP
1024	Metalloproteinase inhibitor 2	TIMP2
1025	Atrial natriuretic peptide receptor 1	NPR1
1026	CD44 antigen	CD44
1027	Integrin beta-4	ITGB4
1028	Carbonyl reductase [NADPH] 1	CBR1
1029	Pancreatic triacylglycerol lipase	PNLIP

1030	Platelet-derived growth factor receptor alpha	PDGFRA
1031	Beta-galactosidase	GLB1
1032	Platelet endothelial cell adhesion molecule	PECAM1
1033	Histone H1.5	HIST1H1B
1034	Dipeptidase 1	DPEP1
1035	Carboxypeptidase E	CPE
1036	Fumarylacetoacetase	FAH
1037	Y-box-binding protein 3	YBX3
1038	Alpha-N-acetylgalactosaminidase	NAGA
1039	Heat shock 70 kDa protein 6	HSPA6
1040	Aspartate aminotransferase, cytoplasmic	GOT1
1041	Interferon alpha/beta receptor 1	IFNAR1
1042	Bactericidal permeability-increasing protein	BPI
1043	Atrial natriuretic peptide receptor 3	NPR3
1044	Sphingomyelin phosphodiesterase	SMPD1
1045	Calpain-2 catalytic subunit	CAPN2
1046	Endoglin	ENG
1047	Ganglioside GM2 activator	GM2A
1048	Galectin-3	LGALS3
1049	Insulin-like growth factor-binding protein 2	IGFBP2
1050	Ig kappa chain V-III region HAH	
1051	Ig kappa chain V-III region HIC	
1052	Vinculin	VCL
1053	Lipopolysaccharide-binding protein	LBP
1054	Interleukin-1 receptor antagonist protein	IL1RN
1055	Phosphoglycerate mutase 1	PGAM1
1056	Syndecan-1	SDC1
1057	Peptidyl-glycine alpha-amidating monooxygenase	PAM
1058	Cadherin-2	CDH2
1059	Vascular cell adhesion protein 1	VCAM1
1060	Tumor necrosis factor receptor superfamily member 1A	TNFRSF1A
1061	Gamma-glutamyltranspeptidase 1	GGT1
1062	Alpha-1-acid glycoprotein 2	ORM2
1063	Amiloride-sensitive amine oxidase [copper-containing]	AOC1
1064	Inter-alpha-trypsin inhibitor heavy chain H2	ITIH2
1065	Inter-alpha-trypsin inhibitor heavy chain H1	ITIH1
1066	Elafin	PI3
1067	Alpha-amylase 2B	AMY2B
1068	Thymidine phosphorylase	TYMP
1069	Annexin A7	ANXA7
1070	Myeloid cell surface antigen CD33	CD33
1071	Gastricsin	PGC
1072	Kallikrein-2	KLK2

1073	Azurocidin	AZU1
1074	Ras-related protein Rab-6A	RAB6A
1075	Lamin-B1	LMNB1
1076	Pregnancy zone protein	PZP
1077	Mimecan	OGN
1078	Ephrin-A1	EFNA1
1079	C4b-binding protein beta chain	C4BPB
1080	Myelin-associated glycoprotein	MAG
1081	N(4)-(beta-N-acetylglucosaminyl)-L-asparaginase	AGA
1082	Glutathione S-transferase Mu 3	GSTM3
1083	V-type proton ATPase subunit B, brain isoform	ATP6V1B2
1084	Filamin-A	FLNA
1085	Cytoplasmic aconitate hydratase	ACO1
1086	Glycerol-3-phosphate dehydrogenase [NAD(+)], cytoplasmic	GPD1
1087	Ephrin type-A receptor 1	EPHA1
1088	Fibroblast growth factor receptor 2	FGFR2
1089	Biglycan	BGN
1090	Oxysterol-binding protein 1	OSBP
1091	Tenascin-X	TNXB
1092	Cadherin-3	CDH3
1093	Iduronate 2-sulfatase	IDS
1094	Ubiquitin-like modifier-activating enzyme 1	UBA1
1095	Cornifin-B	SPRR1B
1096	Insulin-like growth factor-binding protein 4	IGFBP4
1097	Solute carrier family 2, facilitated glucose transporter member 5	SLC2A5
1098	Carbonic anhydrase 4	CA4
1099	Carboxypeptidase N subunit 2	CPN2
1100	Vitamin K-dependent protein Z	PROZ
1101	Neutrophil collagenase	MMP8
1102	Macrophage mannose receptor 1	MRC1
1103	Ig heavy chain V-I region V35	
1104	Fibulin-1	FBLN1
1105	Fibulin-1	FBLN1
1106	Peptidyl-prolyl cis-trans isomerase B	PPIB
1107	Protein S100-A1	S100A1
1108	Receptor-type tyrosine-protein phosphatase delta	PTPRD
1109	Receptor-type tyrosine-protein phosphatase gamma	PTPRG
1110	Receptor-type tyrosine-protein phosphatase zeta	PTPRZ1
1111	Adenosylhomocysteinase	AHCY
1112	Cofilin-1	CFL1
1113	Myeloblastin	PRTN3
1114	Endothelin B receptor	EDNRB
1115	Insulin-like growth factor-binding protein 6	IGFBP6

1116	Acetyl-CoA acetyltransferase, mitochondrial	ACAT1
1117	Tenascin	TNC
1118	Deoxyribonuclease-1	DNASE1
1119	Proteinase-activated receptor 1	F2R
1120	Zinc-alpha-2-glycoprotein	AZGP1
1121	Cathepsin S	CTSS
1122	Proteasome subunit alpha type-1	PSMA1
1123	Proteasome subunit alpha type-3	PSMA3
1124	Protein S100-P	S100P
1125	Collagen alpha-3(V) chain	COL5A3
1126	Tumor necrosis factor receptor superfamily member 5	CD40
1127	Moesin	MSN
1128	Alpha-1,3-mannosyl-glycoprotein 2-beta-N-acetylglucosaminyltransferase	MGAT1
1129	High mobility group protein B2	HMGB2
1130	Elongation factor 1-gamma	EEF1G
1131	CD27 antigen	CD27
1132	Ciliary neurotrophic factor receptor subunit alpha	CNTFR
1133	Erythrocyte band 7 integral membrane protein	STOM
1134	Serum paraoxonase/arylesterase 1	PON1
1135	14-3-3 protein theta	YWHAQ
1136	Calmodulin-like protein 3	CALML3
1137	Dipeptidyl peptidase 4	DPP4
1138	Calreticulin	CALR
1139	Calnexin	CANX
1140	Interleukin-1 receptor type 2	IL1R2
1141	Proteasome subunit alpha type-5	PSMA5
1142	Proteasome subunit beta type-4	PSMB4
1143	Protein-lysine 6-oxidase	LOX
1144	Cystatin-D	CST5
1145	Granulins	GRN
1146	Cytosol aminopeptidase	LAP3
1147	Hematopoietic progenitor cell antigen CD34	CD34
1148	Tumor necrosis factor receptor superfamily member 8	TNFRSF8
1149	Connective tissue growth factor	CTGF
1150	Ephrin type-A receptor 2	EPHA2
1151	Tyrosine-protein phosphatase non-receptor type 6	PTPN6
1152	Cellular retinoic acid-binding protein 2	CRABP2
1153	Transketolase	TKT
1154	Serpin B3	SERPINB3
1155	Kallistatin	SERPINA4
1156	Guanine nucleotide-binding protein subunit alpha-11	GNA11
1157	Delta-1-pyrroline-5-carboxylate dehydrogenase, mitochondrial	ALDH4A1
1158	Phenazine biosynthesis-like domain-containing protein	PBLD

1159	Peroxiredoxin-6	PRDX6
1160	Flavin reductase (NADPH)	BLVRB
1161	Peroxiredoxin-5, mitochondrial	PRDX5
1162	D-dopachrome decarboxylase	DDT
1163	GTP cyclohydrolase 1 feedback regulatory protein	GCHFR
1164	Thioredoxin-dependent peroxide reductase, mitochondrial	PRDX3
1165	Phosphatidylethanolamine-binding protein 1	PEBP1
1166	Protein disulfide-isomerase A3	PDIA3
1167	HLA class I histocompatibility antigen, A-34 alpha chain	HLA-A
1168	HLA class I histocompatibility antigen, B-42 alpha chain	HLA-B
1169	Tyrosine-protein kinase receptor UFO	AXL
1170	Sodium- and chloride-dependent GABA transporter 1	SLC6A1
1171	Leukocyte elastase inhibitor	SERPINB1
1172	Lipocalin-1	LCN1
1173	Coronin-1A	CORO1A
1174	Rab GDP dissociation inhibitor alpha	GDI1
1175	Protein S100-A7	S100A7
1176	Fibroblast growth factor 9	FGF9
1177	Syndecan-4	SDC4
1178	Caspase-14	CASP14
1179	14-3-3 protein beta/alpha	YWHAB
1180	14-3-3 protein sigma	SFN
1181	Protein S100-A11	S100A11
1182	Neural cell adhesion molecule L1	L1CAM
1183	Peroxiredoxin-2	PRDX2
1184	4-hydroxyphenylpyruvate dioxygenase	HPD
1185	Desmoglein-3	DSG3
1186	Cadherin-5	CDH5
1187	Kinesin-1 heavy chain	KIF5B
1188	Mannosyl-oligosaccharide 1,2-alpha-mannosidase IA	MAN1A1
1189	N-acetylgalactosamine-6-sulfatase	GALNS
1190	Ribonuclease 4	RNASE4
1191	Macrosialin	CD68
1192	Serine hydroxymethyltransferase, cytosolic	SHMT1
1193	Protein EVI2B	EVI2B
1194	Heat shock 70 kDa protein 4	HSPA4
1195	Glypican-1	GPC1
1196	Radixin	RDX
1197	Sepiapterin reductase	SPR
1198	Cornifin-A	SPRR1A
1199	Small proline-rich protein 2B	SPRR2B
1200	Small proline-rich protein 2A	SPRR2A
1201	Fibrillin-1	FBN1

1202	Phosphoenolpyruvate carboxykinase, cytosolic [GTP]	PCK1
1203	Myosin-9	MYH9
1204	Tyrosine-protein kinase receptor Tie-1	TIE1
1205	Coatomer subunit beta	COPB2
1206	Basigin	BSG
1207	Glutaredoxin-1	GLRX
1208	Insulin-like growth factor-binding protein complex acid labile subunit	IGFALS
1209	Vascular endothelial growth factor receptor 2	KDR
1210	26S protease regulatory subunit 7	PSMC2
1211	Chitinase-3-like protein 1	CHI3L1
1212	V-type proton ATPase subunit E 1	ATP6V1E1
1213	7,8-dihydro-8-oxoguanine triphosphatase	NUDT1
1214	Phosphoglucomutase-1	PGM1
1215	Tumor necrosis factor receptor superfamily member 3	LTBR
1216	Serpin B5	SERPINB5
1217	Pigment epithelium-derived factor	SERPINF1
1218	Dihydrolipoyllysine-residue succinyltransferase component of 2-oxoglutarate dehydrogenase complex, mitochondrial	DLST
1219	Complement factor H-related protein 2	CFHR2
1220	TGF-beta receptor type-2	TGFBR2
1221	Transgelin-2	TAGLN2
1222	Transaldolase	TALDO1
1223	V-type proton ATPase catalytic subunit A	ATP6V1A
1224	Collagen alpha-1(XVIII) chain	COL18A1
1225	Macrophage-capping protein	CAPG
1226	Interleukin-6 receptor subunit beta	IL6ST
1227	Carcinoembryonic antigen-related cell adhesion molecule 6	CEACAM6
1228	Malate dehydrogenase, cytoplasmic	MDH1
1229	Malate dehydrogenase, mitochondrial	MDH2
1230	Leptin	LEP
1231	Aquaporin-2	AQP2
1232	Myeloid cell nuclear differentiation antigen	MNDA
1233	Prostaglandin-H2 D-isomerase	PTGDS
1234	Aldo-keto reductase family 1 member C3	AKR1C3
1235	Tyrosine-protein kinase FRK	FRK
1236	Leukemia inhibitory factor receptor	LIFR
1237	Lysosomal Pro-X carboxypeptidase	PRCP
1238	Cell surface glycoprotein MUC18	MCAM
1239	Biotinidase	BTD
1240	Nicotinamide phosphoribosyltransferase	NAMPT
1241	Killer cell immunoglobulin-like receptor 2DL1	KIR2DL1
1242	Afamin	AFM
1243	Peptidyl-prolyl cis-trans isomerase C	PPIC

1244	Adapter molecule crk	CRK
1245	Neurogenic locus notch homolog protein 1	NOTCH1
1246	Utrophin	UTRN
1247	Ras GTPase-activating-like protein IQGAP1	IQGAP1
1248	3-hydroxyanthranilate 3,4-dioxygenase	HAAO
1249	F-actin-capping protein subunit beta	CAPZB
1250	Stromal cell-derived factor 1	CXCL12
1251	Lithostathine-1-beta	REG1B
1252	Interferon alpha/beta receptor 2	IFNAR2
1253	Serpin B4	SERPINB4
1254	Glutathione synthetase	GSS
1255	Mannan-binding lectin serine protease 1	MASP1
1256	Protein NOV homolog	NOV
1257	CD97 antigen	CD97
1258	4-trimethylaminobutyraldehyde dehydrogenase	ALDH9A1
1259	Protein-glutamine gamma-glutamyltransferase 4	TGM4
1260	Alpha-aminoadipic semialdehyde dehydrogenase	ALDH7A1
1261	Proteasome subunit beta type-3	PSMB3
1262	Proteasome subunit beta type-2	PSMB2
1263	Histidine triad nucleotide-binding protein 1	HINT1
1264	Retinoic acid receptor responder protein 1	RARRES1
1265	Selenoprotein P	SEPP1
1266	Ketohexokinase	KHK
1267	Retinol-binding protein 2	RBP2
1268	Histamine N-methyltransferase	HNMT
1269	Guanine nucleotide-binding protein G(q) subunit alpha	GNAQ
1270	Rab GDP dissociation inhibitor beta	GDI2
1271	Vasodilator-stimulated phosphoprotein	VASP
1272	Dynamin-2	DNM2
1273	Palmitoyl-protein thioesterase 1	PPT1
1274	T-complex protein 1 subunit theta	CCT8
1275	T-complex protein 1 subunit delta	CCT4
1276	Annexin A11	ANXA11
1277	Ras-related protein Rab-5C	RAB5C
1278	Ras-related protein Rab-7a	RAB7A
1279	Gastrotropin	FABP6
1280	Amiloride-sensitive sodium channel subunit gamma	SCNN1G
1281	Galactokinase	GALK1
1282	Glypican-3	GPC3
1283	N-sulphoglucosamine sulphohydrolase	SGSH
1284	Hepatoma-derived growth factor	HDGF
1285	Lumican	LUM
1286	Prolargin	PRELP

1287	Heterogeneous nuclear ribonucleoprotein A3	HNRNPA3
1288	6-phosphogluconate dehydrogenase, decarboxylating	PGD
1289	Rho GDP-dissociation inhibitor 2	ARHGDIB
1290	Ribonuclease UK114	HRSP12
1291	Hexokinase-3	HK3
1292	Ephrin-B2	EFNB2
1293	Stanniocalcin-1	STC1
1294	F-actin-capping protein subunit alpha-1	CAPZA1
1295	Biliverdin reductase A	BLVRA
1296	Dipeptidyl peptidase 1	CTSC
1297	IST1 homolog	IST1
1298	Cysteine-rich secretory protein 1	CRISP1
1299	Voltage-dependent calcium channel subunit alpha-2/delta-1	CACNA2D1
1300	Heat shock-related 70 kDa protein 2	HSPA2
1301	Sodium/potassium-transporting ATPase subunit gamma	FXYD2
1302	UV excision repair protein RAD23 homolog A	RAD23A
1303	UV excision repair protein RAD23 homolog B	RAD23B
1304	Ephrin type-B receptor 3	EPHB3
1305	Arylsulfatase F	ARSF
1306	Alpha-N-acetylglucosaminidase	NAGLU
1307	Galactocerebrosidase	GALC
1308	Growth arrest-specific protein 1	GAS1
1309	Secreted Ly-6/uPAR-related protein 1	SLURP1
1310	Solute carrier family 12 member 3	SLC12A3
1311	Phospholipid transfer protein	PLTP
1312	Transitional endoplasmic reticulum ATPase	VCP
1313	Inhibin beta C chain	INHBC
1314	Pancreatic secretory granule membrane major glycoprotein GP2	GP2
1315	Laminin subunit beta-2	LAMB2
1316	Cadherin-11	CDH11
1317	Cadherin-13	CDH13
1318	Cadherin-15	CDH15
1319	BH3-interacting domain death agonist	BID
1320	GDNF family receptor alpha-1	GFRA1
1321	Eukaryotic translation initiation factor 6	EIF6
1322	Junctional adhesion molecule B	JAM2
1323	Ras-related protein Rab-25	RAB25
1324	Neutrophil defensin 3	DEFA3
1325	Actin-related protein 2/3 complex subunit 4	ARPC4
1326	Beta-defensin 1	DEFB1
1327	Triosephosphate isomerase	TPI1
1328	Keratin-associated protein 10-6	KRTAP10-6
1329	Actin, cytoplasmic 1	ACTB

1330	Cell division control protein 42 homolog	CDC42
1331	Ras-related protein Rab-5B	RAB5B
1332	Ras-related protein Rab-10	RAB10
1333	Ubiquitin-conjugating enzyme E2 N	UBE2N
1334	Ras-related protein Rab-14	RAB14
1335	Actin-related protein 3	ACTR3
1336	Actin-related protein 2	ACTR2
1337	Ras-related protein Rap-1b	RAP1B
1338	Pterin-4-alpha-carbinolamine dehydratase	PCBD1
1339	Lysozyme C	LYZ
1340	Epididymal secretory protein E1	NPC2
1341	Ubiquitin-fold modifier 1	UFM1
1342	Nuclear transport factor 2	NUTF2
1343	14-3-3 protein gamma	YWHAG
1344	14-3-3 protein epsilon	YWHAE
1345	Thymosin beta-4	TMSB4X
1346	ADP-ribosylation factor 6	ARF6
1347	Histone H4	HIST1H4A
1348	Ras-related protein Rap-1A	RAP1A
1349	Guanine nucleotide-binding protein G(I)/G(S)/G(T) subunit beta-2	GNB2
1350	Peptidyl-prolyl cis-trans isomerase A	PPIA
1351	Peptidyl-prolyl cis-trans isomerase FKBP1A	FKBP1A
1352	Growth factor receptor-bound protein 2	GRB2
1353	Ras-related C3 botulinum toxin substrate 1	RAC1
1354	Guanine nucleotide-binding protein G(s) subunit alpha isoforms short	GNAS
1355	14-3-3 protein zeta/delta	YWHAZ
1356	Actin, cytoplasmic 2	ACTG1
1357	Thymosin beta-10	TMSB10
1358	Tropomyosin alpha-4 chain	TPM4
1359	Actin, alpha skeletal muscle	ACTA1
1360	Tubulin alpha-1B chain	TUBA1B
1361	Tubulin beta-4B chain	TUBB4B
1362	Hemoglobin subunit beta	HBB
1363	Hemoglobin subunit gamma-1	HBG1
1364	Hemoglobin subunit alpha	HBA1
1365	Coxsackievirus and adenovirus receptor	CXADR
1366	Tyrosine-protein phosphatase non-receptor type substrate 1	SIRPA
1367	Disintegrin and metalloproteinase domain-containing protein 8	ADAM8
1368	Glutathione S-transferase omega-1	GSTO1
1369	Protein jagged-1	JAG1
1370	Interleukin-13 receptor subunit alpha-1	IL13RA1
1371	Phosphatidylinositol-glycan-specific phospholipase D	GPLD1
1372	Neutrophil gelatinase-associated lipocalin	LCN2

1373	Metallothionein-1H	MT1H
1374	Protein delta homolog 1	DLK1
1375	Ig heavy chain V-III region GAR	
1376	Protein S100-A12	S100A12
1377	Brain acid soluble protein 1	BASP1
1378	Ig lambda chain V-III region LOI	
1379	Hepcidin	HAMP
1380	Dermcidin	DCD
1381	Retinol-binding protein 5	RBP5
1382	ADAMTS-like protein 3	ADAMTSL3
1383	Serine protease HTRA3	HTRA3
1384	Ig kappa chain V-IV region STH	
1385	ADP-ribosylation factor 1	ARF1
1386	Fibulin-2	FBLN2
1387	Basement membrane-specific heparan sulfate proteoglycan core protein	HSPG2
1388	Polycystin-1	PKD1
1389	Low-density lipoprotein receptor-related protein 2	LRP2
1390	Ephrin-B1	EFNB1
1391	Sorbitol dehydrogenase	SORD
1392	Heterogeneous nuclear ribonucleoprotein U	HNRNPU
1393	CD83 antigen	CD83
1394	Di-N-acetylchitobiase	CTBS
1395	Fatty acid-binding protein, epidermal	FABP5
1396	Adenylyl cyclase-associated protein 1	CAP1
1397	Interferon-induced transmembrane protein 3	IFITM3
1398	Tyrosine-protein kinase transmembrane receptor ROR1	ROR1
1399	Tyrosine-protein kinase transmembrane receptor ROR2	ROR2
1400	Transgelin	TAGLN
1401	N-acylethanolamine-hydrolyzing acid amidase	NAAA
1402	Semenogelin-2	SEMG2
1403	Collagen alpha-1(VII) chain	COL7A1
1404	Desmoglein-1	DSG1
1405	Desmocollin-2	DSC2
1406	Guanylin	GUCA2A
1407	Nucleobindin-1	NUCB1
1408	A-kinase anchor protein 12	AKAP12
1409	Complement factor H-related protein 3	CFHR3
1410	Aminoacylase-1	ACY1
1411	Transforming growth factor beta receptor type 3	TGFBR3
1412	Trefoil factor 2	TFF2
1413	Urokinase plasminogen activator surface receptor	PLAUR
1414	Complement factor H-related protein 1	CFHR1
1415	Glutamate carboxypeptidase 2	FOLH1

1416	Neurogenic locus notch homolog protein 2	NOTCH2
1417	Hepatocyte growth factor activator	HGFAC
1418	Lactoylglutathione lyase	GLO1
1419	Activin receptor type-1	ACVR1
1420	14-3-3 protein eta	YWHAH
1421	Galectin-10	CLC
1422	Inter-alpha-trypsin inhibitor heavy chain H3	ITIH3
1423	Regenerating islet-derived protein 3-alpha	REG3A
1424	Proteasome activator complex subunit 1	PSME1
1425	Tyrosine-protein kinase receptor TYRO3	TYRO3
1426	Amyloid-like protein 2	APLP2
1427	Fibromodulin	FMOD
1428	Peroxiredoxin-1	PRDX1
1429	Glutamyl aminopeptidase	ENPEP
1430	Dermatopontin	DPT
1431	Trefoil factor 3	TFF3
1432	Apoptosis regulator BAX	BAX
1433	Prolow-density lipoprotein receptor-related protein 1	LRP1
1434	Rho GTPase-activating protein 1	ARHGAP1
1435	Protocadherin-1	PCDH1
1436	Protein-glutamine gamma-glutamyltransferase E	TGM3
1437	Quinone oxidoreductase	CRYZ
1438	Epithelial discoidin domain-containing receptor 1	DDR1
1439	Galectin-3-binding protein	LGALS3BP
1440	Desmocollin-1	DSC1
1441	Testican-1	SPOCK1
1442	Fibrinogen-like protein 1	FGL1
1443	Sialic acid-binding Ig-like lectin 14	SIGLEC14
1444	Neuroblast differentiation-associated protein AHNAK	AHNAK
1445	Apolipoprotein B receptor	APOBR
1446	Polypeptide N-acetylgalactosaminyltransferase 1	GALNT1
1447	Bone marrow stromal antigen 2	BST2
1448	Hyaluronidase-1	HYAL1
1449	EGF-containing fibulin-like extracellular matrix protein 1	EFEMP1
1450	EGF-containing fibulin-like extracellular matrix protein 1	EFEMP1
1451	Follistatin-related protein 1	FSTL1
1452	Contactin-1	CNTN1
1453	Cadherin-17	CDH17
1454	Receptor-type tyrosine-protein phosphatase eta	PTPRJ
1455	Tyrosine-protein phosphatase non-receptor type 13	PTPN13
1456	Epidermal growth factor receptor kinase substrate 8	EPS8
1457	Transcription initiation factor TFIID subunit 10	TAF10
1458	T-lymphoma invasion and metastasis-inducing protein 1	TIAM1

1459	Secretory phospholipase A2 receptor	PLA2R1
1460	Secreted phosphoprotein 24	SPP2
1461	PDZK1-interacting protein 1	PDZK1IP1
1462	BMP and activin membrane-bound inhibitor homolog	BAMBI
1463	Multimerin-1	MMRN1
1464	Selenium-binding protein 1	SELENBP1
1465	Chitotriosidase-1	CHIT1
1466	Inactive tyrosine-protein kinase 7	PTK7
1467	Receptor-type tyrosine-protein phosphatase S	PTPRS
1468	Mesothelin	MSLN
1469	Insulin-like growth factor I	IGF-I
1470	Disintegrin and metalloproteinase domain-containing protein 15	ADAM15
1471	Transmembrane emp24 domain-containing protein 1	TMED1
1472	Sequestosome-1	SQSTM1
1473	Ecto-ADP-ribosyltransferase 3	ART3
1474	Acid ceramidase	ASAH1
1475	Polycystin-2	PKD2
1476	Semaphorin-5A	SEMA5A
1477	Solute carrier family 12 member 1	SLC12A1
1478	Ras-related protein Rab-32	RAB32
1479	CD166 antigen	ALCAM
1480	Apolipoprotein F	APOF
1481	Spectrin alpha chain, non-erythrocytic 1	SPTAN1
1482	Bone morphogenetic protein receptor type-2	BMPR2
1483	Carcinoembryonic antigen-related cell adhesion molecule 7	CEACAM7
1484	Coactosin-like protein	COTL1
1485	Lysosome membrane protein 2	SCARB2
1486	Nidogen-2	NID2
1487	Dystroglycan	DAG1
1488	Desmoglein-2	DSG2
1489	Tripartite motif-containing protein 29	TRIM29
1490	Dihydropyrimidinase-related protein 3	DPYSL3
1491	Lymphocyte antigen 6D	LY6D
1492	Src substrate cortactin	CTTN
1493	Fibroleukin	FGL2
1494	Filamin-C	FLNC
1495	Frizzled-2	FZD2
1496	Guanine nucleotide-binding protein subunit alpha-13	GNA13
1497	Growth arrest-specific protein 6	GAS6
1498	cGMP-inhibited 3,5-cyclic phosphodiesterase A	PDE3A
1499	WAP four-disulfide core domain protein 2	WFDC2
1500	SPARC-like protein 1	SPARCL1
1501	Hyaluronan-binding protein 2	HABP2

1502	Desmocollin-3	DSC3
1503	Plastin-1	PLS1
1504	Major vault protein	MVP
1505	LIM and SH3 domain protein 1	LASP1
1506	Ketimine reductase mu-crystallin	CRYM
1507	Prostaglandin reductase 1	PTGR1
1508	Transmembrane glycoprotein NMB	GPNMB
1509	Opioid-binding protein/cell adhesion molecule	OPCML
1510	Calcium-activated chloride channel regulator 4	CLCA4
1511	C-type lectin domain family 5 member A	CLEC5A
1512	Early endosome antigen 1	EEA1
1513	Protein disulfide-isomerase A6	PDIA6
1514	Procollagen C-endopeptidase enhancer 1	PCOLCE
1515	Plectin	PLEC
1516	Inorganic pyrophosphatase	PPA1
1517	Nectin-1	PVRL1
1518	Nicotinate-nucleotide pyrophosphorylase [carboxylating]	QPRT
1519	Reticulocalbin-1	RCN1
1520	Receptor tyrosine-protein kinase erbB-4	ERBB4
1521	Poly(rC)-binding protein 1	PCBP1
1522	Ephrin type-A receptor 7	EPHA7
1523	Ficolin-2	FCN2
1524	Transforming growth factor-beta-induced protein ig-h3	TGFBI
1525	Na(+)/H(+) exchange regulatory cofactor NHE-RF2	SLC9A3R2
1526	Myosin light chain kinase, smooth muscle	MYLK
1527	Probable E3 ubiquitin-protein ligase HERC1	HERC1
1528	Cystatin-M	CST6
1529	Adipogenesis regulatory factor	ADIRF
1530	Adiponectin	ADIPOQ
1531	V-type proton ATPase subunit S1	ATP6AP1
1532	Ras-related protein Rab-11B	RAB11B
1533	Insulin-like growth factor-binding protein 7	IGFBP7
1534	Laminin subunit alpha-4	LAMA4
1535	C3a anaphylatoxin chemotactic receptor	C3AR1
1536	Extracellular matrix protein 1	ECM1
1537	C-C motif chemokine 14	CCL14
1538	Drebrin	DBN1
1539	Prostasin	PRSS8
1540	Guanylate cyclase activator 2B	GUCA2B
1541	2,4-dienoyl-CoA reductase, mitochondrial	DECR1
1542	Alpha-mannosidase 2	MAN2A1
1543	Glutaminyl-peptide cyclotransferase	QPCT
1544	Discoidin domain-containing receptor 2	DDR2

1545	Receptor-type tyrosine-protein phosphatase-like N	PTPRN
1546	V-type proton ATPase subunit F	ATP6V1F
1547	Prostate-associated microseminoprotein	MSMP
1548	Transmembrane protein 132A	TMEM132A
1549	Inverted formin-2	INF2
1550	Fer-1-like protein 6	FER1L6
1551	HLA class II histocompatibility antigen, DRB1-8 beta chain	HLA-DRB1
1552	Leucine-rich repeat flightless-interacting protein 1	LRRFIP1
1553	Nucleoside diphosphate kinase	NME1-NME2
1554	Chromodomain-helicase-DNA-binding protein 9	CHD9
1555	CMRF35-like molecule 2	CD300E
1556	Hydrocephalus-inducing protein homolog	HYDIN
1557	Cell adhesion molecule-related/down-regulated by oncogenes	CDON
1558	TBC1 domain family member 10B	TBC1D10B
1559	Choline transporter-like protein 4	SLC44A4
1560	Fibulin-7	FBLN7
1561	Cytochrome b reductase 1	CYBRD1
1562	Proline-rich transmembrane protein 3	PRRT3
1563	Metalloproteinase inhibitor 1	TIMP1
1564	Protein crumbs homolog 2	CRB2
1565	Rho-related GTP-binding protein RhoC	RHOC
1566	Melanoma inhibitory activity protein 3	MIA3
1567	NHL repeat-containing protein 3	NHLRC3
1568	Olfactomedin-like protein 2A	OLFML2A
1569	Serine/threonine-protein kinase 24	STK24
1570	Forkhead-associated domain-containing protein 1	FHAD1
1571		SERPINB3
1572	Collectin-12	COLEC12
1573	Sorting nexin-5	SNX5
1574	Proteasome inhibitor PI31 subunit	PSMF1
1575	P-selectin	SELP
1576	Tetratricopeptide repeat protein 38	TTC38
1577	Protein S100-A2	S100A2
1578	HLA class I histocompatibility antigen, alpha chain G	HLA-G
1579	Chloride intracellular channel protein 3	CLIC3
1580	Complement receptor type 1	CR1
1581	Calsyntenin-1	CLSTN1
1582	Allograft inflammatory factor 1	AIF1
1583	Protein FAM171A1	FAM171A1
1584	FRAS1-related extracellular matrix protein 2	FREM2
1585	D-3-phosphoglycerate dehydrogenase	PHGDH
1586	UMP-CMP kinase	CMPK1
1587	Slit homolog 1 protein	SLIT1

1588	SH3 domain-binding glutamic acid-rich-like protein 3	SH3BGRL3
1589	Nicastrin	NCSTN
1590	V-set domain-containing T-cell activation inhibitor 1	VTCN1
1591	Na(+)/H(+) exchange regulatory cofactor NHE-RF3	PDZK1
1592	Protein delta homolog 2	DLK2
1593	Tubulointerstitial nephritis antigen	TINAG
1594	Probable G-protein coupled receptor 110	GPR110
1595	Transmembrane protein 59	TMEM59
1596	Glutathione S-transferase Mu 5	GSTM5
1597	Ribosyldihydronicotinamide dehydrogenase [quinone]	NQO2
1598		CFH
1599	Signal-regulatory protein beta-1 isoform 3	SIRPB1
1600	Protein-tyrosine-phosphatase	PTPRK
1601	Protocadherin-9	PCDH9
1602	Putative elongation factor 1-alpha-like 3	EEF1A1P5
1603	BRO1 domain-containing protein BROX	BROX
1604	Retinol-binding protein 4	RBP4
1605	Platelet endothelial aggregation receptor 1	PEAR1
1606	Low-density lipoprotein receptor-related protein 11	LRP11
1607	Golgi-associated plant pathogenesis-related protein 1	GLIPR2
1608	Interleukin-2 receptor subunit alpha	IL2RA
1609	Translationally-controlled tumor protein	TPT1
1610	CD276 antigen	CD276
1611	Carboxypeptidase Z	CPZ
1612	Cyclic AMP-responsive element-binding protein 3-like protein 3	CREB3L3
1613	Natural cytotoxicity triggering receptor 3 ligand 1	NCR3LG1
1614	Transmembrane protein PVRIG	PVRIG
1615	Vasorin	VASN
1616	Secreted frizzled-related protein 4	SFRP4
1617	Leukocyte-associated immunoglobulin-like receptor 1	LAIR1
1618	Twinfilin-2	TWF2
1619	Leukocyte-associated immunoglobulin-like receptor 2	LAIR2
1620	Uncharacterized protein C16orf46	C16orf46
1621	Annexin	ANXA4
1622	Phospholipase B-like 1	PLBD1
1623	Protein CASC4	CASC4
1624	von Willebrand factor A domain-containing protein 1	VWA1
1625	2-oxoglutarate and iron-dependent oxygenase domain-containing protein 3	OGFOD3
1626	Chondroitin sulfate proteoglycan 4	CSPG4
1627	Protein FAM198B	FAM198B
1628	Protein shisa-2 homolog	SHISA2
1629	Suprabasin	SBSN
1630	Suprabasin	SBSN

1631	Ectonucleotide pyrophosphatase/phosphodiesterase family member 7	ENPP7
1632	Lipocalin-15	LCN15
1633	Olfactomedin-4	OLFM4
1634	Plexin domain-containing protein 2	PLXDC2
1635	UPF0764 protein C16orf89	C16orf89
1636	Ly6/PLAUR domain-containing protein 2	LYPD2
1637	C-type lectin domain family 4 member G	CLEC4G
1638	Peptidase inhibitor 16	PI16
1639	CMRF35-like molecule 9	CD300LG
1640	Leucine-rich repeat neuronal protein 1	LRRN1
1641	C-type lectin domain family 9 member A	CLEC9A
1642	ADAMTS-like protein 4	ADAMTSL4
1643	Protocadherin Fat 4	FAT4
1644	Mucin-6	MUC6
1645	Nicotinate phosphoribosyltransferase	NAPRT
1646	Gliomedin	GLDN
1647	Scavenger receptor class A member 5	SCARA5
1648	Tropomyosin alpha-1 chain	TPM1
1649	Ferric-chelate reductase 1	FRRS1
1650	Protein shisa-6 homolog	SHISA6
1651	Hemojuvelin	HFE2
1652	F-box only protein 50	NCCRP1
1653	Cyclic AMP-responsive element-binding protein 3-like protein 2	CREB3L2
1654	Small integral membrane protein 5	SMIM5
1655	Isoaspartyl peptidase/L-asparaginase	ASRGL1
1656	Glycerophosphodiester phosphodiesterase domain-containing protein 3	GDPD3
1657	Charged multivesicular body protein 1b	CHMP1B
1658	Neuronal growth regulator 1	NEGR1
1659	Low-density lipoprotein receptor-related protein 10	LRP10
1660	Growth/differentiation factor 7	GDF7
1661	UPF0669 protein C6orf120	C6orf120
1662	Vitelline membrane outer layer protein 1 homolog	VMO1
1663	Podocan	PODN
1664	B- and T-lymphocyte attenuator	BTLA
1665	E3 ubiquitin-protein ligase HUWE1	HUWE1
1666	Transmembrane emp24 domain-containing protein 4	TMED4
1667	Multiple epidermal growth factor-like domains protein 8	MEGF8
1668	N-acetylgalactosaminyltransferase 7	GALNT7
1669	G-protein coupled receptor 126	GPR126
1670	C-type lectin domain family 14 member A	CLEC14A
1671	Uncharacterized protein C14orf37	C14orf37
1672	Serpin A11	SERPINA11
1673	Out at first protein homolog	OAF

1674	Reticulon-4 receptor-like 2	RTN4RL2
1675	Fermitin family homolog 3	FERMT3
1676	Thioredoxin domain-containing protein 5	TXNDC5
1677	Integral membrane protein GPR180	GPR180
1678	Cullin-associated NEDD8-dissociated protein 1	CAND1
1679	Transmembrane emp24 domain-containing protein 7	TMED7
1680	Xylosyltransferase 1	XYLT1
1681	Copine-8	CPNE8
1682	Plexin domain-containing protein 1	PLXDC1
1683	Adipocyte enhancer-binding protein 1	AEBP1
1684	Phospholipase D3	PLD3
1685	Protein AHNAK2	AHNAK2
1686	SLIT and NTRK-like protein 4	SLITRK4
1687	Choline transporter-like protein 2	SLC44A2
1688	MAX gene-associated protein	MGA
1689	Extracellular sulfatase Sulf-2	SULF2
1690	Ubiquitin-conjugating enzyme E2 variant 3	UEVLD
1691	Transmembrane protein 192	TMEM192
1692	Osteoclast-associated immunoglobulin-like receptor	OSCAR
1693	Probable G-protein coupled receptor 116	GPR116
1694	G-protein coupled receptor 64	GPR64
1695	Cell adhesion molecule 3	CADM3
1696	Prominin-2	PROM2
1697	Protein unc-80 homolog	UNC80
1698	Ly6/PLAUR domain-containing protein 1	LYPD1
1699	Latent-transforming growth factor beta-binding protein 4	LTBP4
1700	Leucine-rich repeat-containing protein 25	LRRC25
1701	Maturin	MTURN
1702	Cell adhesion molecule 2	CADM2
1703	Secreted frizzled-related protein 1	SFRP1
1704	Leukocyte immunoglobulin-like receptor subfamily A member 3	LILRA3
1705	Discoidin, CUB and LCCL domain-containing protein 1	DCBLD1
1706	Golgi membrane protein 1	GOLM1
1707	E3 ubiquitin-protein ligase RNF149	RNF149
1708	Keratinocyte-associated transmembrane protein 2	KCT2
1709	Group XV phospholipase A2	PLA2G15
1710	NAD(P)H-hydrate epimerase	APOA1BP
1711	Hemicentin-2	HMCN2
1712	MAPK-interacting and spindle-stabilizing protein-like	MAPK1IP1L
1713	Beta-1,3-N-acetylglucosaminyltransferase lunatic fringe	LFNG
1714	DCC-interacting protein 13-beta	APPL2
1715	Retinoic acid-induced protein 3	GPRC5A
1716	Torsin-1A-interacting protein 2	TOR1AIP2

1717	Delta and Notch-like epidermal growth factor-related receptor	DNER
1718	Thiosulfate sulfurtransferase/rhodanese-like domain-containing protein 1	TSTD1
1719	Cell adhesion molecule 4	CADM4
1720	Putative phospholipase B-like 2	PLBD2
1721	Protocadherin-19	PCDH19
1722	T-cell immunomodulatory protein	ITFG1
1723	Membrane protein FAM174A	FAM174A
1724	5(3)-deoxyribonucleotidase, cytosolic type	NT5C
1725	BPI fold-containing family B member 1	BPIFB1
1726	Hepatitis A virus cellular receptor 2	HAVCR2
1727	Immunoglobulin superfamily DCC subclass member 4	IGDCC4
1728	Epidermal growth factor receptor kinase substrate 8-like protein 1	EPS8L1
1729	WASP homolog-associated protein with actin, membranes and microtubules	WHAMM
1730	Leucine-rich repeat-containing protein 15	LRRC15
1731	Marginal zone B- and B1-cell-specific protein	MZB1
1732	Programmed cell death 6-interacting protein	PDCD6IP
1733	Leucine-rich repeat neuronal protein 4	LRRN4
1734	Soluble calcium-activated nucleotidase 1	CANT1
1735	Intelectin-1	ITLN1
1736	Stabilin-2	STAB2
1737	High affinity immunoglobulin alpha and immunoglobulin mu Fc receptor	FCAMR
1738	Oncoprotein-induced transcript 3 protein	OIT3
1739	Titin	TTN
1740	Roundabout homolog 4	ROBO4
1741	Acid sphingomyelinase-like phosphodiesterase 3a	SMPDL3A
1742	Acid sphingomyelinase-like phosphodiesterase 3b	SMPDL3B
1743	Complement factor H-related protein 4	CFHR4
1744	Protein FAM3C	FAM3C
1745	Protein NDRG1	NDRG1
1746	Peroxidasin homolog	PXDN
1747	Sortilin-related receptor	SORL1
1748	Nectin-2	PVRL2
1749	Serine protease HTRA1	HTRA1
1750	Tenascin-R	TNR
1751	Secreted frizzled-related protein 3	FRZB
1752	Gamma-glutamyl hydrolase	GGH
1753	Neogenin	NEO1
1754	Kallikrein-6	KLK6
1755	Ubiquitin fusion degradation protein 1 homolog	UFD1L
1756	Golgi apparatus protein 1	GLG1
1757	Proteoglycan 4	PRG4
1758	Betaine--homocysteine S-methyltransferase 1	BHMT
1759	Homogentisate 1,2-dioxygenase	HGD

1760	Liver-expressed antimicrobial peptide 2	LEAP2
1761	Myeloid-derived growth factor	MYDGF
1762	Tumor necrosis factor receptor superfamily member 19L	RELT
1763	Uncharacterized protein C11orf52	C11orf52
1764	Mas-related G-protein coupled receptor member F	MRGPRF
1765	Phosphotriesterase-related protein	PTER
1766	EF-hand domain-containing protein D2	EFHD2
1767	Aldose 1-epimerase	GALM
1768	Collagen triple helix repeat-containing protein 1	CTHRC1
1769	BTB/POZ domain-containing protein KCTD12	KCTD12
1770	Reticulocalbin-3	RCN3
1771	Zymogen granule protein 16 homolog B	ZG16B
1772	Carboxymethylenebutenolidase homolog	CMBL
1773	Phosphoinositide-3-kinase-interacting protein 1	PIK3IP1
1774	Kinesin-like protein KIF12	KIF12
1775	Protein S100-A16	S100A16
1776	DPH3 homolog	DPH3
1777	Phosphoglucomutase-2	PGM2
1778	Brevican core protein	BCAN
1779	PDZ and LIM domain protein 5	PDLIM5
1780	Cysteine-rich with EGF-like domain protein 1	CRELD1
1781	N-acyl-aromatic-L-amino acid amidohydrolase (carboxylate-forming)	ACY3
1782	ERO1-like protein alpha	ERO1L
1783	Immunoglobulin superfamily member 21	IGSF21
1784	V-set and immunoglobulin domain-containing protein 2	VSIG2
1785	Alpha/beta hydrolase domain-containing protein 14B	ABHD14B
1786	Carboxypeptidase B2	CPB2
1787	Kin of IRRE-like protein 1	KIRREL
1788	Beta-galactoside alpha-2,6-sialyltransferase 2	ST6GAL2
1789	Protocadherin-16	DCHS1
1790	Beta-Ala-His dipeptidase	CNDP1
1791	Cytosolic non-specific dipeptidase	CNDP2
1792	Receptor protein-tyrosine kinase	EPHB4
1793	Fc receptor-like protein 1	FCRL1
1794	Intraflagellar transport protein 74 homolog	IFT74
1795	Junctional sarcoplasmic reticulum protein 1	JSRP1
1796	Kremen protein 1	KREMEN1
1797	Nectin-4	PVRL4
1798	Serpin B12	SERPINB12
1799	N-acetylmuramoyl-L-alanine amidase	PGLYRP2
1800	Erythroid membrane-associated protein	ERMAP
1801	SLIT and NTRK-like protein 1	SLITRK1
1802	Proton myo-inositol cotransporter	SLC2A13

1803	Vacuolar protein sorting-associated protein 35	VPS35
1804	Vacuolar protein sorting-associated protein 13A	VPS13A
1805	Hemicentin-1	HMCN1
1806	Phosphatidylethanolamine-binding protein 4	PEBP4
1807	Probable carboxypeptidase X1	CPXM1
1808	Niban-like protein 1	FAM129B
1809	Protein deglycase DJ-1	PARK7
1810	Sialidase-1	NEU1
1811	Sortilin	SORT1
1812	Synaptic vesicle membrane protein VAT-1 homolog	VAT1
1813	Legumain	LGMN
1814	Neuroserpin	SERPINI1
1815	Protein S100-A13	S100A13
1816	Oncostatin-M-specific receptor subunit beta	OSMR
1817	Cell growth regulator with EF hand domain protein 1	CGREF1
1818	Cell surface A33 antigen	GPA33
1819	Smoothened homolog	SMO
1820	Histone H2A type 1-J	HIST1H2AJ
1821	Retinoic acid receptor responder protein 2	RARRES2
1822	Myocilin	MYOC
1823	Osteomodulin	OMD
1824	Growth/differentiation factor 15	GDF15
1825	Programmed cell death 1 ligand 2	PDCD1LG2
1826	Calsyntenin-3	CLSTN3
1827	Coronin-1B	CORO1B
1828	Thioredoxin domain-containing protein 17	TXNDC17
1829	Serine/threonine-protein phosphatase CPPED1	CPPED1
1830	Matrix-remodeling-associated protein 8	MXRA8
1831	45 kDa calcium-binding protein	SDF4
1832	Migration and invasion enhancer 1	MIEN1
1833	Endoplasmic reticulum resident protein 44	ERP44
1834	Protease-associated domain-containing protein 1	PRADC1
1835	Synaptotagmin-11	SYT11
1836	Ubiquitin-related modifier 1	URM1
1837	Plasma alpha-L-fucosidase	FUCA2
1838	Chordin-like protein 1	CHRDL1
1839	Spondin-2	SPON2
1840	Protein crumbs homolog 3	CRB3
1841	Protein MENT	MENT
1842	3-hydroxybutyrate dehydrogenase type 2	BDH2
1843	Vesicle-associated membrane protein 8	VAMP8
1844	Gamma-glutamylaminecyclotransferase	GGACT
1845	Specifically androgen-regulated gene protein	SARG

1846	Junctional adhesion molecule C	JAM3
1847	TBC1 domain family member 10A	TBC1D10A
1848	C-type lectin domain family 7 member A	CLEC7A
1849	Pappalysin-2	PAPPA2
1850	Complement factor H-related protein 5	CFHR5
1851	EMILIN-2	EMILIN2
1852	Charged multivesicular body protein 4a	CHMP4A
1853	Cell adhesion molecule 1	CADM1
1854	Cadherin-related family member 2	CDHR2
1855	Angiotensin-converting enzyme 2	ACE2
1856	Fibroblast growth factor-binding protein 2	FGFBP2
1857	Ly-6/neurotoxin-like protein 1	LYNX1
1858	Sialoadhesin	SIGLEC1
1859	Tubulointerstitial nephritis antigen-like	TINAGL1
1860	Twisted gastrulation protein homolog 1	TWSG1
1861	Toll-interacting protein	TOLLIP
1862	Protein ITFG3	ITFG3
1863	Cysteine-rich and transmembrane domain-containing protein 1	CYSTM1
1864	Multiple epidermal growth factor-like domains protein 9	MEGF9
1865	EH domain-containing protein 4	EHD4
1866	Caspase recruitment domain-containing protein 9	CARD9
1867	C-X-C motif chemokine 16	CXCL16
1868	STE20-like serine/threonine-protein kinase	SLK
1869	Probable serine carboxypeptidase CPVL	CPVL
1870	Charged multivesicular body protein 4b	CHMP4B
1871	Frizzled-8	FZD8
1872	Rab GTPase-binding effector protein 2	RABEP2
1873	CXADR-like membrane protein	CLMP
1874	Epidermal growth factor receptor kinase substrate 8-like protein 2	EPS8L2
1875	Anthrax toxin receptor 1	ANTXR1
1876	UPF0454 protein C12orf49	C12orf49
1877	Leucine-rich repeat-containing protein 19	LRRC19
1878	MANSC domain-containing protein 1	MANSC1
1879	Multimerin-2	MMRN2
1880	Chondrolectin	CHODL
1881	Sialate O-acetylesterase	SIAE
1882	Tumor necrosis factor receptor superfamily member 27	EDA2R
1883	Retinoid-inducible serine carboxypeptidase	SCPEP1
1884	Cadherin-related family member 5	CDHR5
1885	Collectrin	TMEM27
1886	Putative sodium-coupled neutral amino acid transporter 10	SLC38A10
1887	Cadherin-20	CDH20
1888	EGF, latrophilin and seven transmembrane domain-containing protein 1	ELTD1

1889	Otoferlin	OTOF
1890	Mucin-5B	MUC5B
1891	Copine-5	CPNE5
1892	UPF0606 protein KIAA1549	KIAA1549
1893	Platelet glycoprotein VI	GP6
1894	Endosialin	CD248
1895	Cadherin EGF LAG seven-pass G-type receptor 2	CELSR2
1896	Resistin	RETN
1897	Tumor necrosis factor receptor superfamily member 12A	TNFRSF12A
1898	CD320 antigen	CD320
1899	Protocadherin-12	PCDH12
1900	Interleukin-1 receptor accessory protein	IL1RAP
1901	Complement component C1q receptor	CD93
1902	Signal peptide, CUB and EGF-like domain-containing protein 2	SCUBE2
1903	Serine protease inhibitor Kazal-type 5	SPINK5
1904	Cartilage acidic protein 1	CRTAC1
1905	Omega-amidase NIT2	NIT2
1906	Nectin-3	PVRL3
1907	Baculoviral IAP repeat-containing protein 6	BIRC6
1908	Scavenger receptor cysteine-rich type 1 protein M160	CD163L1
1909	Matrix-remodeling-associated protein 5	MXRA5
1910	Cytokine-like protein 1	CYTL1
1911	14 kDa phosphohistidine phosphatase	PHPT1
1912	Tumor necrosis factor receptor superfamily member 19	TNFRSF19
1913	Gastrokine-1	GKN1
1914	EMILIN-3	EMILIN3
1915	Glycoprotein integral membrane protein 1	GINM1
1916	Transmembrane protein 106B	TMEM106B
1917	Protein FAM49B	FAM49B
1918	UPF0587 protein C1orf123	C1orf123
1919	Stabilin-1	STAB1
1920	N-acetyllactosaminide beta-1,3-N-acetylglucosaminyltransferase 2	B3GNT2
1921	Cadherin EGF LAG seven-pass G-type receptor 1	CELSR1
1922	Podocalyxin-like protein 2	PODXL2
1923	Alpha-hemoglobin-stabilizing protein	AHSP
1924	G-protein coupled receptor family C group 5 member B	GPRC5B
1925	Eukaryotic translation initiation factor 2-alpha kinase 3	EIF2AK3
1926	Methionine adenosyltransferase 2 subunit beta	MAT2B
1927	Interleukin-1 receptor accessory protein-like 1	IL1RAPL1
1928	Complement C1r subcomponent-like protein	C1RL
1929	Calmodulin-like protein 5	CALML5
1930	Leucine-rich repeat transmembrane protein FLRT3	FLRT3
1931	Cysteine-rich motor neuron 1 protein	CRIM1

1932	Charged multivesicular body protein 5	CHMP5
1933	Neurotrimin	NTM
1934	Costars family protein ABRACL	ABRACL
1935	Prostaglandin F2 receptor negative regulator	PTGFRN
1936	Small proline-rich protein 3	SPRR3
1937	Ammonium transporter Rh type C	RHCG
1938	C-type mannose receptor 2	MRC2
1939	Cornulin	CRNN
1940	Guanine nucleotide-binding protein G(I)/G(S)/G(O) subunit gamma-12	GNG12
1941	Glyoxylate reductase/hydroxypyruvate reductase	GRHPR
1942	Cathepsin Z	CTSZ
1943	Peflin	PEF1
1944	Cathepsin F	CTSF
1945	Kallikrein-11	KLK11
1946	DnaJ homolog subfamily B member 4	DNAJB4
1947	Klotho	KL
1948	Myelin protein zero-like protein 1	MPZL1
1949	Neuroplastin	DKFZp566H1924
1950	CGG triplet repeat-binding protein 1	CGGBP1
1951	Deleted in malignant brain tumors 1 protein	DMBT1
1952	Fetuin-B	FETUB
1953	CMRF35-like molecule 8	CD300A
1954	Sushi domain-containing protein 2	SUSD2
1955	Niemann-Pick C1-like protein 1	NPC1L1
1956	Tachykinin-3	TAC3
1957	ProSAAS	PCSK1N
1958	Prenylcysteine oxidase 1	PCYOX1
1959	A disintegrin and metalloproteinase with thrombospondin motifs 1	ADAMTS1
1960	Dipeptidyl peptidase 2	DPP7
1961	Brain-specific angiogenesis inhibitor 1-associated protein 2-like protein 1	BAIAP2L1
1962	Enolase-phosphatase E1	ENOPH1
1963	SLAM family member 5	CD84
1964	Leucyl-cystinyl aminopeptidase	LNPEP
1965	Serpin B13	SERPINB13
1966	N-acetyl-D-glucosamine kinase	NAGK
1967	Annexin A10	ANXA10
1968	N-acetylglucosamine-1-phosphotransferase subunit gamma	GNPTG
1969	N-acetylglucosamine-1-phosphodiester alpha-N-acetylglucosaminidase	NAGPA
1970	Vacuolar protein sorting-associated protein 28 homolog	VPS28
1971	Kallikrein-13	KLK13
1972	Protein kinase C and casein kinase substrate in neurons protein 3	PACSIN3
1973	Thyrotropin-releasing hormone-degrading ectoenzyme	TRHDE
1974	Angiopoietin-related protein 2	ANGPTL2

1975	Prion-like protein doppel	PRND
1976	Endomucin	EMCN
1977	Protein HEG homolog 1	HEG1
1978	RING finger protein 150	RNF150
1979	Unconventional myosin-Vb	MYO5B
1980	Frizzled-4	FZD4
1981	Coronin-1C	CORO1C
1982	Apoptosis-associated speck-like protein containing a CARD	PYCARD
1983	Mammalian ependymin-related protein 1	EPDR1
1984	Neurogenic locus notch homolog protein 3	NOTCH3
1985	Unconventional myosin-VI	MYO6
1986	Lysosomal thioesterase PPT2	PPT2
1987	Neudesin	NENF
1988	Vacuolar protein sorting-associated protein 4A	VPS4A
1989	Protocadherin beta-8	PCDHB8
1990	Protocadherin gamma-C3	PCDHGC3
1991	Protocadherin alpha-6	PCDHA6
1992	Protein kinase C and casein kinase substrate in neurons protein 2	PACSIN2
1993	Endothelial protein C receptor	PROCR
1994	Multiple inositol polyphosphate phosphatase 1	MINPP1
1995	NSFL1 cofactor p47	NSFL1C
1996	Frizzled-1	FZD1
1997		
1998	V-set and immunoglobulin domain-containing protein 4	VSIG4
1999	Integral membrane protein 2B	ITM2B
2000	Band 4.1-like protein 3	EPB41L3
2001	Lambda-crystallin homolog	CRYL1
2002	von Willebrand factor A domain-containing protein 7	VWA7
2003	Calcium-binding protein 39	CAB39
2004	Talin-1	TLN1
2005	Neurexin-3	NRXN3
2006	Plexin-D1	PLXND1
2007	Low-density lipoprotein receptor-related protein 12	LRP12
2008	Angiopoietin-related protein 3	ANGPTL3
2009	Protocadherin gamma-C5	PCDHGC5
2010	Protocadherin alpha-3	PCDHA3
2011	Suppressor of tumorigenicity 14 protein	ST14
2012	Lymphatic vessel endothelial hyaluronic acid receptor 1	LYVE1
2013	Heme-binding protein 2	HEBP2
2014	Phosphoserine aminotransferase	PSAT1
2015	Junctional adhesion molecule A	F11R
2016	Carboxypeptidase Q	CPQ
2017	G-protein coupled receptor 56	GPR56

2018	Chloride intracellular channel protein 4	CLIC4
2019	EMILIN-1	EMILIN1
2020	Tumor necrosis factor receptor superfamily member 11A	TNFRSF11A
2021	Adseverin	SCIN
2022	Calpain-7	CAPN7
2023	Bis(5-adenosyl)-triphosphatase ENPP4	ENPP4
2024	Protein S100	S100A6
2025	DENN domain-containing protein 4C	DENND4C
2026	Fatty acid-binding protein, heart	FABP3
2027	Lipolysis-stimulated lipoprotein receptor	LSR
2028		AMBP
2029	Calpain small subunit 1	CAPNS1
2030	OX-2 membrane glycoprotein	CD200
2031	Histone H2B	HIST1H2BN
2032	Low-density lipoprotein receptor-related protein 3	LRP3
2033		APOC2
2034	Apolipoprotein A-II	APOA2
2035	Signaling lymphocytic activation molecule	SLAMF1
2036	Carboxypeptidase	CTSA
2037	Carboxylic ester hydrolase	CEL
2038	Uromodulin	UMOD
2039	Complement C1q subcomponent subunit A	C1QA

Supplementary Table 5. Molecular Pathways

Pathway Number	Pathway Name
1	ESRD - Coagulation
2	ESRD - Acute Phase Response
3	ESRD - Intrinsic Prothrombin Activation
4	ESRD - GP6
5	Control - Acute Phase Response Signaling
6	Control - Cardiac Hypertrophy Signaling
7	Control - Gα12/13 Signaling
8	Control - Glioma Signaling
9	Control - IL-15 Signaling
10	Control - LXR-RXR Activation
11	Control - NF-κB Signaling
12	Control - PTEN Signaling
13	Control - Regulation of the Epithelial-Mesenchymal Transition by Growth Factors Pathway
14	Control - Stat3 Pathway
15	Control - Tumor Microenvironment Pathway
16	Control T-Cell Exhaustion Signaling Pathway
17	Control - Complement System
18	Control - Neuroprotective Role of THOP1 in Alzheimer's Disease
19	Control - Coagulation System
20	Control - Intrinsic Prothrombin Activation Pathway
21	Control - Production of Nitric Oxide and Reactive Oxygen Species